Spring 2014

Analysis of hydrologic systems at multiple spatial scales and its implications for aggregating hydrologic process

Bo Chen
University of Iowa

ANALYSIS OF HYDROLOGIC SYSTEMS AT MULTIPLE SPATIAL SCALES AND ITS IMPLICATIONS FOR AGGREGATING HYDROLOGIC PROCESS

by

Bo Chen

A thesis submitted in partial fulfillment of the
requirements for the Doctor of Philosophy degree
in Civil and Environmental Engineering
in the Graduate College of
The University of Iowa

May 2014

Thesis Supervisor: Professor Witold F. Krajewski

Graduate College
The University of Iowa
Iowa City, Iowa

CERTIFICATE OF APPROVAL

_____

PH.D. THESIS

_____

This is to certify that the Ph.D. thesis of

Bo Chen

has been approved by the Examining Committee
for the thesis requirement for the Doctor of Philosophy degree
in Civil and Environmental Engineering at the May 2014 graduation.

Thesis Committee: _____
Witold F. Krajewski, Thesis Supervisor

_____
Larry Weber

_____
Allen Bradley

_____
Ricardo Mantilla

_____
You-Kuan Zhang

_____
Keith Schilling

To my parents, Weichen, and Zhifei

ACKNOWLEDGMENTS

Many individuals have contributed to this thesis in various ways. Special thanks to Dr. Witold F. Krajewski for his thoughtful guidance, encouragement, patience, efforts, and wisdom. He gave me the absolute freedom to explore engaging topics and always kept his door open for insightful discussions which propelled me forward. I will benefit throughout my life from his training that extended from scientific research to daily life, and I hope to continue to learn from him. I wish to express my sincere gratitude to Dr. Larry Weber for his generosity and his initiating my study at IIHR. Great appreciation is extended to Drs. Allen Bradley, Ricardo Mantilla, You-Kuan Zhang, and Keith Schilling for their valuable suggestions concerning my research and for their serving on my committee. I thank Drs. Helmers Matthew and Xiaobo Zhou for their kindness in sharing their invaluable data and in organizing the field trips for us that contributed significantly to Chapter 2 of this thesis.

I thank Radoslaw Goska for his help pertaining to my research on LiDAR topography and radar rainfall, although they are not included in this thesis. I thank Scott Small for his helping me running numeric simulations and Bongchul for his providing radar rainfall for my research. Thanks also go to Dr. Marian Muste, James Niemeier, and Nathan Young for their guidance in field work and insightful discussions. I thank my lab mates Luciana and Tibebu for their help and availability for research discussions. I would also like to thank the administrative and computer staff of IIHR-Hydroscience and Engineering for their timely and patient help with all non-research matters.

I wish I could list all of the names of the friends at UI to whom I am thankful. I would also like to thank my friends in China for all the help they offered. I thank my brother and parents-in-law for their love and support. Lastly, my most heartfelt thanks go to my wife, Weichen, for her unconditional love, tolerance, and encouragement. The kindness, unselfishness, and strength of my parents will remain with me forever. I feel indebted to my little daughter, Zhifei, for my not being able to spend the amount of time

that a dad should spend with his kids. This Ph.D. degree is dedicated to you all, my family members and friends.

ABSTRACT

The representation and aggregation of the variability of small scale processes are fundamental to distributed hydrologic modeling. Addressing these issues via the examination of detailed information with large spatiotemporal coverage is infeasible due to the limitations of hydrological measurement techniques; however, data collected at discrete spatial scales are available. The main objective of this thesis is to explore how useful insights into aggregating hydrologic processes can be obtained through 1) analyzing hydrologic systems at multiple spatial scales to identify patterns of hydrologic processes at various scales and 2) conducting diagnostic simulations to understand how these patterns are linked. I first identified patterns of hydrologic processes by 1) comparing the surface runoff hydrographs (area-averaged discharges) from 12 hillslopes (0.5~3 ha) with spatial proximity in agricultural land in Iowa over 72 runoff events; 2) using consistent methods to analyze ~1000 recession curves observed in the nested Iowa and Cedar River basins (7~17000km^2) over the period of 1995-2010; and 3) examining the long recession curves in the nested Iowa and Cedar River basins during the 1988 and 2012 droughts. I then developed a distributed model as a diagnostic tool to explore the controls on the aggregation of hydrologic processes. In order to avoid other complex processes (e.g., partitioning of rainfall), I simplified the investigation by focusing on recession processes rather than on the entire response. The diagnostic simulations in the Cedar River basins reproduced the observed patterns of hydrologic recessions, which allowed us to decipher the link between the spatial pattern of processes at the small scale and that at larger scales. The results from this thesis demonstrate the usefulness of the "multiscale-analysis" approach and suggest that both the organization and randomness of process variability at the small scale should be considered for the spatial aggregation of the hydrologic response.

TABLE OF CONTENTS

LIST OF TABLES ix

LIST OF FIGURES x

CHAPTER 1 INTRODUCTION 1

1.1 PROBLEM STATEMENT 1
1.2 APPROACH 2
1.3 STRUCTURAL OVERVIEW 2
1.4 LITERATURE REVIEW 3
1.4.1 Distributed hydrologic modeling 4
1.4.2 Hydrologic processes at the hillslope scale 7
1.4.3 Hydrologic processes at the catchment scale 8
1.4.4 Connecting and aggregating hillslope to catchment processes 9
1.4.5 Summary of literature review 12

CHAPTER 2 ORGANIZED VARIABILITY OF SURFACE RUNOFF PROCESSES ACROSS NEIGHBORING HILLSLOPES IN IOWA 14

2.1 INTRODUCTION 14
2.2 STUDY SITE AND DATA 16
2.2.1 Site description 16
2.2.2 Surface runoff and rainfall measurements 17
2.2.3 Soil moisture data 18
2.3 METHOD 18
2.4 RESULTS 21
2.4.1 General rainfall and runoff characteristics 21
2.4.2 Shape similarity and magnitude variability: analysis of a single event 21
2.4.3 Shape similarity and magnitude variability: analysis of multiple events 22
2.4.4 Controls of the spatial variation of shape similarity and scaling factor 23
2.4.5 Temporal variation of scaling factor and its controls 25
2.5 DISCUSSION 27
2.5.1 Organized variability of small-scale hydrologic responses 27
2.5.2 Controls on the organized variability of small-scale hydrologic responses 28
2.5.3 Implications for distributed hydrologic modeling 30
2.6 CONCLUSION 31

CHAPTER 3 RECESSION DATA ANALYSIS: SENSITIVITY OF PARAMETER ESTIMATION TO THE CALCULATION PROCEDURE 40

3.1 INTRODUCTION 40
3.2 DATA AND METHOD 44
3.2.1 Data and study area 45
3.2.2 Selection of complete recession curves and recession segments 46
3.2.3 Parameter estimation methods 47
3.3 RESULTS 51

3.3.1 Variability due to starting point....51
3.3.2 Variability due to recession length....52
3.3.3 Variability due to parameter estimation methods....53
3.3.4 Effect of uncertainties in streamflow....55
3.4 Discussion....57
3.5 Conclusion....59

CHAPTER 4 DISSECTING RECESSION CURVES....71

4.1 Introduction....71
4.2 Data....73
4.3 Method....74
4.3.1 Selection of recession segments....74
4.3.2 Method to calculate event-based recession exponent....75
4.4 Results of data analysis....76
4.5 A theoretical explanation....78
4.6 Discussion....82
4.6.1 Ideal vs. real evolution paths of recession exponent....82
4.6.2 Application: dissecting recession curves....84
4.6.3 Application: within- and between- basin comparisons....86
4.6.4 Application: importance of groundwater contribution to streamflow....87
4.6.5 Limitations....88
4.7 Conclusions....89

CHAPTER 5 RECESSION ANALYSIS ACROSS SCALES: IMPORTANCE OF ORGANIZED-RANDOM SPATIAL VARIABILITY FOR AGGREGATING HYDROLOGIC RESPONSES....99

5.1 Introduction....99
5.2 Recession data analysis for the 2012-2013 drought....101
5.2.1 Site description....101
5.2.2 Recession analysis using individual events....102
5.2.3 Quantifying late-time recession characteristics....103
5.3 Results of data analysis....106
5.4 Diagnostic drainage experiment....107
5.4.1 Conceptual design of the simulation study....108
5.4.2 Structure of the distributed drainage model....109
5.4.3 Parameterization of the distributed drainage model....110
5.4.4 Steady-state drainage experiment for the Cedar River basin....111
5.4.5 Analyses of the simulated recession curves....111
5.5 Discussion....113
5.5.1 On the Linearity and homogeneity of recession processes....114
5.5.2 A random or organized representation of watersheds?....115
5.6 Conclusion....117

CHAPTER 6 SUMMARY AND FUTURE RESEARCH....124

6.1 Conclusions....124
6.2 Limitations....125
6.3 Future research....126

APPENDIX A CONTROLS OF THE SCALING FACTOR....129

APPENDIX B SENSITIVITY OF RECESSION ANALYSIS TO THE CHOICE OF ΔT 135

APPENDIX C ANALYSIS OF LATE-TIME RECESSIONS DURING SEVERE DROUGHT EVENTS 141

REFERENCES 151

LIST OF TABLES

Table 2-1. Hillslope characteristics..... 32

Table 3-1. Comparison of the estimates of recession parameters *A* and *B* at Clear Creek near Coralville, Iowa (USGS 454300) calculated using the CTS, VTS and the NDF methods. All recession segments have a starting point of 2 days and a length of 7 days.....60

Table 3-2. Comparison of the estimates of *B* at 25 gauges calculated with the CTS, VTS and NDF methods. All gauges are located within the HUC05 of the United States, and we use only the last six digits of their complete USGS gauge ID. NRec is the number of recession events analyzed; Median of *B* are the median values of *B* for multiple events at a gauge; IQR of *B* is the interquartile range of *B* estimates for multiple events at a gauge; Modeling error (%) is the median of the relative differences between the volumes of modeled and observed recession flows; *p* value is for the paired t-test; ΔB is the median value of absolute difference of *B* estimates given by two methods.....61

Table 4-1. Description of the USGS stream gauges investigated in this study 91

Table 5-2. Parameterization schemes of the recession timescales *K* over hillslopes..... 119

LIST OF FIGURES

Figure 1-1. Approach adopted to pursue the research goal of this thesis.. 13

Figure 2-1. Location and experiment design of the 12 hillslopes at Basswood, Orbweaver, and Interim.....33

Figure 2-2. Time series of 5-minute accumulation of runoff at hillslope Basswood #6 and 5-minute accumulation of rainfall at the NOAA weather station during the growing season over the period from 2008 to 2011.....34

Figure 2-3. Lagged regression analysis of hydrographs between paired hillslopes (hillslope B6 as the benchmark). Left to right are the hydrographs plotted in the same vertical scale, the cross correlation of hydrographs, the lagged regression of hydrographs, and the hydrographs plotted with different vertical scales for each paired hillslopes. Top to bottom are comparisons for different pairs of hillslopes (e.g., B1 VS. B6). The solid gray lines represent the hydrographs at B6, and the dashed black lines represent hydrographs at other hillslopes (y-axis unit: mm/5min). Lagged regression was done at the time lag that cross-correlation achieves maximum. In the last column, the vertical scaling ad horizontal shift was determined according to the associated lagged regression analysis. 35

Figure 2-4. Event-based comparison of shape similarity and scaling factor at the twelve experimental hillslopes in Iowa. 36

Figure 2-5. Annual distribution of single-event shape similarity (i.e., maximum cross-correlation ρ_{max}), and scaling factor (i.e., lagged regression slope k). Values of ρ_{max} and k were calculated between each hillslope and B6 for 72 events observed from 2008 to 2011. 37

Figure 2-6. Scatterplots of scaling factor k versus width of prairie strip width at footslope (a), maximum slope length (b), slope (c), and size (d) of the hillslopes.....38

Figure 2-7. Comparison of the model versus data estimates of scaling factor *k*. The 1:1 line is superimposed to the scatter plot. Independent variables *MHRA* and *VSMC* are the maximum hourly rain accumulation, and the volumetric soil moisture content averaged over the top 50cm of soil, respectively. Both *MHRA* and *VSMC* are observed at the same NOAA weather station about 1.1~3.3km away. 39

Figure 3-1. Location of the USGS stream gauges used in this study. 63

Figure 3-2. The schematic of selecting recession segments from a complete recession curve by fixing the length while varying the starting points (upper panels) and by fixing the starting point while varying the lengths (lower panels). The starting point of a recession segment is measured from the hydrograph peak that is marked by the red dashed-line. The blue curve is the recession segment used to estimate the recession parameters *A* and *B*. This is a 27-day long complete recession curve observed at Clear Creek near Coralville, Iowa (USGS 454300) and spanned from June 24, 2007 until July 19, 2007. 64

Figure 3-3. Variability of *B* estimates due to the change in starting points of recession segments (a single event). The same example recession event as in Figure 3-2 is used here. The text at the top right corner is the length of the recession segments used to estimate *B*. At each fixed recession length, we first extracted recession segments using different starting points (0~7 days after hydrograph peak) and then estimated the values of *B* using the NDF method. The range of *B* values (defined as $\Delta B = B_{max} - B_{min}$) due to the change in starting points is about 1.5 for this example event. 65

Figure 3-4. Variability of *B* estimates due to the change in starting points of recession segments (multiple events). For each USGS gauge (see gauge ID at the top right corner), we repeated the analysis in Figure 3-3 to obtain ΔB values for all of the recession events. Each red dot is the median value and each gray line segment represents the range of ΔB at a fixed recession length. The median values of ΔB for all gauges are around 1.0. 66

Figure 3-5. Variability of *B* estimates due to the change in lengths of recession segments (a single event). The same example recession event as in Figure 3-2 is used here. The text at the top right corner is the starting point (number of days after hydrograph peak) of the recession segments used to estimate *B*. At each fixed starting point, we first extracted recession segments using different lengths (4~12 days) and then estimated the values of *B* using the NDF method. The range of *B* values (defined as $\Delta B = B_{max} - B_{min}$) due to the change in recession lengths is about 0.5 for this example event. 67

Figure 3-6. Variability of *B* estimates due to the change in lengths of recession segments (multiple events). For each USGS gauge (see gauge ID at the top right corner), we repeated the analysis in Figure 3-5 to obtain ΔB values for all of the recession events. Each red dot is the median value and each gray line segment represents the range of ΔB at a fixed starting point. The median values of ΔB for all gauges are around 0.5. 68

Figure 3-7. Variability of parameter estimates due to method choices. The same example recession event as in Figure 3-2 is used here. We extracted the recession segment from the complete recession curve using a starting point of 2 days and a length of 7 days. The parameters for the selected segment were estimated using the CTS ((a) and (c)), VTS ((b) and (d)) and NDF ((e)) methods. In (b), (d), and (e), the open circles are the measured streamflow values, and the lines are the modeled recession segments using the estimated parameters. For the VTS method, the value $C = 0.001$ was used to reduce the impact of the noise in streamflow data on the estimation of recession parameters. The modeling error was calculated as the relative difference between the volumes of modeled and observed recession flows. 69

Figure 3-8. Robustness of the VTS (blue) and the NDF (red) methods to the noise in streamflow data. The true value of *B* is 2. Filled circles represent the mean values of *B*. Error bars show the standard deviation of *B* estimates at each magnitude of error. The mean and standard deviation were obtained based on the results of 1000 simulations. The length of the recession segment used is 7 days (168 hourly flow values). The uncorrelated noise are generated from a normal distribution $N(0, \sigma)$. The correlated noise are generated from the AR(1) model $E(t) = \rho E(t-1) + \varepsilon(t)$,

where ρ is the correlation coefficient (ρ = 0.6 for this figure), $\varepsilon(t)$ is an i.i.d. random variable with mean 0 and standard deviation $\sqrt{1-\rho^2}\sigma$, and σ is the magnitude of data noise in percentage.....70

Figure 4-1. Schematic of the evolution path of an individual recession event. The lag represents the starting point of a recession segment, and it is measured from the hydrograph peak marked by the red dashed-line. The blue curve is the recession segment used to estimate the recession exponent *B*. In the lower panel of Figure 4-2, each circle represents the *B* value that is calculated using a specific starting point (horizontal axis) and recession length (the text at the upper right corner.). For example, the first circle in the lower panel represents the value of exponent *B* calculated using the selected recession segment starting from the hydrograph peak with a recession length of 5 days. 92

Figure 4-2. Flowchart of constructing the evolution path of the recession exponent *B* for an individual recession event (a) and a basin (b).....93

Figure 4-3. Evolution paths of recession exponent *B* for individual recession events: June 24, 2007 (a), August 25, 2007 (b), July 25, 2009 (c), and August 28, 2009 (d) at USGS454300, Clear Creek near Coralville, area = 254.0 km^2. Each panel in this figure is similar to the lower panel in Figure 4-2. 94

Figure 4-4. The characteristic evolution path of recession exponent *B* at USGS454300, Clear Creek near Coralville, area = 254.0 km^2. Each gray dot is the exponent *B* calculated from a recession segment with a certain starting point and recession length. Gray dots along the same vertical line represent *B* values calculated using different recession segments that are selected with the same starting point and recession length. The red dots are the medians of the *B* values along the same vertical line. The text at the upper right corner is the length of the recession segment used to estimate exponent *B*. For example, the first red dot in the first panel represents the median value of exponent *B* calculated for all of the selected recession segments starting from the hydrograph peak with a recession length of 1 day. 95

Figure 4-5. Characteristic evolution paths of recession exponent *B* for USGS streamflow gauges in the Iowa and Cedar River basins, Iowa. Two out of 27 gauges are not shown here because of the small numbers of recession events available. The explanation of the plot is the same as that for Figure 4-5. For simplicity and clarity, we do not plot the gray dots as in Figure 4-5. 96

Figure 4-6. Dissecting hydrograph recessions according to the evolution path of *B*. Upper panel: evolution of the recession exponent *B*; Middle panel: contributors to streamflow for different periods of recession; Bottom panel: periods for soil water and groundwater recession analysis. The periods are identified according to the evolution path of *B*. 97

Figure 4-7. Characteristic evolution paths of recession exponent *B* for nested USGS streamflow gauges in the Iowa River basin, Iowa during the lengthy and widespread drought in 2012. The recession lengths used were 90 days for each basin. The horizontal and vertical axes are the same as that for the plot at USGS gauge 451210. 98

Figure 5-1. Performance and parameters of the $dQ/dt = -AQ^B$ model plotted as a function of the drainage area top: modeling error of reproducing the observed recession curves; middle: parameter *B*; and bottom: parameter *A*. The horizontal gray lines represent the corresponding median values. The result is obtained by analyzing the observed recession curves (late-time) in the Iowa and Cedar River basins during the 2012-2013 drought. The starting point used is 12 days after hydrograph peak and the recession length is 120 days. 120

Figure 5-2. Comparison between the observed (gray) and modeled (red) recession curves. Constant values of $A = 0.029$ and $B = 1$are used for modeling recession curves at all gauges. 121

Figure 5-3. Structure of the Cedar River basin. 122

Figure 5-4. Parameters and performance of the $dQ/dt = -AQ^B$ model versus drainage area. In the vertical direction, top: parameter *A*; middle: parameter *B*; and bottom: relative error of reproducing the simulated recession curves. In the horizontal direction, left: the organized scenario; middle: the random scenario; right: the organized-random scenario. The solid gray lines represent the corresponding median values. This result is obtained by analyzing simulated recession curves (late-time) for the Cedar River basin. The starting point used is 12 days after hydrograph peak and the recession length is 120 days. 123

Figure A-1. Scatterplots of scaling factor *k* versus width of prairie strip widths at footslope (a), maximum slope lengths (b), slopes (c), and sizes (d) of the hillslopes for the event on May 25 of 2008. 130

Figure A-2. The same as Figure A-1but for the event on June 12 of 2009. 131

Figure A-3. The same as Figure A-1but for the event on June 20 of 2011. 132

Figure A-4. Relationship between the scaling factor and the total amount of rainfall of each storm event. 133

Figure A-5. Relationship between the scaling factor and the peak flow of each storm event. 134

Figure B-1. Comparison of *A* and *B* estimated using three methods and streamflow data with three temporal resolutions. This 27-day long recession segment was observed at the USGS gauge at Clear Creek near Coralville (USGS05454300) with an observational interval of 15 minutes. We extracted the recession segment from the complete recession curve using a starting point of 2 days and a length of 7 days. We aggregated the 15-minute streamflow data to hourly and daily data by taking the mean values. The open circles are the observed streamflow values, and the lines are the modeled recession segments using the estimated parameters. For the variable time step method, the value $C = 0.001$ was used to reduce the impact of the noise in streamflow data on the estimation of recession parameters. The modeling error was calculated as the relative difference between the volumes of modeled and observed recession flows. 139

Figure B-2. Estimating the recession parameters using the CTS and the VTS methods in Excel. The same hourly data as that in the middle panel of Figure B-1 is used here. This figure is used to verify the results given by our code. 140

Figure C-1. Performance and parameters of the $dQ/dt = -AQ^B$ model plotted as a function of the drainage area top: modeling error of reproducing the observed recession curves; middle: parameter *B*; and bottom: parameter *A*. The horizontal gray lines represent the corresponding median values. The result is obtained by analyzing the observed recession curves (late-time) in the Iowa and Cedar River basins during the 2012-2013 drought. The starting point used is 10 days after hydrograph peak and the recession length is 120 days. 144

Figure C-2. Similar to Figure C-1 but the starting point used is 20 days after hydrograph peak and the recession length is 120 days. 145

Figure C-3. Similar to Figure c-1 but the starting point used is 10 days after hydrograph peak and the recession length is 90 days. 146

Figure C-4. Performance and parameters of the $dQ/dt = -AQ^B$ model plotted as a function of the drainage area top: modeling error of reproducing the observed recession curves; and bottom: recession timescale ($1/A$). The horizontal gray lines represent the corresponding median values. The result is obtained by analyzing the observed recession curves (late-time) in the Iowa and Cedar River basins during the 1988 drought. The starting point used is 5 days after hydrograph peak and the recession length is 30 days.....147

Figure C-5. Similar to Figure C-4 but the starting point used is 5 days after hydrograph peak and the recession length is 45 days. 148

Figure C-6. Comparison between the observed (gray) and modeled (red) recession curves during the 1988 drought. Constant values of $A = 0.028$ (recession timescale of 36 days) and $B = 1$ are used for modeling recession curves at all gauges.....149

Figure C-7. Recession timescales of late-time drainage processes plotted as a function of the drainage area for a) the 1988 drought; and b) the 2012 drought. The horizontal gray lines represent the corresponding median values. The result is obtained by analyzing the observed recession curves (late-time) in the Iowa and Cedar River basins. 150

CHAPTER 1
INTRODUCTION

1.1 Problem statement

Integrated catchment management aims to secure the water supply for human beings and ecosystems and to manage the flood and drought risks under the changing climate and environment (e.g., Sivapalan et al., 2003; Beven, 2011; Blöschl et al., 2013). The decision-making process is constrained by our abilities to collect the required information about hydrologic systems at various spatiotemporal scales. Hydrologic modeling everywhere has been expected to help fill this information gap by allowing us to extrapolate our sparse and historical hydrologic variables in space and time. However, hydrologic processes occur at a wide range of scales in space and time (e.g., Klemeš, 1983; Blöschl and Sivapalan, 1995), and data about hydrologic processes are often collected at scales much larger or smaller than the scale of interest in hydrologic modeling. Therefore, hydrologic modeling often involves either upscaling or downscaling, i.e., transferring the information from the small to the large scale or vice versa.

Hydrologic modeling across scales, often using distributed models, has been acknowledged to be challenging due to the lack of effective approaches to represent and aggregate the spatial variability of small-scale hydrologic processes (e.g., Wood et al., 1988; Seyfried and Wilcox, 1995; Woods, 2006). Addressing this issue by examining detailed information with large spatiotemporal coverage is infeasible due to the limitations of hydrological measurement techniques; however, data collected at discrete spatial scales are available. Consequently, the main objective of this thesis is to explore how useful insights for aggregating hydrologic processes can be obtained through examining hydrologic processes over a range of spatial scales. The two primary research

questions that I will address in this study through the use of a "multiscale-analysis" approach are:

1) Can we identify some patterns of hydrologic processes at multiple spatial scales?
2) Can we obtain useful insight for the aggregation of hydrologic processes by investigating the connection between hydrologic processes at various spatial scales?

1.2 Approach

I address these research questions by 1) analyzing hydrologic systems at multiple spatial scales to identify patterns of hydrologic processes at various scales and 2) conducting diagnostic simulations to understand how these patterns are linked (Figure 1-1). Two hydrologic signatures, including the surface runoff responses and the recession processes, are used for data analyses. I first identified patterns of hydrologic processes by 1) comparing the surface runoff hydrographs (area-averaged discharges) observed at neighboring hillslopes in agricultural land in Iowa; 2) analyzing recession curves observed in the nested Iowa and Cedar River basins over the period of 1995-2010; and 3) examining the long recession curves in the nested Iowa and Cedar River basins during the 1988 and 2012 droughts. I then developed a distributed model as a diagnostic tool and used it to explore the link between the spatial pattern of processes at the small scale and that found at larger scales. In order to avoid other complex processes (e.g., partitioning of rainfall), I simplified this investigation by focusing on recession processes rather than on the entire response. The diagnostic simulations were run for the Cedar River basins.

1.3 Structural overview

In this thesis, the research questions have been addressed in the manuscripts of four studies that have been prepared for submission to research journals. Chapter 2

compares the surface runoff hydrographs from 12 hillslopes with spatial proximity in agricultural land in Iowa over 72 runoff events. The goal was to explore how the variability of surface runoff processes from areas with spatial proximity is organized in space. Chapter 3 assesses the sensitivity of the analyses of individual recession events to the selection of recession segments and parameter estimation methods. On the basis of Chapter 3, Chapter 4 analyzes recession curves observed in the nested Iowa and Cedar River basins over the period of 1995-2010, using consistent methods to identify the patterns in recession processes. The implications of the identified evolution patterns of the recession exponent for hydrologic modeling are discussed. Chapter 5 examines the effects of the spatial pattern of the drainage processes at the hillslope scale on the recession behaviors at the catchment scale. First, the characteristics of late-time recession processes in the Iowa and Cedar River basins during the 1988 and 2012 severe droughts were identified using a consistent method. Then, a distributed drainage model was developed in order to reproduce the observed catchment-scale recession characteristics. Lastly, Chapter 6 summarizes this research and discusses its limitations and implications for future research. Overall, the results from this thesis suggest that 1) analyzing hydrologic systems at multiple spatial scales can provide useful insight into the spatial aggregation of hydrologic processes and 2) both the organization and randomness of the process variability at the small scale should be considered for aggregating hydrologic responses.

1.4 LITERATURE REVIEW

The literature review first summarizes previous work related to the challenges of distributed hydrologic modeling, i.e., the representation and aggregation of the variability of hydrologic processes at the small scales, then presents current knowledge about the characteristics of hydrologic processes at the hillslope scale and at the catchment scale, and finally summarizes the attempts to connect hydrologic processes across spatial scales.

1.4.1 Distributed hydrologic modeling

Hydrologic modeling across scales can be achieved in two ways: using scaling relationships and using distributed hydrologic models. An example of the first approach entails designing hydrologic/hydraulic structures using the power-law relationship between peak discharge and basin drainage area (and maybe also some other variables). This thesis focuses on the second approach. Distributed hydrologic modeling typically consists of two steps: distributing and aggregating. Distributing refers to decomposing a catchment into elements and applying some governing equations to describe the hydrologic processes at the elementary scale. Aggregating denotes collecting the responses from the elements to obtain the responses at larger scales.

Distributed models make spatially distributed predictions, and their state variables and parameters represent averages over a local element area. This type of model decomposes a catchment into a large number of elements and solves for the state variables for each element. Conversely, lumped hydrologic models treat a basin as a single unit, and the spatial variability of their state variables and parameters are assumed to be unimportant and are therefore ignored. A lumped hydrologic model becomes more distributed by splitting a basin into sub-units to account for the spatial variability. Inversely, a distributed hydrologic model becomes lumped by coarsening the size of the elements. There is no clear boundary between distributed and lumped models.

Distributed hydrologic modeling is preferred in hydrologic applications, though lumped models have relatively simpler structures and fewer parameters and furthermore require fewer inputs. Distributed models require inputs and parameters to be specified for each element. These requirements lead to the difficulties in preparing model inputs and calibrating model parameters. The great amount of computation needed to solve for the multiple state variables at many time steps is another obstacle of distributed modeling. These burdens have been greatly reduced due to the rapid development of measuring techniques (e.g., Robinson et al., 2008; Entekhabi et al., 2010; Berne and Krajewski,

2013), the efforts dedicated to improving or avoiding the calibration process (e.g., Kirchner, 2006; Beven, 2012; Juston et al., 2013), and the advances in computer power (Small et al., 2013). Despite more progress is needed, distributed hydrologic modeling has been gaining attention due to the demand for hydrologic prediction everywhere, its ability to account for small-scale variability, its potential to couple other types of modeling (e.g., transport of sediments and contaminants), and its potential to assess the impacts of land use (e.g., Foley et al., 2005) and climate (e.g., Milly et al., 2008) change.

The spatial variability in distributed hydrologic models is commonly resolved to the levels of grids or representative elementary areas (REA). For the grid-based distributed models, different cell sizes can be used, and they generalize the spatial variability to different degrees. This artifact leads to the grid size dependency of the representation of the drainage features (e.g., Garbrecht and Martz, 1994; Zhang and Montgomery, 1994) and ultimately to the grid size dependency of the results of hydrologic modeling (e.g., Wolock and Price, 1994; Kuo et al., 1999). The REA (Wood et al., 1988) concept proposes that there is a threshold scale above which the average hydrologic response occurs, indicating that the within-unit spatial variability is not important and can be ignored at a certain scale. This hypothesis has the potential to reduce the complexity of hydrologic models and has been tested by numeric simulations (e.g., Blöschl et al., 1995; Fan and Bras, 1995) and filed studies (e.g., Woods et al., 1995; Wolock et al., 1997; Shaman et al., 2004; Uchida et al., 2005a; Asano and Uchida, 2010). However, the threshold values varied from 1 to 8 km^2, and they depend on factors such as topography, storm duration, spatial variability of rainfall, and antecedent wetness (Blöschl et al., 1995). Furthermore, at the scale of 1 to 8 km^2, a significant variability of hydrologic processes (e.g., Loague and Gander, 1990; Faures et al., 1995; Grayson and Western, 1998; Krajewski et al., 2003) has been identified. Overall, the optimal decomposition of watersheds into grids or REAs in distributed modeling needs further investigation.

To avoid the difficulty of optimizing the size of elementary areas, in this thesis, we adopt the geomorphologic decomposition of a basin into hillslope-channel links. The hillslopes and channel links are used as sub-units in our distributed hydrologic model. Hillslopes are the smallest natural unit for the ecologic processes and for the cycling of water, sediment, and chemicals. They can be defined easily from topographic information, and they integrate every component of the hydrologic cycle (e.g., Band, 1986; Mantilla and Gupta, 2005). The well-defined shapes make them easier to monitor and study. In this dissertation, we adopt this hillslope-channel link based decomposition of a basin. In our numerical simulations, the channel links and hillslopes are treated as the natural control volume, which is similar to the representative elementary watershed concept (e.g., Reggiani et al., 1998; Reggiani et al., 1999; Reggiani et al., 2000; Reggiani and Rientjes, 2005).

However, regardless of how a catchment is partitioned, the representation of between-element variability in distributed hydrologic models is unavoidable, and simple yet effective approaches for this purpose remain a challenging and active research area. The representation of between-element variability has been performed by simply using statistical distributions, i.e., the variability is assumed to be randomly distributed or variable in a certain sense (e.g., Dagan and Bresler, 1983; Moore, 1985; Mantoglou and Gelhar, 1987; Bierkens et al., 2000; Harman et al., 2009), or by using some deterministic functions, i.e., the variability is a function of the state variable of hydrologic systems and/or characteristics of catchments (e.g., Beven and Kirkby, 1979; Wood et al., 1990; Moore and Grayson, 1991; McGlynn et al., 2003; Jencso et al., 2009). Both types of watershed representations have shown some success, which raises the question: which one should be chosen?

Overall, the lack of effective ways to represent small-scale variability and the limited knowledge about how extensively we should resolve it are major obstacles with respect to distributed hydrologic modeling. Identifying emergent patterns of hydrologic

processes at multiple spatial scales and understanding the connections between them may provide useful insight into effectively addressing these issues. To this end, we will review the current understanding of hydrologic processes at various spatial scales in the following sections.

1.4.2 Hydrologic processes at the hillslope scale

Hydrologic processes at the small scales are investigated through comprehensive field experiments and through detailed numeric modeling. Hydrologic investigations at the small scales involving single or multiple processes are conducted in a wide variety of environments that are subject to diverse climates, topography, soils, vegetation, and land use manipulated by human activities. Diverse results, e.g., different aspects of small-scale hydrologic process, are seen and contribute to the difficulties of hydrologic understanding and modeling.

Analyses of the intensive collected data reveal the heterogeneous and complex nature of the hydrologic processes at the hillslope scale. Extensive monitoring and investigation of small sub-systems of a larger hydrologic system, i.e., experimental hillslopes, plots, or soil columns, is a commonly used approach to deepening our understanding of hydrologic processes. Such studies generally reveal great complexities and variability in the hydrologic process. For example, there are several classical perceptual runoff generation mechanisms that include the infiltration excess overland flow (Horton, 1933), the partial area infiltration excess overland flow (Betson, 1964), the saturation excess overland flow (Dunne and Black, 1970), the subsurface stormflow (Hewlett and Hibbert, 1967), and the perched subsurface stormflow (Weyman, 1970). It is possible that infiltration excess, saturation excess, or purely subsurface responses may all occur in the same catchment at different times or different places due to different land uses, antecedent conditions, soil properties, or rainfall intensities and amounts. Furthermore, the rainfall-runoff relationship at the hillslope scale tends to be highly

nonlinear and dynamic (e.g., Minshall, 1960; Tromp-van Meerveld and McDonnell, 2006b; Zehe and Sivapalan, 2009) and is very sensitive to the spatial variability of rainfall (e.g., Ogden and Julien, 1993; Faurès et al., 1995) and other factors. Accordingly, complex numerical models with large number of parameters are required to capture the dominant hydrologic processes at the hillslope scale.

Interestingly, the hydrologic processes at the hillslope scale also show some spatial organization due to the spatial patterns of the landscape (e.g., McGlynn et al., 2003; McGlynn et al., 2004; Jencso et al., 2009), terrain (e.g., Western et al., 1999; McGuire et al., 2005), vegetation (e.g., Bautista et al., 2007), and soil properties (e.g., Tromp-van Meerveld and McDonnell, 2006a). For example, the hydrologic connectivity to streams tends to be longer for hillslopes near the streams than for hillslopes in the uplands (e.g., Jencso et al., 2010). The importance of such a spatial pattern (structures) in advancing hydrologic sciences has been recognized (e.g., Schulz et al., 2006).

In summary, there is consensus that hydrologic responses at the hillslope scale are highly variable and complex yet show some degree of organization due to the spatial patterns of geology, soil, vegetation, rainfall, and soil moisture.

1.4.3 Hydrologic processes at the catchment scale

Hydrologic processes at the catchment scale (especially at large scales) are often sparsely monitored at the point scale. On the one hand, comprehensive field campaigns that cover large areas require substantial budgets, while on the other hand, some hydrologic variables, such as rainfall and evapotranspiration, are difficult to accurately measure at the areal scale. Therefore, hydrologic processes at the catchment scale are primarily investigated through data analyses and numeric modeling that use the limited data available.

Hydrologic responses at the catchment scale are relatively "simpler," though hydrologic processes at the hillslope scale are heterogeneous and complex. For example,

hydrologic responses at larger catchment scales tend to be more linear (e.g., Wang et al., 1981; Beven et al., 1988), less variable (e.g., Woods et al., 1995; Wolock et al., 1997; Asano and Uchida, 2010), and less sensitive to the spatial variability of rainfall (e.g., Mandapaka et al., 2009). Also, it is commonly accepted that simple models, such as the unit hydrograph (e.g., Nash, 1957; Dooge, 1973) and the storage-discharge model (e.g., Klemeš, 1983; Kirchner, 2009), can reasonably reproduce some of the key aspects of the catchment-scale hydrologic processes under some circumstances. Another example entails the modeling of groundwater. The groundwater depletion at larger catchment scales can be represented by a simple linear model (e.g., Zecharias and Brutsaert, 1988; Fenicia et al., 2006; Brutsaert, 2008), while it needs to be described using the more complex, nonlinear Darcy's equation at the soil-column scale.

1.4.4 Connecting and aggregating hillslope to catchment processes

Demands from both hydrologic sciences and practices are the major driving forces behind synthesizing hydrologic knowledge at the hillslope and the catchment scales. From the perspective of hydrologic practices, the hydrologic prediction is often required at the catchment scale, and we consequently have to extrapolate our small-scale information to the various scales of interest. From the standpoint of the development of hydrologic science, understanding the linkage between the hydrologic processes at the hillslope and the catchment scales can potentially reveal the universal and fundamental governing laws of hydrologic systems (e.g., Dooge, 1986; Council, 1991; Eagleson, 1994; Sivapalan et al., 2003; Wagener et al., 2010; Beven, 2012; Council, 2012; Blöschl et al., 2013).

For distributed hydrologic modeling, directly linking the hydrologic responses at the hillslope scale to that at the catchment scale, i.e., applying hydrologic response mechanisms (represented by mathematic equations) to each elementary area and collecting the elementary responses to obtain the watershed response, is hindered by

several factors. Firstly, because the number of parameters and inputs increases linearly with the number of hillslopes, simply connecting the similar detailed hillslopes models through channel routing will not reduce the complexity of the model at the catchment scale. This large number of parameters in the catchment model may also lead to the calibration dilemma (e.g., Beven and Binley, 1992; Duan et al., 1992; Beven and Freer, 2001b; Kirchner, 2006). Secondly, it is likely that several hillslope models are needed to represent the multiple runoff mechanisms within a catchment across space and time. However, some of the details of small-scale processes variability may not be important for the hydrologic response at larger scales.

Field experiments and numeric simulations highlight the connection between hydrologic processes at both smaller and larger scales. For example, previous studies demonstrate that spatial averaging plays an important role in hydrologic aggregation. Analysis of experimental data showed that the variation of area-averaged streamflow magnitude (e.g., Woods et al., 1995; Shaman et al., 2004; Lyon et al., 2012) and stream chemistry (e.g., Wolock et al., 1997; Shaman et al., 2004; Asano and Uchida, 2010) tend to decrease with the space scale. This observation is supported by numeric simulations (e.g., Blöschl et al., 1995; Fan and Bras, 1995). These results indicate that as the spatial scale increases, the catchment-scale hydrologic behavior converges to the representative path of the geomorphologically-determined distribution of hillslope-scale hydrologic processes (e.g., Savenije, 2001). Spatial averaging is an inherent property for distributed models.

Another interesting example of hydrologic modeling across scales, i.e., the application of the TOPMODEL (e.g., Beven and Kirkby, 1979; Beven, 1997), implies the importance of spatial organization of small-scale hydrologic processes. This model has been widely used around the world because it is simple, has a low demand for inputs, and performs acceptably well in some cases. The simplicity originates by incorporating into

the model a topographic index as a quantitative measure of grid-scale spatial pattern (e.g., Beven and Freer, 2001a).

Importantly, the spatial averaging is conducted within the framework of the self-organization of the river networks (e.g., Rodr ́guez-Iturbe and Vald ́s, 1979; Gupta et al., 1980; Rodriguez-Iturbe and Rinaldo, 1997). The self-organized nature of the river network has been fundamental to explaining the observed spatial scaling of peak discharge (e.g., Gupta and Dawdy, 1995; Ogden and Dawdy, 2003; Gupta et al., 2010) and the physical origins of the unit hydrograph concept (e.g., Rodr ́guez-Iturbe et al., 1979; Rodr ́guez-Iturbe and Vald ́s, 1979) and recession processes (e.g., Biswal and Marani, 2010; Mutzner et al., 2013; Biswal and Marani, 2014). These successful applications suggest the importance of incorporating the self-similarity of the river network into hydrologic models.

Simple means of aggregating hydrologic processes in space may be discovered by searching for concepts that can be easily connected across scales. However, we have to find simple indicators to quantify the spatial organization. For example, the spatial correlation function is mathematically sophisticated difficult to incorporate into distributed models. Quantities including, but are not limited to, land use type, topographic indices, soil properties, and Strahler order can be good candidates. The Strahler order, for example, reflects the hierarchical nature of the branching river network, which has been found to impose spatial organizations of bioecologic processes (e.g., Vannote et al., 1980; Gomi et al., 2002; Benda et al., 2004) and the hillslope hydrologic connectivity to the stream (e.g., McGlynn et al., 2003; McGlynn et al., 2004; Jencso et al., 2009).

Overall, the attempts to link hydrologic processes at various spatial scales have advanced our understanding of the spatial aggregation of hydrologic process. However, most of the data analyses-based studies have small spatial scales (less than 10 km^2) and small sample sizes in space due to the limited resources available for data collection.

Until significant advances in the capability of hydrologic measurement occur, directly connecting the processes at the small scale to that at larger scales will remain difficult. For modeling-based studies, consideration of the random yet organized small-scale process variability deserves more investigation.

1.4.5 Summary of literature review

The foregoing review illustrates that understanding the spatial aggregation of hydrologic processes remains challenging. This challenge stems from the facts that 1) hydrologic processes observed at different spatial scales may show different patterns that vary with time and 2) it is difficult to measure and represent the pattern of small-scale process variability. Based on the discipline of thermal dynamics, useful insight may be obtained through examining the patterns of collective hydrologic responses over a range of spatial scales rather than through examining the variability of individual response from each elementary area of a basin. This work follows this notion and aspires to shed light on resolving the challenging issue of aggregating hydrologic processes across scales.

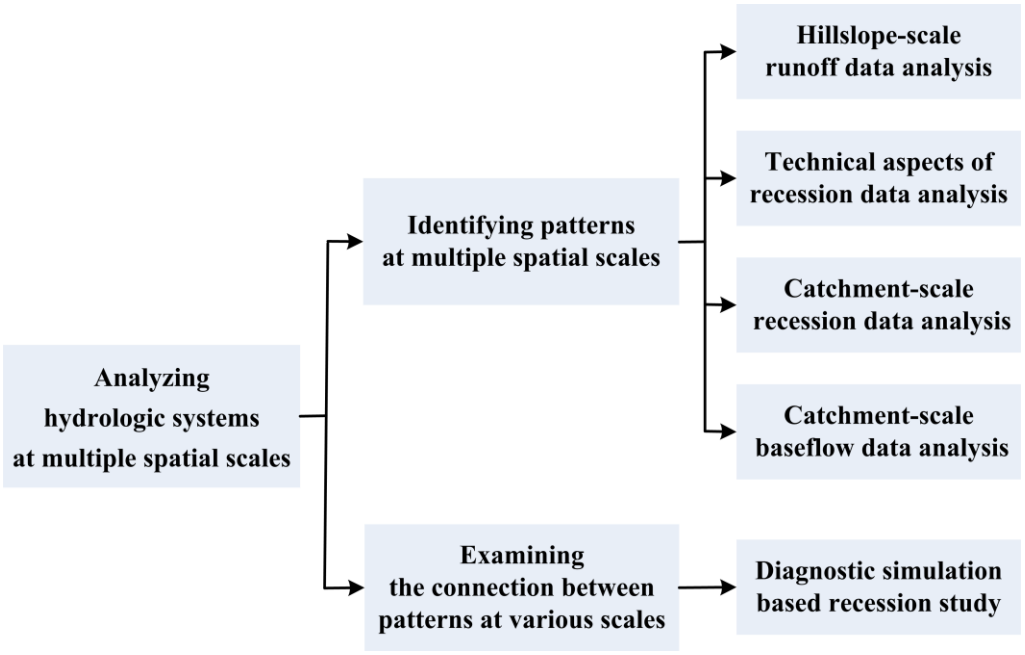

Figure 1-1. Approach adopted to pursue the research goal of this thesis.

CHAPTER 2

ORGANIZED VARIABILITY OF SURFACE RUNOFF PROCESSES ACROSS NEIGHBORING HILLSLOPES IN IOWA

2.1 Introduction

Variability in space and time is fundamental to hydrologic science and practice. Three comparative methods that can be used to study the variability of hydrologic responses are: 1) comparing the hydrologic responses to various atmospheric forcings observed at a fixed experimental watershed, which allows examining the temporal variability of hydrologic responses; 2) comparing the hydrologic responses observed at places with contrasting climates or physiographic conditions, i.e., investigating the space-time variability of hydrologic responses; and 3) comparing the hydrologic responses to similar atmospheric forcings observed at watersheds with spatial proximity, which allows studying the spatial variability of hydrologic responses. It seems that many aspects about the temporal variability of hydrologic responses are better understood, due to the relative ease with which we can measure at high temporal resolution for a long period. For example, by adopting the first method, the nonlinearity of hydrologic responses has been recognized. This widely accepted nonlinearity emphasizes the dynamical property of rainfall-runoff relationship at a site and it rises from the dependence of storm response on antecedent conditions and rainfall inputs (e.g., Minshall, 1960; Grayson et al., 1997; Sivapalan et al., 2002; Zehe and Bloschl, 2004; Tromp-van Meerveld and McDonnell, 2006b; Graham et al., 2010). Many applications of the second method, i.e., comparing the hydrologic responses observed at different places, (e.g., Chapman and Falkenmark, 1989; Whitehead and Robinson, 1993; Jones, 2006) have demonstrated that hydrologic processes at the hillslope scale are rich in complexity and heterogeneity. For example, different runoff generation mechanisms exist (e.g., Sivapalan, 2003; Uchida et al., 2005b;

Scherrer et al., 2007; Kienzler and Naef, 2008a; Kienzler and Naef, 2008b; de Araújo and González Piedra, 2009; Beven, 2012).

However, applying the third method in the field is rare, due to the difficulties of making comprehensive spatial measurements covering area large enough and period long enough to be hydrologically meaningful. One example is that Bachmair examined the effects of vegetation cover on the subsurface flow processes at neighboring hillslopes with similar slope, exposure, curvature, geologic, and pedologic properties but different in vegetation cover (e.g., Bachmair et al., 2012). The third method has the potential to answer the question - What is the relation between the hydrologic responses to similar rainfall but from different locations with geographic vicinity? A good understanding of this issue is particularly helpful for distributed hydrologic modeling for a specific region. Distributed hydrologic models attempt to represent hydrological variability by partitioning watersheds into multiple computational elements. Examples of such computational elements are the representative elementary watershed (REW) (e.g., Hubbert, 1957; Wood et al., 1988; Reggiani et al., 1998), hillslopes (e.g., Band, 1986; Yang et al., 2002; McGlynn and Seibert, 2003; Mantilla and Gupta, 2005), and grids (e.g., Liang et al., 1994; Arnold et al., 1998). However, the challenge still remains in characterizing the spatial variability of hydrologic response between elements (e.g., hillslopes). Applying the third method in the field, which allows exploring the organization (or pattern) of the spatial variability of hillslope hydrologic responses at the event scale (about few hours), is a first step to address this question.

In this study, we investigated the spatial variability of surface runoff processes at the event scale (~few hours), i.e., how runoff processes are related across multiple instrumented hillslopes. We used a unique data set of 5-min runoff records over 12 agricultural experimental hillslopes in central Iowa, USA. These hillslopes are clustered in three blocks and the distances between the clusters are about 2 km. The hillslopes within each cluster locate closely and drain areas ranging from 0.48 to3.19 hectares.

We used the inter-site comparison method. By pairing up the rest 11 hillslopes to the benchmark hillslope (i.e., hillslope B6 with no treatment), we investigated the relationship between the event scale surface runoff processes from these neighboring hillslopes. We concerned about both the similarity and dissimilarity of the hydrologic responses. Our comparison of neighboring hillslopes alleviates the common challenge of the inter-site comparison technique, i.e., its difficulty in differentiating whether the variability in hydrologic responses is caused by different underlying basin response mechanisms or variations in affecting factors including but not limited to rainfall forcings, soil properties, topology, and geology.

We adopted the lagged regression method, which is a well-established approach to describe and model the relationship between two time series and to quantify the association between the rainfall-runoff behaviors of paired hillslopes. In contrast to the commonly used runoff ratio, peak discharge, and total runoff volume based inter-site comparison, the lagged regression technique provides information about relation between the hydrologic responses at paired hillslopes from the perspectives of both magnitude and shape.

In all, the large number and the spatial vicinity of these monitored hillslopes allow us to study the relation between rainfall-runoff processes across hillslopes. We will first evaluate the variability/similarity of the hydrographs of these neighboring hillslopes for individual runoff events. We then investigate how this variability/similarity in hydrologic responses from these hillslopes varies in space and time. Finally, we explore the factors that control the characteristics of the hydrologic variability/similarity between these hillslopes.

2.2 Study site and data

2.2.1 Site description

We use the data sample collected from three clusters of hillslopes designed and maintained by the ecohydrology research group at Iowa State University (Helmers et al., 2012). A total of twelve hillslopes (Basswood (B1~B6), Interim (I1, I2, I3), and Orbweaver (O1, O2, O3)) were selected in the Neal Smith National Wildlife Refuge in central Iowa (Figure 2-1). Their sizes range from 0.48 to3.19 hectares. These hillslopes are distributed in three clusters and are monitored to evaluate the benefits of integrating prairie filter strips (PFS) in row crop agriculture for enhancing water quality. They receive various treatments specified by the amounts and the planting positions of the PFSs (Table 2-1). The PFSs were seeded on 7 July 2007. Starting in spring 2007, a 2-yr, no-till corn–soybean rotation (soybeans in 2007) was grown in areas receiving row crop. The soil properties and agricultural management are similar over these hillslopes. Annual precipitation in the study area is about 900mm, and the majority occurs through May to August. Detailed description about these hillslopes and the experiments can be found in the paper by Helmers and Zhou (2012). In all, the physiographic and climatic characteristics of these hillslopes are similar.

2.2.2 Surface runoff and rainfall measurements

Overland flow at the bottom of each hillslope was measured by an H-flume at 5-minute interval since 2007. These hillslopes are drained by poorly defined ephemeral channels. We did not use the data observed in 2007 to avoid the extensive disturbance due to site equipment malfunction. To eliminate the size effect, we average the flow at the bottom of each hillslope over its drainage area in this study. We use the rainfall data collected at a U.S. Climate Reference Network weather station maintained by the National Oceanic and Atmospheric Administration (NOAA), which is 1.1~3.3 km from the hillslopes. The observational frequency is 5-minute for rainfall from 2008 to 2011. Another nearby Mesonet weather station operated by the National Weather, which is 1.3 to 3.6 km from the hillslopes, collects hourly rainfall data. Our comparison at the hourly

time scale showed that the rainfall data from these two stations are highly correlated with limited differences, indicating relatively similar storm events over this small region. This is consistent with the analysis by Helmers and Zhou (2012).

2.2.3 Soil moisture data

Hourly soil moisture data is also collected from 2010 to 2011at the same NOAA weather station. Soil dielectric permittivity are measured by the Hydra Probe soil water sensors installed in a vertical profile at depths 5 cm, 10 cm, 20 cm, 50 cm, and 100 cm, and are then converted to volumetric soil moisture content using an empirical relationship (Seyfried et al., 2005). We calculated the depth-weighted soil moisture for the top 10, 20, and 50 centimeters layers at the weather station based on the point measurements. Prior to the runoff events investigated in this study, the maximum depth-weighted soil moisture for the top 10, 20, and 50 centimeters layers was 0.50, 0.51, and 0.54 and the minimum was 0.29, 0.33, and 0.37, respectively.

2.3 Method

We use the paired basin technique combined with lagged regression method to quantify the relation between the runoff processes across the neighboring hillslopes in this study. Magnitude, time to peak, and shape (i.e. the overall runoff process,) are important characteristics of a hydrologic response (Ehret and Zehe, 2011). When comparing hydrologic responses from two hillslopes, we focus on the similarity in the overall shapes of hydrographs (hereafter referred to as shape similarity), and the similarity in magnitude of the flow values (hereafter referred to as scaling factor). We chose to use B6 as our benchmark hillslope and paired it with each of the other 11 hillslopes for two reasons. First, B6 is a treatment-free (100% cropland) hillslope. Additionally, we have six side-by-side hillslopes clustered at Basswood, indicating a larger chance of smaller differences in the factors that affect their hydrologic responses. This second fact is advantageous, for example, it makes the event-based comparison

between Basswood hillslopes conditioned on the same rainfall process (at least very similar), which means that for each runoff event, discrepancies in the hydrologic responses over these hillslopes are caused by the differences in their response mechanisms rather than rainfall forcings.

The lagged regression method consists of cross-correlation analysis and simple linear regression. Cross-correlation analysis describes the similarity and alignment in time between two signals, and linear regression gives the scaling of magnitude of two signals. Cross-correlation has been used as a metric to measure the shape similarity between two signals in many fields, including, but not limited to, neuroscience (e.g., Ts'o et al., 1986; Avants et al., 2008), , image processing (e.g., Van Heel, 1987), and it has also been employed by hydrologist to predict time series of streamflow for ungauged basins (e.g., Smakhtin et al., 1997; Hortness, 2006; Zhang and Kroll, 2007; Oudin et al., 2010). Linear regression of streamflow at one site against another has been used to study the relative runoff yield and the slope of a regression line can be used as an indicator of runoff reduction or increase (Jones and Grant, 1996; Beschta et al., 2000). The lagged regression analysis can be mathematically expressed as

$$Q_B(t) = kQ_A(t-\tau) + e_t \qquad (2\text{-}1)$$

where $Q_A(t-\tau)$ is the flow per unit area at time $(t-\tau)$ at site A, $Q_B(t)$ is the flow per unit area at time t at site B, k is the slope of the simple linear model and it can only take positive values, e_t is independent and identically distributed (i.i.d.) random error with zero mean. There is no intercept in equation (2-1) because our analysis of real data showed that the intercept was seldom different from zero at the significance level of 95%. By taking the variance for both sides of equation (2-1) we get

$$\sigma_B^2 = k^2\sigma_A^2 + \sigma_e^2, \qquad (2\text{-}2)$$

where σ_A is the standard deviation of flow at site A, σ_B is the standard deviation of flow at site B, σ_e is the standard deviation of random error. Based on equation (2-1) and (2-2), the cross-correlation $\rho_{AB}(\tau)$ between time series of flow at site A and B at time lag τ is

$$\boldsymbol{\rho_{AB}(\tau)} = \frac{\boldsymbol{Cov[Q_B(t), Q_A(t-\tau)]}}{\sqrt{\boldsymbol{Var[Q_A(t-\tau)] * Var[Q_B(t)]}}} = \frac{\boldsymbol{k\sigma_A^2}}{\sqrt{\boldsymbol{\sigma_A^2 * (k^2\sigma_A^2 + \sigma_e^2)}}} = \frac{\mathbf{1}}{\sqrt{\mathbf{1} + (\frac{\sigma_e}{k\sigma_A})^2}}. \quad (2\text{-}3)$$

For two given hydrographs (thus σ_A and σ_B are determined), equation (2-3) indicates that the maximization of cross-correlation $\rho_{AB}(\tau)$ is achieved by maximizing k and minimizing σ_e. Interestingly, maximizing k and minimizing σ_e can be accomplished simultaneously, according to equation (2-2). Therefore, the maximization of cross-correlation $\rho_{AB}(\tau)$ is equivalent to the maximization of k. The maximum of cross-correlation $\rho_{max} = \max(\rho_{AB}(\tau))$ can be determined based on cross-correlograms.

Base on the derivation above, we quantify the relation between the hydrologic responses from paired hillslopes using two measures. One is the shape similarity (irrespective to the magnitude of runoff volume), which describes the degree of coincidence of two rescaled hydrographs, i.e., the concurrence in the sequence of occurrence of high-, mid-range, and low- flows. It is defined as the maximum of cross-correlation ρ_{max} and takes values from 0 to 1. Another measure is the scaling factor, which represents the relative magnitude of hydrologic response, i.e., relative efficiency of runoff production. It is defined as the slope k of lagged regression analysis and takes positive values. The closer the values of shape similarity ρ_{max} and scaling factor k to unity, the more similar the hydrologic responses from the paired hillslopes are. When applying this lagged regression analysis, we first construct a cross- correlogram to determine the maximum cross-correlation ρ_{max} and the associated time lag τ_{max}. Time lag τ_{max} between two hydrographs is the time shift at which the cross-correlation functional achieves maximum ρ_{max}. We then conduct simple linear regression analysis

at the time lag τ_{max}. Time lag will not be discussed in this paper because we are interested in the overall runoff process and the efficiency of runoff generation.

2.4 Results

We first examine the general rainfall and runoff characteristics of the hillslopes over the study period, then investigate the variation of shape similarity and the scaling factor in space conditioned on time, i.e., the relation between hydrologic responses triggered by similar rainfall forcing but from different hillslopes. Last, we explore the variation of shape similarity and the scaling factor in time conditioned on space, i.e., the relation between hydrologic responses from the same paired-hillslopes but triggered by different storms.

2.4.1 General rainfall and runoff characteristics

The total depths of rainfall during the sampling periods from 2008 to 2011 are 951, 798, 1198, and 703 mm, and the corresponding total depth of runoff at the hillslope B6 are 278, 166, 640, and 213 mm. As the wettest year among the investigated, one half of the number of the runoff events occurred in 2011. Figure 2-2 shows the temporal patterns of rainfall and runoff events at the hillslope B6 over the study period. The rainfall events tend to cluster between middle May to middle August, and the clustering is most significant in June and August of 2010. The spiky hydrographs indicate that short-duration is another major characteristic of the runoff process over this hillslope. A closer look at the original rainfall and runoff data shows that the runoff processes over these hillslopes last for about 2-8 hours (see the first column in Figure 2-3 for example), depending on the rainfall durations.

2.4.2 Shape similarity and magnitude variability:

analysis of a single event

We chose the storm occurred in middle May, 2010 as our example event for detailed analysis. Corn development was at the very early stage and the vegetation cover condition was close to bare earth. The depth-weighted soil moisture for the top 10, 20, and 50 centimeters at the weather station was 0.40, 0.42, and 0.44 before the beginning of rainfall. This can be considered as wet condition when compared to the observed wettest condition. The total amount of rainfall was 28.8mm and its temporal distribution can be seen in Figure 2-3. Figure 2-3 shows the relation between hydrologic responses of each hillslope and the benchmark hillslope B6 for the selected example event.

The overall shapes of the hydrographs among these hillslopes are highly similar. This high shape similarity can be reflected from three aspects. First, the maximum cross-correlation coefficients between the hydrologic responses of each hillslope and B6 are greater than 0.90 (the second column in Figure 2-3). Second, the coefficients of determination of the lagged regression analysis are greater than 0.88 (the third column in Figure 2-3). Lastly, the alignments between the rescaled hydrograph of each hillslope and the benchmark hydrograph are extraordinary (the last column in Figure 2-3).

However, the magnitudes of hydrologic responses vary dramatically among these hillslopes. This substantial variation in the scaling factor can be seen from the first column of Figure 2-3, which displays the direct comparison of hydrographs plotted with the same vertical scale. It is also evidenced from the fact that the slopes of lagged linear regression varies from 0.3 to 1 (the third column of Figure 2-3), though we exclude the hillslope size impact by analyzing the area averaged flows.

2.4.3 Shape similarity and magnitude variability: analysis of multiple events

The analysis described above shows evident shape similarity but high spatial variation of scaling factor between the hydrologic responses from these hillslopes for a single runoff event. To examine whether this relation sustained across runoff events, we

analyzed 72 individual runoff events following the same procedure. The selection of runoff events is based on the runoff characteristics. For example, sometimes short duration heavy rainfall occurred while none of the hillslopes produced notable flow because of dry field conditions. This zero overland flow response would not help much in deepening our understanding of hydrologic process, and thus we chose events that flow were noticeable for at least most of the hillslopes.

Figure 2-4 shows the results of the analysis on the 72 runoff events. The upper panel confirms the high shape similarity among the hydrologic responses of theses hillslopes. For each runoff event, the shape similarity values for most of the hillslopes are above 0.80 with few exceptions. We find that for some events many hillslopes have low shape similarity values. An example is event #22 occurred on June 12, 2009 under dry soil moisture condition. We also find that some hillslopes tend to have larger chances to have low shape similarity values (e.g., I1 and I2). We will investigate these exceptions in the following sections. The lower panel of Figure 2-4 confirms the high spatial variation of the scaling factor between the hydrologic responses from these hillslopes. For most of the runoff events, the scaling factor range from about 0 to 1.0. Extremely, for some sizable runoff events, the scaling factor varies from 0.3 to about 1.5 (The largest scaling factor values were obtained at I3, which is another 100% cropland hillslope).

2.4.4 Controls of the spatial variation of shape similarity and scaling factor

In the previous two sections, we assessed the shape similarity and scaling factor between the hydrologic responses from the hillslopes, and we will investigate the control factors of the spatial variation in the shape similarity and scaling factor in this section. Figure 2-5 shows the annual distribution of events, estimated shape similarity ρ_{max}, and scaling factor k for each hillslope. The majority of the events occurred during the period from May to mid-August, which is the rainy season for the study area.

The shapes of hydrographs are more similar between areas that are closer than those are further apart. In Figure 2-5, the red pluses represent events with shape similarity lower than 0.8, and the red circles are the associated scaling factor. There are few red pluses in the panels for the Basswood hillslopes (B1 to B5), while many more in the panels for I1, I2, I3, O1, O2, O3. This indicates hillslopes from the Interim and Orbweaver blocks tend to have bigger chances to have low values in shape similarity. The hillslopes at Interim and Orbweaver are relatively further from B6. Many other reasons, for example, the small-scale variability in soil moisture condition and rainfall field may also contribute to this low shape similarity.

Moreover, the occasionally low shape similarity tends to accompany low runoff responses (Figure 2-5). The data in Figure 2-5 shows that events with scaling factor lower than 0.05 (i.e., the runoff at a targeting hillslope is less than 5% of the runoff at B6) tend more often to have low shape similarity. We applied a threshold of scaling factor $k=0.05$ to exclude the cases that some hillslopes did not generate noticeable runoff, and found that the shape similarity tends to be high with small variation across hillslopes and events.

The spatial variation of the scaling factor conditioned on individual events cannot be consistently explained by structural characteristics of the hillslopes we investigated in this study (Figure 2-6). For each event, we plotted the scaling factor against four possible predictive variables including width of prairie filter strips at footslope, maximum slope length, slope, and size of the hillslopes. We also conducted simple linear regression analysis to reveal the predictive value of each of these variables alone for the scaling factor. Figure 2-6 is one of such scatterplots constructed for the example runoff event occurred in middle May, 2010 (our example event), and it suggests weak relationships between scaling factor and the independent variables tested. We did not find consistent pattern in similar scatterplots for other events (see Appendix A), indicating there is no

apparent relationship between the scaling factor and the independent variables investigated.

Land use tends to affect the scaling factor, but its impact can be masked by others (Figure 2-5). The within-cluster comparison shows that 100% cropland hillslopes (B6, O3, and I3) produced more runoff than the other hillslopes receiving prairie strip treatment for most of the events. Note that for the Basswood block the scaling factors for B1~B5 are less than unity for most events, indicating B6 is more productive in runoff generation. However, the inter-cluster comparison shows that 100% cropland hillslopes do not grantee higher runoff generation efficiency than those hillslopes receiving prairie strip treatment. For example, B4 (20% of its total area receives prairie treatment) could be more productive in runoff generation than I3 and O3.

2.4.5 Temporal variation of scaling factor and its controls

The data analysis thus far is confined to the comparison of hydrologic responses among all of the hillslopes, and the goal was to explore how the shape similarity and scaling factor change across hillslopes conditioned on the same storm event. We showed in Sections 2.4.3 and 2.4.4 that the shape similarity tends to be high and static among these hillslopes across events, and we will concentrate on exploring the dynamics of the scaling factor and its control factors in this section.

The scaling factor for each hillslope shows high temporal variation, indicating substantial differences in the relative runoff generation efficiency across runoff events. Figure 2-5 shows that the scaling factors can vary from about 0 to 1 for nine of the hillslopes and a relatively narrower range for B1 and O1. However, no apparent seasonal pattern of the scaling factor is detected.

Given the spatial proximity of these hillslopes, the short-term factors, i.e., the antecedent soil moisture condition and the rainfall characteristics may lead to the observed substantial dynamics in the scaling factor for each hillslope. We apply the

multiple linear regression technique to test this hypothesis. The antecedent wetness and rainfall at the study hillslopes are repented by the soil moisture and rainfall measurements at the NOAA weather station. Though the measurements at the weather station may not precisely represent those at the hillslopes but they provide good approximations to the dry/wet field conditions and rainfall characteristics. This idea is similar to the concept of the widely used antecedent precipitation index (API). Note that this approach neglects the spatial variability of soil wetness and rainfall between the hillslopes. The antecedent wetness indices include the depth weighted average volumetric soil moisture contents (VSMC) for the top 10-, 20-, and 50-cm layers. The variables describing rainfall characteristics include the total amount of rainfall, rainfall duration, maximum 5-minute rain accumulation, maximum hourly rain accumulation (MHRA), and the coefficient of variation of rain rate for each storm event (as a measure of the temporal variability of rain rate). We used the 44 events occurred in 2010 and 2011 in our regression analysis because the soil moisture data is available starting from 2010.

Multivariate linear regression analysis suggests a moderate functional relationship between the scaling factor and short-term factors (Figure 2-7). Forward stepwise least squares linear regression shows that the volumetric soil moisture content (VSMC in top 50cm) and maximum hourly rain accumulation (MHRA) account for about 36% to 75% of the temporal variation of the scaling factor. As expected, the coefficients of volumetric soil moisture content and maximum hourly rain accumulation are positive and statistically significant at the $p=0.05$ level, indicating that the wetter the hillslopes are and the heavier the rain intensity is, the more similar the runoff generation efficiencies are. The consistent relationship at the other 9 hillslopes does not apply for B1 and O1 (negative coefficient of volumetric soil moisture content). B1 tends to have low and relatively constant scaling factor (the first panel in Figure 2-5) across events and hillslope O1 have relatively fewer points available for analysis. Further investigation on these two hillslopes is needed in the future.

2.5 Discussion

The effect of spatial variability of hydrologic processes at the small scale on the hydrologic responses at larger scales is essential for scaling in hydrologic modeling. However, the characteristics of the small-scale variability remain poorly understood. The approach of inter-site comparison at the same storm event, as a complement to the approaches of inter-site comparison across climate regions and inter-event comparison at a fixed site, is adopted in this study to investigate the property of the variability of small-scale surface runoff processes. We calculated the shape similarities and scaling factors between surface hydrographs observed over 12 neighboring hillslopes for each individual runoff event. We analyzed 72 runoff events over 4 years and examined the spatial and temporal variability of the shape similarity and scaling factors.

2.5.1 Organized variability of small-scale hydrologic responses

Our data analysis suggests that hillslopes with spatial proximity respond to the same storm event similarly in shapes but differently in magnitudes (section 2.4.3). The spatial variability in the scaling factor for each storm event supports the finding established via inter-site comparisons across land use and climate regions that hydrologic processes at the hillslope scale are heterogeneous and complex (e.g., Sivapalan, 2003; Uchida et al., 2005b; Scherrer et al., 2007; Kienzler and Naef, 2008a; Kienzler and Naef, 2008b; de Araújo and González Piedra, 2009; Beven, 2012). The temporal variability in the scaling factor for each paired hillslopes agrees with the notion recognized through across-event comparison at a fixed site that hydrologic responses at the small scale are nonlinear (e.g., Minshall, 1960; Grayson et al., 1997; Sivapalan et al., 2002; Zehe and Bloschl, 2004; Tromp-van Meerveld and McDonnell, 2006b; Graham et al., 2010). In contrast to the remarkable spatial and temporal variability of the scaling factor, the extraordinary high shape similarity of surface runoff processes across neighboring hillslopes for each storm event tends to be persistent. These results indicate that the

small-scale surface runoff processes are spatially variable but organized in a linear manner. It would be valuable to test this new feature of the variability of small-scale runoff responses in other land use and climate regions such that we can generalize and use it to assist distributed hydrologic modeling.

2.5.2 Controls on the organized variability of small-scale hydrologic responses

It is difficult to explain the spatial and temporal characteristics of the shape similarity and the scaling factor. On the one hand, factors including antecedent soil moisture, rainfall characteristics, and hillslope properties individually are influential in determining the runoff responses, and probably more realistic, their complex nonlinear interactions control the runoff processes. On the other hand, there is only limited data available and some of the key information is very challenging to be measured with high accuracy and spatiotemporal resolution. These process complexity and measurement difficulty hamper us from deciphering the controlling factors using the simple linear regression tools and the incomplete information. Nevertheless, we try to understand this organized-variability using the data available.

The persistent high shape similarity in space and time may result from the spatial proximity of these hillslopes and the spatiotemporal characteristics of the rainfall field. These hillslopes have similar sizes ranging from 0.5 to 3 hectares and have major land use of crop land covering at least 80% of their total areas. Furthermore, these hillslopes are closely located in space, indicating that 1) they have large chance to have similar soil and geology, and thus have relatively similar wetness condition though not exactly the same; 2) they subject to similar temporal configuration of rainfall processes. It is quite possible that the states of these hillslopes are spatially similar prior to each storm event, and thus the shapes of the hydrologic responses are determined by the temporal characteristics of rainfall.

The high spatiotemporal variability of the scaling factor can be moderately (40%~70%) explained by the variability of rainfall intensity and antecedent soil moisture content. We first investigated the impact of hillslope characteristics (slope, size, prairie-strip width and slope) on their scaling factors but our scatterplots do not show consistent simple relationships across runoff events. However, this does not exclude the potential that some other factors may affect the scaling factor. For example, the various combinations of the locations and the amount of the prairie strips (see Table 2-1) installed on these hillslopes have been reported to have impact on the scaling factor (Hernandez-Santana et al., 2013). Furthermore, the lack of relationship does not mean that they are not important-maybe their importance is masked by other factors such as the variation in the antecedent conditions and rainfall at these hillslopes. This hypothesis cannot be directly tested because we currently do not have the detailed measurements at each hillslope, while the theory of ergodicity or space-for-time substitution (e.g., Birkhoff, 1931; Neumann, 1932; Harvey, 1968; Pickett, 1989) allows us to indirectly test it by analyzing the temporal variation of the scaling factor. Our multivariate linear regression shows that 40%~70% of the temporal variability of the scaling factor can be attributed to the variability of rainfall intensity and antecedent soil moisture content. Interestingly, the coefficients of rainfall intensity in Figure 2-7 are the same for all of the hillslopes (except for B1) while it is not the case for soil moisture content. In other words, for a storm event, rainfall intensity contributed equally in determining the scaling factors across hillslopes if its spatial variability is neglected and the spatial variability of the scaling factor is cause by the spatial variability of soil moisture content. This is consistent with our conscious that given similar rainfall, the runoff responses of areas with spatial proximity tend to rely on antecedent soil moisture condition.

The results and discussions above suggest it will be interesting to explore the interaction between the spatial structures of rainfall(e.g., Krajewski et al., 2003), soil moisture (e.g., Western et al., 2004) and runoff processes at small scales (~ 3 kilometers).

To pursue this goal, we installed soil moisture and rain gauge platforms in 2013 to collect more data at the three clusters of hillslopes for future investigation. This may allow us to gain more solid insights about the organized variability of small-scale runoff processes. For example, with the more detail rainfall measurements we can conduct the lagged regression analysis between rainfall measurements over these hillslopes to explore the control of the high shape similarity of the hydrographs. Furthermore, this increase in instrumentation may also help to reduce the scatters in Figure 2-7 by using data at the hillslopes rather than that at the NOAA weather station.

2.5.3 Implications for distributed hydrologic modeling

Successful applications of spatial organization of hydrologic response have been applied both at the small and large scales. At the extreme case of small scale – the grid scale, the widely applied TOPMODEL assumes that all locations within the catchment having the same topographic index respond similarly to similar inputs. This assumption of topography based local hydrologic similarity has been recognized as an important contributor to the simplicity and success of the TOPMODEL (e.g., Beven, 1997). A lesson from this example is that accounting for the relationships between small-scale hydrologic responses can be important for distributed hydrologic modeling at larger scales. At large scale (i.e., the catchment scale ranging from tens to thousands of square kilometers), hydrologic similarity between neighboring catchments has been frequently used for all purposes. Many studies use this idea for regionalization of models and parameters (e.g., Merz and Blöschl, 2004; Oudin et al., 2008; Oudin et al., 2010), some use this concept to predict streamflows for ungauged basins (PUB) (e.g., Hirsch, 1979; Hortness, 2006; Archfield and Vogel, 2010; Ssegane et al., 2013), and others for creating hydrologic models (Andréassian et al., 2012). These studies generally showed the power of spatial organization in hydrologic modeling application, and raise to our question - how we can apply the spatial relationship of small-scale hydrologic response observed in

this study for distributed hydrologic modeling? It would be great if we could explicitly account for it in the process of writing the equations for distributed hydrologic models (see for example, Andréassian et al., 2012), or at least we can use it as a feature to test the capabilities of our elementary models developed for the REWs of a distributed model.

2.6 Conclusion

This study used the lagged regression technique to examine the relationship between surface runoff processes from 12 closely located hillslopes in central Iowa, USA. The results show that areas with spatial proximity respond to the same storm event similarly in shapes but differently in magnitudes, indicating that the small scale surface runoff responses (hydrographs) are spatially variable but organized in a linear manner. We call this phenomenon as organized variability or spatial proportionality of surface runoff processes. Further multivariate regression analysis shows that the organized variability tends to depend on the antecedent wetness condition and rainfall characteristics. These results suggest that except for nonlinearity and heterogeneity, shape similarity in space (or spatial proportionality) is another feature of small-scale runoff process.

On the basis of our analysis in the Iowa climate and agriculture lands, it is not ready to claim that this spatial proportionality in the hydrologic responses from hillslopes in geographic vicinity is universally true. However, it will be interesting to test this possibility out for different geographic and climate regions by designing rigorous experiments and conducting similar data analysis illustrated in this study. The confirmation of the existence of this between-element feature for other regions would benefit distributed hydrologic modeling.

Table 2-1. Hillslope characteristics

Site	Size (ha)	Slope (%)	Max. Slope Lengths (m)	Width of PFS at footslope (m)	Location and percent of PFS
B1	0.53	7.5	120	38.2	10% footslope
B2	0.48	6.6	113	40.5	5% footslope and 5% upslope
B3	0.47	6.4	110	37.6	10% footslope and 10% upslope
B4	0.55	8.2	118	38.1	10% footslope and 10% upslope
B5	1.24	8.9	144	46.4	5% footslope and 5% upslope
B6	0.84	10.5	140	0	All rowcrops
I1	3	7.7	288	51	3.3% footslope, 3.3% sideslope, and 3.3% upslope
I2	3.19	6.1	284	78.2	10% footslope
I3	0.73	9.3	137	0	All rowcrops
O1	1.18	10.3	187	57.3	10% footslope
O2	2.4	6.7	220	52	6.7% footslope, 6.7% sideslope, and 6.7% upslope
O3	1.24	6.6	230	0	All rowcrops

B: Basswood; I: Interim; O: Orbweaver

Percent of prairie filter strips (PFS) = area of PFS / area of watershed

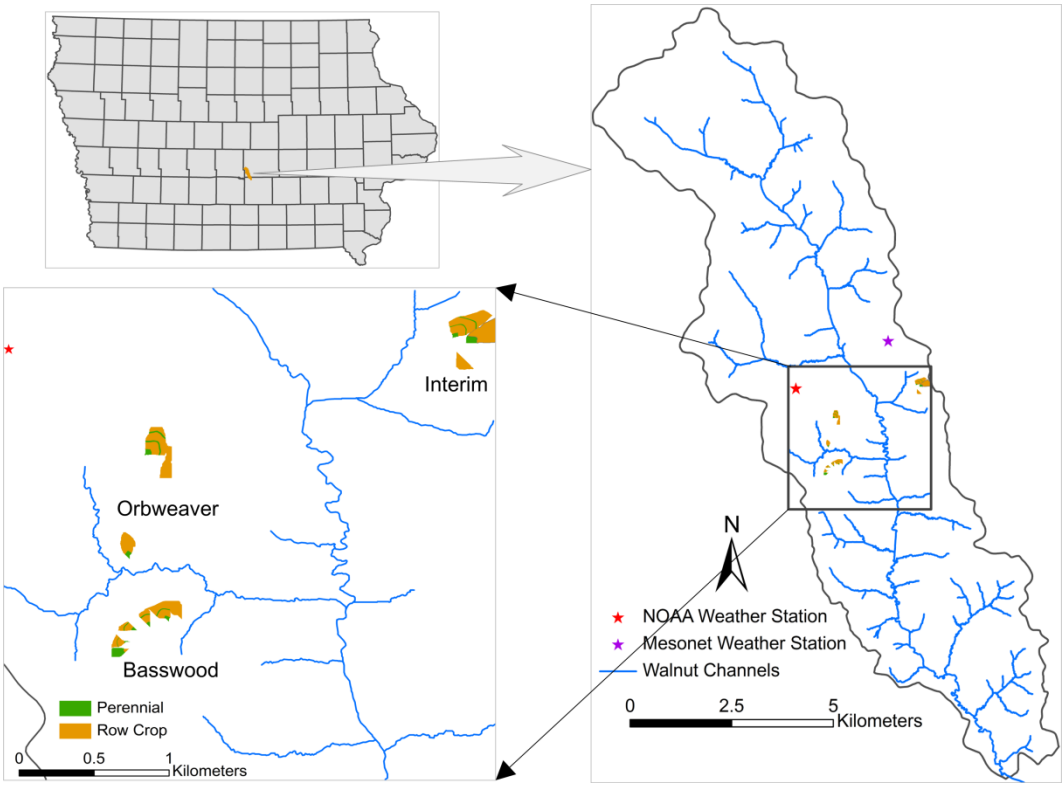

Figure 2-1. Location and experiment design of the 12 hillslopes at Basswood, Orbweaver, and Interim.

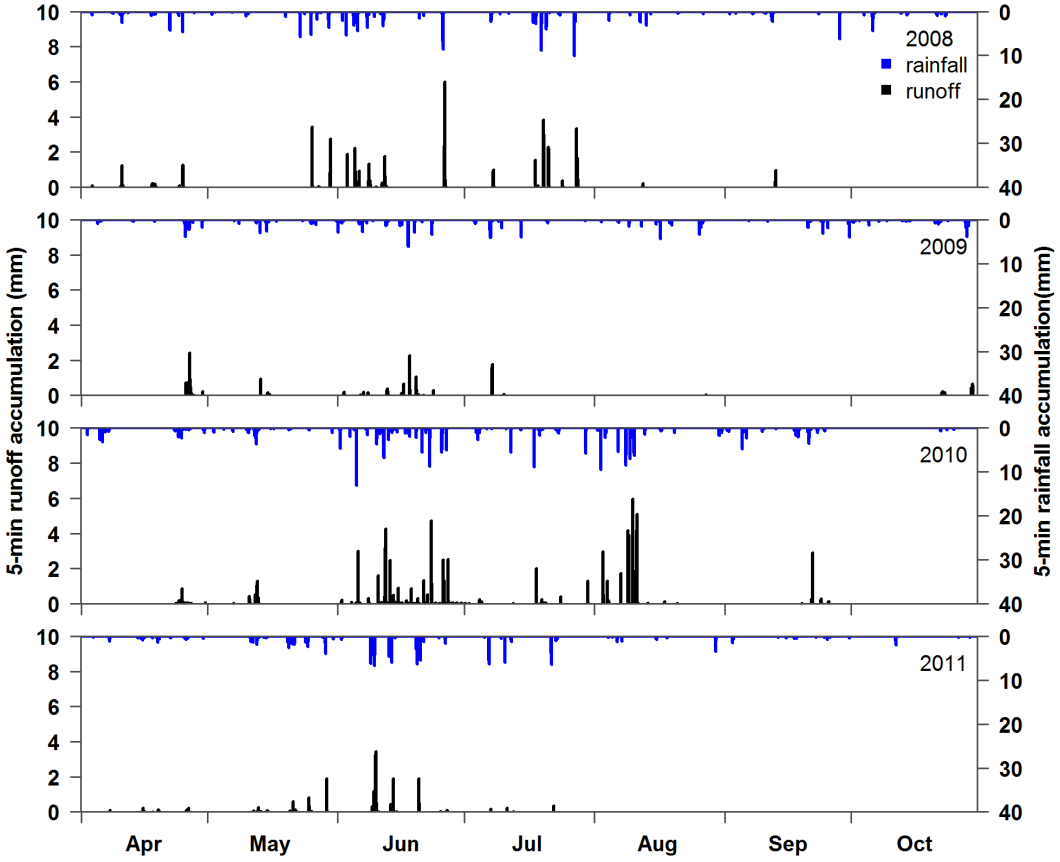

Figure 2-2. Time series of 5-minute accumulation of runoff at hillslope Basswood #6 and 5-minute accumulation of rainfall at the NOAA weather station during the growing season over the period from 2008 to 2011.

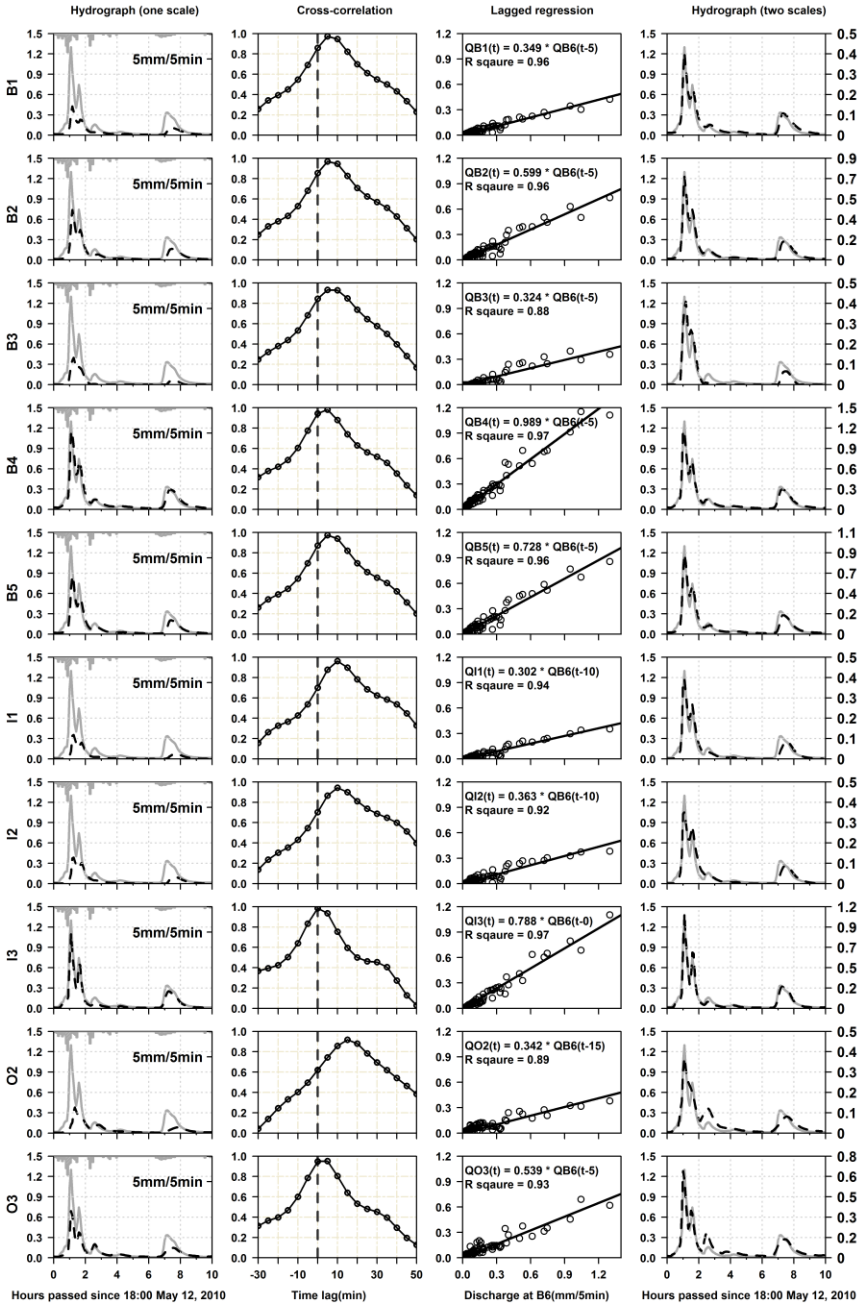

Figure 2-3. Lagged regression analysis of hydrographs between paired hillslopes (hillslope B6 as the benchmark). Left to right are the hydrographs plotted in the same vertical scale, the cross correlation of hydrographs, the lagged regression of hydrographs, and the hydrographs plotted with different vertical scales for each paired hillslopes. Top to bottom are comparisons for different pairs of hillslopes (e.g., B1 VS. B6). The solid gray lines represent the hydrographs at B6, and the dashed black lines represent hydrographs at other hillslopes (y-axis unit: mm/5min). Lagged regression was done at the time lag that cross-correlation achieves maximum. In the last column, the vertical scaling ad horizontal shift was determined according to the associated lagged regression analysis.

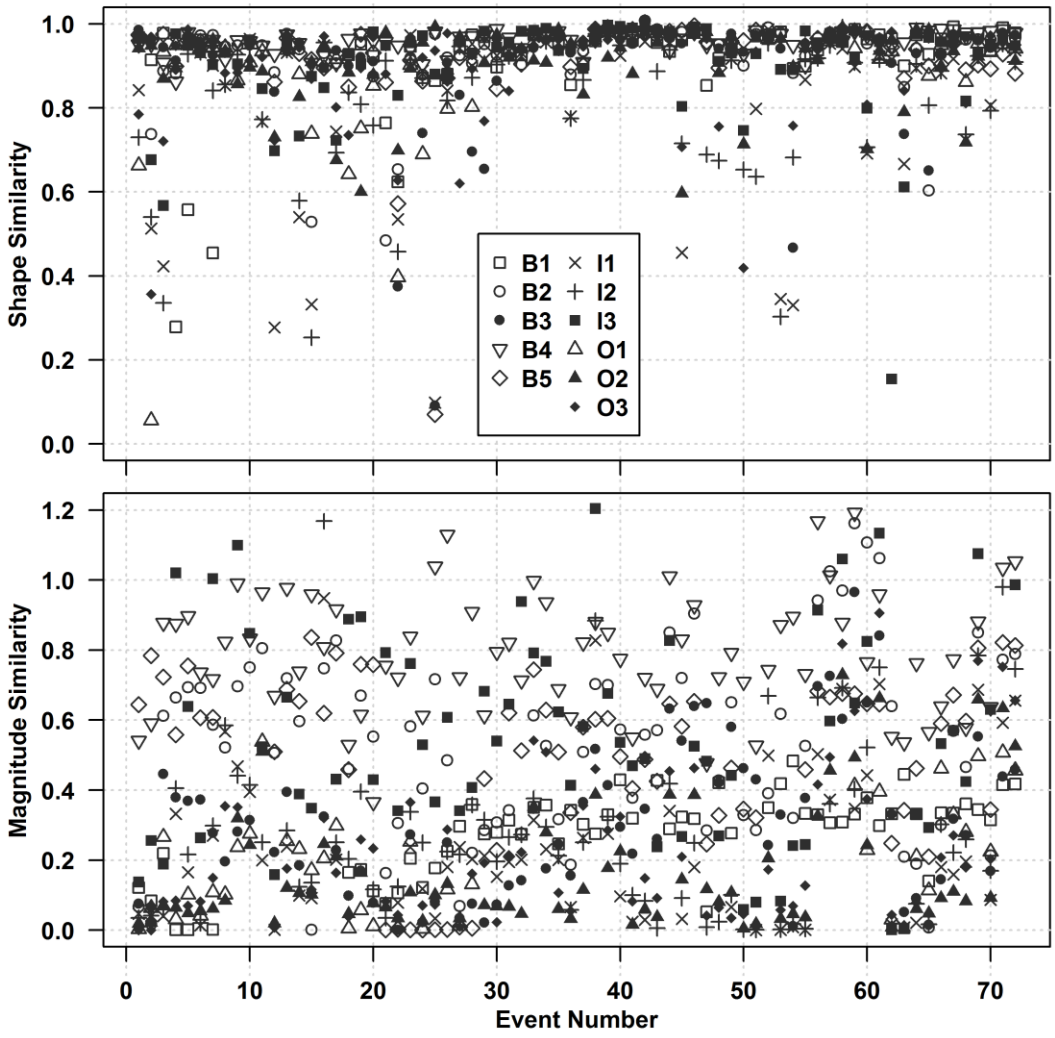

Figure 2-4. Event-based comparison of shape similarity and scaling factor at the twelve experimental hillslopes in Iowa.

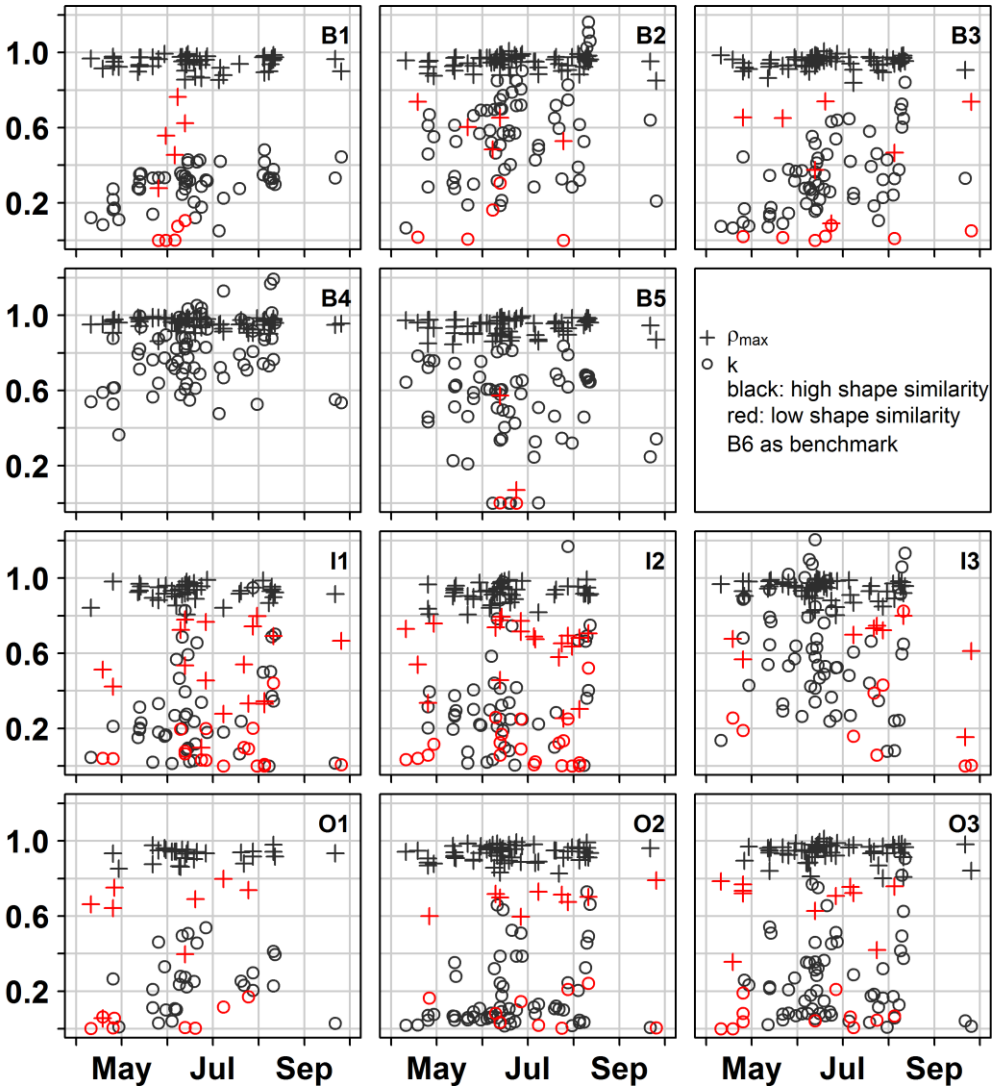

Figure 2-5. Annual distribution of single-event shape similarity (i.e., maximum cross-correlation $\rho_{\max}$), and scaling factor (i.e., lagged regression slope k). Values of $\rho_{\max}$ and k were calculated between each hillslope and B6 for 72 events observed from 2008 to 2011.

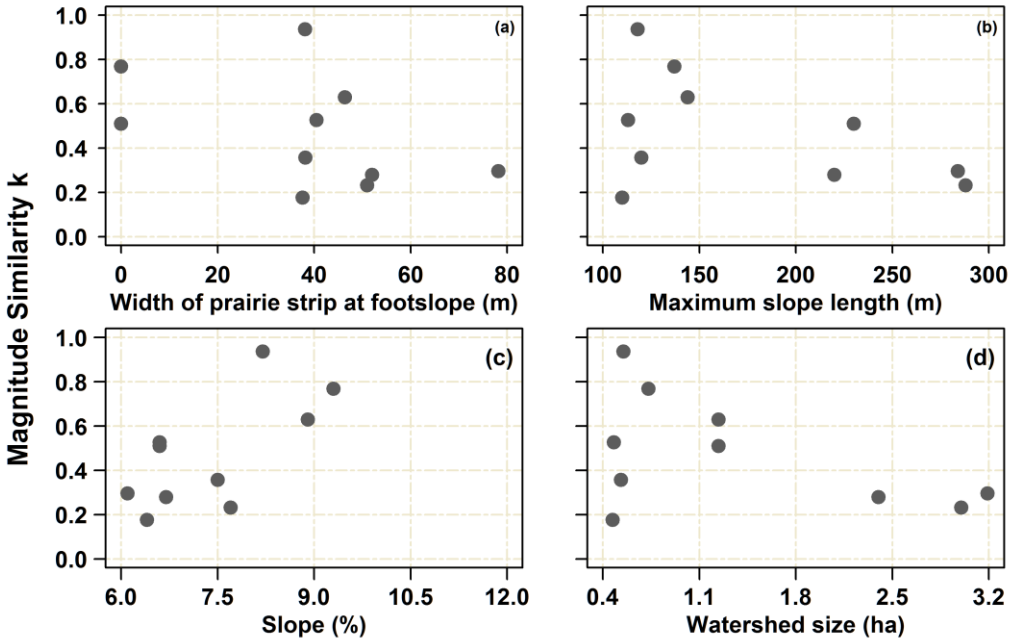

Figure 2-6. Scatterplots of scaling factor k versus width of prairie strip width at footslope (a), maximum slope length (b), slope (c), and size (d) of the hillslopes.

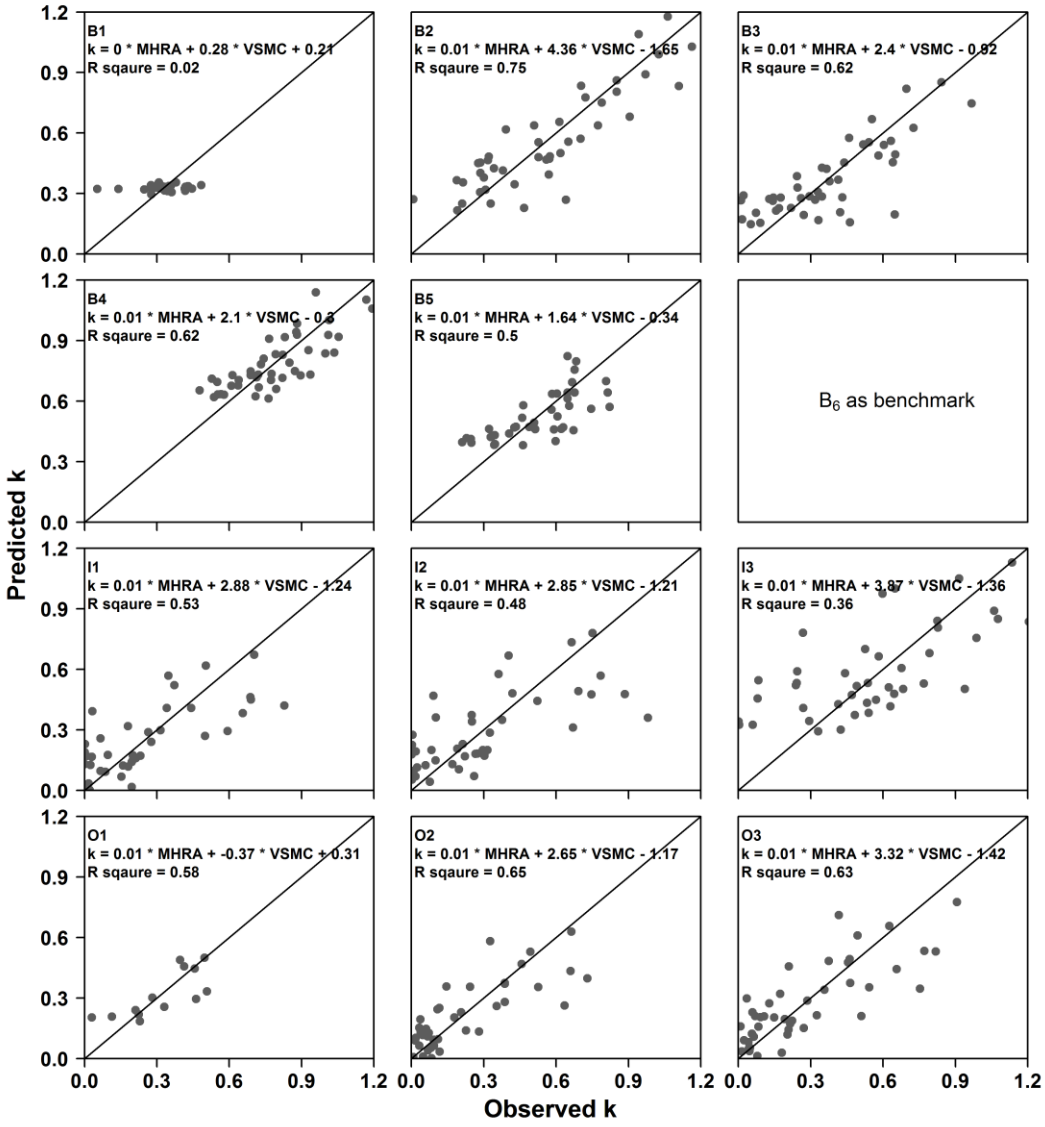

Figure 2-7. Comparison of the model versus data estimates of scaling factor *k*. The 1:1 line is superimposed to the scatter plot. Independent variables *MHRA* and *VSMC* are the maximum hourly rain accumulation, and the volumetric soil moisture content averaged over the top 50cm of soil, respectively. Both *MHRA* and *VSMC* are observed at the same NOAA weather station about 1.1~3.3km away.

CHAPTER 3

RECESSION DATA ANALYSIS: SENSITIVITY OF PARAMETER ESTIMATION TO THE CALCULATION PROCEDURE

3.1 Introduction

Quantitative analyses of recession curves involve the selection of mathematical expression and the estimation of the recession parameters. Among the mathematical models, the power-law function proposed by Brutsaert and Nieber (1977) is widely adopted:

$$\frac{dQ}{dt} = -AQ^{B}, \qquad (3\text{-}1)$$

where dQ/dt is the time rate of change in streamflow Q, and recession intercept A and recession slope B are model parameters. Examining the variability of recession behaviors, i.e., the variability of A and B, across and within basins has long been used to understand the functioning of watersheds.

A number of factors can contribute to the variability of the parameters A and B. Some studies related the variability of A and B to the aquifer characteristics (e.g., Brutsaert and Nieber, 1977; Troch et al., 1993; Brutsaert and Lopez, 1998; Szilagyi et al., 1998; Eng and Brutsaert, 1999; Mendoza et al., 2003; Rupp et al., 2004; Troch et al., 2013), which are summarized as the hydraulic theory based interpretation of recession behavior (e.g., Harman et al., 2009; Troch et al., 2013). Recent development linked variability of A and B to other physical factors. To name a few, Rupp and Selker (2006b) showed that the vertical heterogeneity of hydraulic conductivity and Harman et al. (2009) presented that the spatial heterogeneity of linear recession processes across hillslopes could influence the variability of B. Clark et al. (2009) demonstrated the importance of landscape organization in shaping the recession behavior across scales. Biswal and

Marani (2010) and Mutzner et al. (2013) linked the recession slope *B* to the shrink of the feeding river network or area to streamflow. Shaw et al. (2013) found that the change in recession intercept *A* was moderately related to watershed moisture storage during the recession events.

These studies unveiled various natural causes of recession variability, while little attention has been paid to the contribution by the artifacts of recession data analysis. There seems to be wide agreement on the functional form (Equation (3-1)) of the recession model, while many procedures have been developed to determine the parameters *A* and *B* (e.g., Brutsaert and Nieber, 1977; Vogel and Kroll, 1996; Wittenberg, 1999; Rupp and Selker, 2006a; Kirchner, 2009). The flexibility in determining model parameters leads to the artificial recession variability and arises from factors that include: 1) deciding whether to examine average recession characteristics or individual recession behavior; 2) selecting starting points and lengths to extract recession segments; and 3) choosing parameter estimation methods. To narrow this gap and thus to raise cautions for interpreting and comparing the results of recession analyses, the sensitivity of parameter estimation to the calculation procedure should be assessed.

The parameters *A* and *B* can be determined by using multiple or individual recession events. For example, Brutsaert and Nieber (1977) used the lower envelope, Vogel and Kroll (1992) employed the best regression line, and Kirchner (2009) used the binned curve fitting of the *dQ/dt*-*Q* data cloud to determine *A* and *B*. Instead of studying multiple recessions that make up the data cloud, there has been increasing effort devoted to analyzing individual recession events. Vogol and Kroll (1996) and Sujono et al. (2004) used different methods to determine the baseflow recession constants (assuming $B = 1$) for individual recession events. Hammond and Han (2006) and Blume et al. (2007) used portions of individual recession curves to determine parameters *A* and *B* for hydrograph separation. Biswal and Marani (2010) and Shaw et al. (2012; 2013) studied individual recession events within data clouds. Van de Giesen et al. (2005), Rupp et al. (2009), and

Biswal and Nagesh Kumar (2014) investigated the relation between the characteristics of aquifer recharge and the temporal variability of *A* and *B* across individual events.

In a systematical comparative study, Stoelzle et al. (2012) found considerable differences between the average recession characteristics (represented by *A* and *B*) obtained for the same basin using different methods of segment selection and parameter estimation. These average recession characteristics were derived using multiple events. Compared to the recession analysis using multiple recession events, we foresee that individual recession analysis may be even more sensitive to the choice of the calculation procedure since, by definition, less information is available. Fewer studies have systematically investigated the sensitivity of recession parameters for individual events to subjective factors such as the selection of recession segments and the choice of the method to calibrate the recession model. This work aims to fill this gap.

This paper will first investigate the sensitivity of the resulting recession model for individual events (Equation (3-1)) with respect to the starting points and lengths used to extract recession segments. The recession segments used to calculate parameters *A* and *B* can be selected according to various criteria with different starting points and lengths (e.g., Brutsaert and Nieber, 1977; Vogel and Kroll, 1992; Tallaksen, 1995; Kirchner, 2009; Aksoy and Wittenberg, 2011). This arbitrariness can affect the estimation of recession parameters. For example, even for baseflow recession analyses with linear assumption (*B = 1*), it has been documented that the estimates of *A* depend on the starting points (Vogel and Kroll, 1992; Tallaksen, 1995) and lengths (Vogel and Kroll, 1996) used to select recession segments. These studies used strict criteria to select recession segments to "ensure" that groundwater was the only flow source. Extending the analyses to include the early stage of recession (e.g., Hammond and Han, 2006; Kirchner, 2009; Biswal and Marani, 2010), which may have multiple flow sources feeding into the streamflow and lead to a higher sensitivity of parameter estimation to the starting points of recession segments. For instance, Hammond and Han (2006) reported sensitivity of

the parameters *A* and *B* to the lengths and starting points of the recession segments. Their goal was to find the optimum recession model for hydrograph separation. This study will quantify the sensitivity of the parameters *A* and *B* with respect to the starting points and lengths used to extract segments from individual recession curves.

We will then investigate how the results of analyzing individual recession events depend on parameter estimation methods. Parameters *A* and *B* in Equation (3-1) can be estimated using the log-log linear least squares fitting method employed by Vogel and Kroll (1992), and the nonlinear direct fitting (hereafter the NDF method) method proposed by Wittenberg (1999). Vogel and Kroll's (1992) method uses constant time steps (hereafter the CTS method) to calculate *dQ/dt* and thus is sensitive to the noise in the recession data. To overcome this restriction, Rupp and Selker (2006a) recommended to use variable time steps (hereafter the VTS method) to calculate *dQ/dt* and further to estimate the recession parameters. This paper will evaluate the performances of these three methods (CTS, VTS, NDF) and investigate if their estimates of *A* and *B* are significantly different.

Lastly, we will investigate the robustness of the parameter estimation methods to the uncertainty in streamflow data. While it is difficult to avoid uncertainty in streamflow data, we can assess the robustness of the parameter estimation methods to data noise. Streamflow data estimated by means of rating curve have substantial combined error, and this error can reach 100% for low flows (Harmel et al., 2006; McMillan et al., 2012). To reduce the impact of the precision of streamflow data on the estimation of recession parameters, some strategies were proposed to tackle this problem. For example, using a scaled time step to calculate *dQ/dt* (Rupp and Selker, 2006a), smoothing the noise in the original streamflow records by applying a moving average (Kroll et al., 2004), and averaging out the noise in the calculated *dQ/dt* by binning (Kirchner, 2009) have been suggested. All of these strategies are designed to smooth the

data noise, while limited effort has been devoted to comparing the robustness of parameter estimation methods with respect to the uncertainty in streamflow data.

In conclusion, the objective of our study was to assess the sensitivity of the resulting model $dQ/dt = -AQ^B$ for individual recession events with respect to: 1) the starting point and length used to extract segments from complete individual recession curves; and 2) the method used to estimate *A* and *B*. We do not pretend to provide new insights into the physical mechanism of the recession processes. We addressed this objective in three steps. First, we compared the values of parameters that were estimated using the same regression method and the recession segments with the same starting point but varying lengths. Second, we compared the values of parameters that estimated using the same regression method and recession segments with the same length but varying starting points. Lastly, we estimated *A* and *B* for the same set of recession segments using multiple methods and tested whether they produce similar results. We further examined the robustness of parameter estimation methods with respect to the noise in the streamflow data through Monte Carlo simulations.

3.2 Data and method

First, we define our terms in this paragraph. A "complete recession curve" is the portion of a discharge hydrograph starting from the peak and extending to the point at which the hydrograph begins to increase. A "recession segment" refers to a portion of a complete recession curve (Tallaksen, 1995; Sujono et al., 2004). Therefore, different recession segments can be extracted from a complete recession curve by changing the starting point and the segment length, i.e., each recession event has one complete recession curve but multiple recession segments. The "starting point" is the time elapsed since the occurrence of the hydrograph peak. These definitions apply to the true hydrograph, i.e., the actual discharge values. However, we only know the observed hydrograph, which is corrupted by the errors. The data uncertainty issues will be

addressed later in the paper. In this study, we focus on the recession slope *B* (see Equation (3-1)) to demonstrate the sensitivity of its estimates with respect to the calculation procedure.

3.2.1 Data and study area

We analyzed about 750 recession events observed over the period from 1995 to 2010 at 25 USGS stream gauges in the Iowa and Cedar River Basins in Iowa, USA (Figure 3-1). The corresponding drainage area at the gauge locations ranges from 7 to 17000 km^2. For this region that has a rather flat terrain, approximately three-fourths of the 900 mm average annual precipitation and 85% of the 45-65 thunderstorms occur from April through September (Villarini et al., 2011). Frozen soils and snow melting near the surface last from late October to early April. Water level is recorded every 15 or 30 minutes and is translated into discharge by applying the stage-discharge relation. We downloaded this sub-hourly streamflow data from the USGS Instantaneous Data Archive and aggregated it to hourly time series.

Most of the area investigated in this study has landforms of the Southern Iowa Drift Plain and the Iowan Surface. These two landscapes both are formed of glacial deposits and have well-defined drainage networks, with the first has steep rolling hills and valleys and the later has gentle rolling slopes and low relief. The width, depth, and alluvial fill of these valleys are shaped by gradual processes (i.e., frost action, wind and water erosion) as well as by intense flood events.

We will show details of our analysis for the recession events observed at the Clear Creek stream gauge near Coralville, Iowa, USA (red dot in Figure 3-1) and present summaries of our analysis for all of the gauges. Clear Creek is one of the U.S. National Science Foundation critical zone observatories and is representative of the U.S. Midwestern watersheds subject to agricultural land use and a humid climate. Clear Creek is an intensively instrumented and studied experimental watershed (e.g., Bradley et al.,

2002; Abaci and Papanicolaou, 2009; Rayburn and Schulte, 2009; Loperfido et al., 2010; Risley et al., 2010; Berne and Krajewski, 2013). This basin drains an area of ~250 km^2 and has the longest flow length of ~50km. The time of centration for this basin is on the order of 1 day if the channel velocity is assumed to be 0.5 m/s. Land cover in this basin is dominated by agricultural uses including corn, soybeans, and pasture.

3.2.2 Selection of complete recession curves and recession segments

Considering the hydroclimatological characteristics of the region mentioned in Section 3.2.1, only summer and autumn recession events were analyzed in this study. For each gauge, isolated events were selected from its continuous discharge hydrograph by applying a threshold. The threshold was the estimate of the 95% quantile of hourly streamflow at the gauge. Then the times of peak discharge for each event were marked and the hydrograph segments between two consecutive peaks (events) were extracted. For each of these selected segments, we identified a complete recession curve starting from the hydrograph peak and extending until the difference between consecutive observations is greater than 0.1mm/day. The threshold of 0.1mm/day rather than 0 was chosen to account for spurious increases and "stair-step" patterns in lowflow measurements. In this study, only complete recession curves longer than 10 days were considered.

Figure 3-2 shows our approach to investigate how parameter estimation depends on the selection of recession segments. Segments from a complete recession curve were extracted with various starting points and lengths. By analyzing recession segments with constant length but varying starting points, as illustrated in Figure 3-2 (a), the dependence of B on the starting point were investigated. Similarly, by analyzing recession segments with the same starting point but changing lengths, as illustrated in Figure 3-2 (b), the dependence of B on the lengths of recession segments were examined. This analysis was

repeated for all hydrographs included in the study. When investigating how the estimation of *B* depends on the starting point, we varied the starting points from 0, 3, 6, 9, 12, 18, 24, 36, 48, 60, 72, 96, 120, 144 and 168 hours after the hydrograph peak. When examining how the estimation of *B* depends on the recession length, we changed the recession lengths from 4, 5, 6,… up to 12 days if the recession was not interrupted by consecutive storms.

3.2.3 Parameter estimation methods

The constant time step method (CTS)

The terms in equation (3-1) can be discretized as $dQ/dt = (Q_t-Q_{t-1})/\Delta t$ and $Q=(Q_t+Q_{t-1})/2$ for a given recession segment, where the time step Δt is constant. The time step can be chosen to be 1 day (e.g., Brutsaert and Nieber, 1977; Vogel and Kroll, 1992), 1 hour (e.g., Clark et al., 2009), or 15 minutes(e.g., Rupp and Selker, 2006a). For the constant time step method investigated in this study, we first calculated *dQ/dt* and *Q* for an individual recession event using constant time step of 1 hour, and then adopted the log-log simple linear least squares regression method used by Vogel and Kroll (1992) to determine *A* and *B*.

The variable time step method (VTS)

Rupp and Selker (2006a) showed that the CTS method may bias the estimates of *A* and *B*, and they recommended to use variable time steps to calculate *dQ/dt* to remove this limitation. For the variable time step method compared in this paper, we first calculated *dQ/dt* and *Q* for an individual recession event using variable time steps, and then adopted the log-log simple linear least squares regression method used by Vogel and Kroll (1992) to estimate *A* and *B*. To implement the VTS method (Rupp and Selker, 2006a), the stage-discharge relationship and the stage measurement accuracy are required to determine the threshold *C* ($\boldsymbol{C} \geq \mathbf{0}$, equation (15) in their paper) and thus Δt. However,

this information is often not available and the value of *C* ends up being arbitrary. Palmroth et al. (2010) proposed to use the criterion

$$Q_t - Q_{t-1} \geq C(Q_t + Q_{t-1})/2 \quad (3\text{-}2)$$

We followed this approach and set the value of *C* to be constant at 0.001 for all our analyses as Palmroth et al. (2010) used in their study.

The nonlinear direct fitting method (NDF)

The third method is the nonlinear direct fitting method recommended by Wittenberg (Wittenberg, 1999). Accordingly, we varied *B* systematically, for example, from 0 to 5 with a step size of 0.01 and calculates the value of *A* at each value of *B* using equation

$$A = \frac{\sum_{t=1}^{n}(Q_{t-1} - Q_t)}{\Delta t \sum_{t=1}^{n}\left(\frac{Q_{t-1} + Q_t}{2}\right)^B} \quad (3\text{-}3)$$

where *n* is the length of the recession segment, and Δt is the observational interval. Solving equation (3-1) for Q_t gives

$$Q_t = Q_0\left[1 - \frac{(1-B)At}{Q_0^{1-B}}\right]^{\frac{1}{1-B}} \quad (3\text{-}4)$$

where Q_0 is the discharge at the starting point of the recession segment used to calculate *B*, and *t* is the number of hours elapsed from the starting point. All recession segments are modeled using their initial discharges Q_0, the values of *A* and *B*, and equation (3-4). The modeling error *E* is defined as

$$E = \frac{V_{\text{mod}} - V_{obs}}{V_{obs}} \times 100\% \quad (3\text{-}5)$$

where V_{obs} and V_{mod} are the volume of the observed and modeled hydrographs, respectively. The optimal paired values of *A* and *B* were selected by minimizing the modeling error.

Data points used by parameter estimation methods

After a recession segment is selected, the three methods are used to estimate its recession parameters. To make *log(-dQ/dt)* valid, the CTS method requires excluding non-negative *dQ/dt* values. This requirement is satisfied in the literature by eliminating the non-negative values after *dQ/dt* are calculated (e.g., Brutsaert, 2008; Stoelzle et al., 2012). We followed this approach in our study. In the VTS method, the criterion (Equation (3-2)) automatically makes *log(-dQ/dt)* valid. When small *C* values are chosen, Equation (3-2) selects strictly monotonically decreasing data points for parameter estimation. The choice of the value of *C* determines the number of points used for parameter estimation. The NDF method uses all of the data points to estimate *A* and *B*. When applying these three methods, possibly different data points from the same recession segment are used in parameter estimation. However, these are the methods commonly used in the literature and little attention is paid to how they may give notably different parameter values for the same recession event.

Comparison of the parameter estimates

Once the estimates of *A* and *B* are obtained for a given recession segment using the three methods described above, Equations (3-4) and (3-5) can be used to assess the goodness of fit. As done in other works (e.g., Wittenberg, 1999; Hammond and Han, 2006), we assume the method producing the smallest modeling error *E* outperforms the others. It is possible to improve the performance of the VTS method by adjusting the threshold *C*, while there is no solid guidance on how to optimize the selection of *C* value. Following Palmroth et al.(2010), we used a constant *C* value of 0.001.

Robustness with respect to uncertainty in streamflow data

Investigating the robustness of the parameter estimation methods to data errors is important because errors in the data may lead to biased estimates of parameters (e.g., Draper et al., 1966; Gupta and Dawdy, 1995; Ciach and Krajewski, 1999; Fuller, 2009; Carroll et al., 2010). Streamflow data are subject to stage measurement and rating curve errors, and the evapotranspiration in the vicinity of streams. The uncertainty in streamflow data is usually described as percentages of flow rates when assessing the quality of streamflow measurements (Harmel et al., 2006; McMillan et al., 2012) and modeling errors in streamflow measurements (e.g., Georgakakos, 1986; Weerts and El Serafy, 2006).

In this study, the Monte Carlo simulation method was used to assess the robustness of the parameter estimation methods with respect to the uncertainty in streamflow data. First, a noise-free ("true") recession segment of 7-day length at an hourly time step (168 values) was generated. Then, for each run, the true curve was corrupted with a vector of noise with 168 elements and the methods discussed in section 3.2.3 were applied to estimate the parameters *A* and *B*. For each magnitude of noise, we ran 1000 simulations and took the mean and standard deviation of the estimates of *A* and *B* given by each of the methods. The means were compared to the true values used to generate the noise-free recession segment.

The noise-free recession segment was corrupted with either multiplicative uncorrelated noise or multiplicative correlated noise. Errors in consecutive streamflow measurements have been assumed to be correlated (e.g., Kitanidis and Bras, 1980; Sorooshian and Dracup, 1980; Foglia et al., 2009) or uncorrelated (e.g., Georgakakos, 1986; Weerts and El Serafy, 2006) in the literature. We tested both cases in this study, and introduced noise to the true recession segments data by

$$Q(t) = [1 + E(t)]Q_{true}(t), \qquad (3\text{-}6)$$

where *E(t)* is the noise process, and *Q(t)*and $Q_{true}(t)$ are the time-varying corrupted and noise-free recession segments. We generated vectors of uncorrelated noise from a normal distribution of *N(0, σ)* following Weerts and El Serafy(2006) and vectors of correlated noise using the first order autoregressive model (Sorooshian and Dracup, 1980)

$$E(t) = \rho E(t-1) + \varepsilon(t) \qquad (3\text{-}7)$$

where σ is the magnitude of noise, $t = 1, 2, \ldots, 168$, ρ is the lag-one serial correlation coefficient for the errors and takes a positive value less than 1, and $\varepsilon(t)$ is an i.i.d. random variable with mean 0 and standard deviation $\sqrt{1-\rho^2}\sigma$. We investigated different magnitudes of noise at σ = 1%, 3%, 5%, 8%, 10%, and 15% and tested six levels of correlation atρ = 0.3, 0.4, 0.5, 0.6, 0.7, and 0.8.

3.3 Results

3.3.1 Variability due to starting point

The analysis of a single event shows that the estimation of *B* varies substantially with the starting points of recession segments (Figure 3-3). To show how the starting points of recession segments affect the estimation of *B*, we took a recession event observed at the Clear Creek stream gauge near Coralville, Iowa as an example. The selected complete recession curve has a total length of 27 days and spanned from June 24, 2007 until July 19, 2007 (Figure 3-2). For each fixed length (e.g., 5, 7, 9,11 days), we first extracted segments from the complete recession curve using various starting points and then estimated the corresponding values of *B*. Finally, we plotted the obtained *B* values against the associated starting points. The result shows that, for the same complete recession curve, the estimates of *B* for its recession segments with the same length but different starting points can differ on the magnitude of 1.5.

Analyses of all of the recession events selected in this study also show a high variation of the *B* estimates due to the change in the starting points of recession segments

(Figure 3-4). For each event at a gauge, recession segments were extracted from the complete recession curve with a fixed length but various starting points. Then the associated estimates of *B* were obtained using the same parameter estimation method. Next, the range of *B* (defined as $\Delta B = B_{max} - B_{min}$) was calculated and used as a measure of the variation of *B* due to the change in starting points for the selected recession event. This analysis was repeated to obtain the values of ΔB for all recession events at each USGS gauge. Figure 3-4 shows that ΔB can take values ranging from 0 to 3 if the values of *B* were estimated using recession segments extracted from the same complete recession curve with fixed length but various starting points. The median values of ΔB (red dots in Figure 3-4) for all gauges are around 1. Similar results (not shown) were obtained when repeating similar analysis using the CTS and VTS methods. Precautions should be taken when using *A* and *B* to characterize individual recession behavior because the estimation of *A* and *B* is sensitive to the starting point of the recession segment.

3.3.2 Variability due to recession length

The analysis of a single event shows that the estimation of *B* tends to be affected by the lengths of recession segments (Figure 3-5). The same recession event as described in Section 3.3.1 was used to investigate the dependence of *B* on the lengths of recession segments. At each fixed starting point (e.g., 1 day, 3, 5, and 7 days after hydrograph peak), we first extracted recession segments using different lengths and then calculated the associated *B* values. Finally, we plotted *B* against the associated lengths of recession segments. The result shows that, for the same complete recession curve, the estimates of *B* for its recession segments with the same starting point but different lengths can vary on the magnitude of 0.5.

Analyses of all of the recession events selected in this study also show that the *B* estimates tend to depend on the lengths of recession segments (Figure 3-6). For each

event at a gauge, recession segments were extracted from the complete recession curve with a fixed starting point but various lengths. Then the associated estimates of *B* were obtained using the same parameter estimation method. Next, the range of *B* (defined as $\Delta B = B_{max} - B_{min}$) was calculated and used as a measure of the variation of *B* due to the change in the segment lengths for the selected recession event. This analysis was repeated to obtain the values of ΔB for all recession events at each USGS gauge. Figure 3-6 shows that ΔB can take values ranging from 0 to 2 (for most gauges) if the values of *B* were estimated using recession segments extracted from the same complete recession curve with fixed starting points but various lengths. The median values of ΔB (red dots in Figure 3-6) for all gauges are around 0.5. Similar results (not shown) were obtained when repeating similar analysis using the CTS and VTS methods. Cautions should be exercised when comparing *A* and *B* values for different events, especially if the difference in the lengths of the two recession segments used to estimate *A* and *B* is large.

3.3.3 Variability due to parameter estimation methods

The analysis of a single event shows considerable differences among the values of *B* estimated by different methods (Figure 3-7). A recession segment was extracted from the same recess event as described in Section 3.3.1 with a starting point of 2 days after the hydrograph peak and a length of 7 days. This segment and the three methods introduced in Section 3.2.3 were used to estimate the value of *B*. Figure 3-7 shows that the parameters estimated by the NDF method are most effective in terms of reproducing the given recession segment. Surprisingly, the difference among the values of *B* estimated by these methods can be as high as ~0.6. Both the CTS and the VTS methods estimate *A* and *B* in the log-log scale using the least squares linear regression, and therefore the goals are to maximize the amount of variation in $log(-dQ/dt)$ rather than that in $-dQ/dt$ that is explained by the power-law recession models. In contrast, the NDF method estimates *A* and *B* in the original units using iterative direct curve fitting. This

leads to different optimal solution for *A* and *B*. A sensitivity analysis of these methods to the choice of Δt is provided in Appendix B at the end of the thesis. The impact of noise in recession data on these discrepancies will be discussed later in Section 3.3.4. We will investigate whether these differences in the values of *B* estimated by different methods are statistically significant.

Analyses of all of the recession events selected at the Clear Creek near Coralville, Iowa shows that the values of *B* estimated by the three methods are statistically different (Table 3-1). We selected one segment from each of the 30 recession events observed at the Clear Creek stream gauge near Coralville using a starting point of 2 days after the hydrograph peak and a length of 7 days. For all recession segments, we estimated *B* values using the three methods and conducted three paired t-tests of the estimates: CTS versus VTS, CTS versus NDF, and VTS versus NDF, respectively. Our paired t-tests showed that the estimates of *B* given by the three methods were different from each other at the significance level of $p = 0.05$.

We repeated the paired t-tests described above for the other 24 sub-basins in the Iowa and Cedar River basins. We extracted ~750 recession segments from observations at 25 USGS gauges using the same starting point of 2 days after the hydrograph peak and the same recession length of 7 days. For 17 out of the 25 gauges investigated, the paired t-tests indicated that *B* estimates given by the three methods were statistically different at the significance level of $p = 0.05$ (Table 3-2). This significant differences suggest that it would be wise to ascertain that recession parameters are estimated using the same method when comparing them across events.

In conclusion, the artificial variability of *B* resulting from the calculation procedure is comparable to the variability of *B* among individual recession events. For the Clear Creek basin, Table 3-1 shows that the variability of *B* among 30 individual recession events measured by interquartile range is about 0.7. Table 3-1 also shows that, for individual events, the differences between estimates of *B* given by the three methods

can vary from 0 to ~1. For multiple basins, Table 3-2 shows that the variability of *B* among individual recession events is around 1.0 (median value) and the difference caused by the method of choice is about 0.3 (median value). Additionally, as we reported in Section 3.3.1 and 3.2, the differences in the estimates of *B* for the same recession event are 1.0 and 0.5 due to changes in the starting points and lengths used to extract recession segments, respectively. These numbers suggest that when interpreting the temporal variability in the recession behavior (e.g., represented by *A* and *B*) of a basin, it is important to reduce the variability in the recession parameters caused by the procedure of recession segment selection and parameter estimation.

Comparison showed that the parameters estimated by the NDF method better reproduced given recession segments (smaller modeling error) than those estimated by the CTS and the VTS methods (Table 3-2). For the majority of ~750 recession events investigated, the given recession segments were the best and worst reproduced by the parameters estimated by the NDF and the CTS methods, respectively. Based on this, it seems that the NDF method outperforms the other two in estimating the recession parameters. It is worthy to note that the NDF method produces more reliable estimates of *A* and *B* at the expense of requiring slightly longer computational time (<1 second). It is interesting to understand why the NDF method is more effective. Probably the noise in recession data contributes to the differences in and the effectiveness of the parameter estimates. Since the VTS method is more advanced in dealing with the noise in recession data than the CTS method is, we will use a Monte Carlo simulation method to compare only the robustness of the VTS and the NDF methods to the uncertainty in recession data in the next section.

3.3.4 Effect of uncertainties in streamflow

This investigation was limited to the Clear Creek basin as its recession analysis results are representative of other basins (Table 3-1 and Table 3-2). We generated the

noise-free ("true") recession segment based on our understanding of the recession behavior at the Clear Creek stream gauge near Coralville, Iowa. A visual examination of the complete recession curves at this gauge reveals that discharge usually drops below 2 mm/day two days after hydrograph peaks. Typical values of *A* and *B* at this gauge are 0.15 and 2.0, respectively, based on the analysis of the recession segments that start two days after a hydrograph peak with a length of seven days (Table 3-2). Thus, we created a seven-day long noise-free recession segment with an hourly time step using the power law function $^{dQ}\!/_{dt} = -0.15Q^{2.0}$ and an initial discharge of 2 mm/day. This noise-free recession segment was corrupted with either multiplicative uncorrelated noise or multiplicative correlated noise.

Among the noise processes we investigated, the NDF method is more robust with respect to data errors and thus is preferred for parameter estimation. Figure 3-8 shows that the mean values of the estimates of *B* given by the NDF method are close to the true value of 2.0, regardless of the existence of correlation in and the magnitude of the data noise. In contrast, the mean values of the estimates of *B* given by the VTS method tend to deviate from 2.0 as the magnitude of uncorrelated error increases. Furthermore, at each magnitude of the noise, the NDF method gives less variable estimates of *B*, indicating that it is more robust with respect to the noise in the recession data. As anticipated, for both methods, the estimation of *B* deteriorates as the magnitude of uncertainty in recession data increases. For the correlated error case shown in Figure 3-8, we contaminated the noise-free recession curve with noise correlated at the level of ρ = 0.6. We decided on this value based on a brief sensitivity study.

We investigated how the levels of correlation of the data noise (ρ) and the length of recession segments affect the comparison results. We first estimated the recession parameters for each of the observed recession events at Clear Creek using the NDF method and subsequently used the estimated *A* and *B* values to reproduce the associated recession segment. We then fitted AR(1) models to the residuals of the recession model

for each of the events and found that the estimated values of ρ vary between 0.3 and 0.8, with a median value of around 0.6. We tested six levels of correlation, ρ = 0.3, 0.4, 0.5, 0.6, 0.7, and 0.8, and found similar results as reported in the previous paragraph. We repeated the analysis for recession segments with lengths of 3, 5, 7, and 9 days and obtained similar results, except that longer segments tend to reduce the variance of the *B* estimates.

3.4 Discussion

Recent research has suggested examining individual recession events to gain insights into hydrological processes at the scale of large watersheds (e.g., Biswal and Marani, 2010; Shaw and Riha, 2012). Such studies revealed some of the natural causes of recession variability by directly relating the recession slope and intercept and their variability to the physical factors such as aquifer recharge (Pauwels et al., 2002; van de Giesen et al., 2005; e.g., Rupp et al., 2009), evapotranspiration process (e.g., Shaw and Riha, 2012), watershed soil moisture storage (e.g., Shaw et al., 2013), and river network morphology (e.g., Biswal and Marani, 2010; Mutzner et al., 2013; Biswal and Nagesh Kumar, 2014). However, the flexibility in the procedures to estimate the recession parameters(e.g., Brutsaert and Nieber, 1977; Vogel and Kroll, 1992; Wittenberg, 1999; Rupp and Selker, 2006a) may challenge the inversion problem of determining natural causes of the recession variability. The results presented in this paper show that the variability of recession parameters due to artifacts of data analysis is comparable to that rising from natural processes. For the same recession event (Figure 3-2), notable differences in the estimates of recession parameters can arise alone from the procedure of data analysis (Figure 3-3, Figure 3-5, Figure 3-7). These differences are remarkable when compared to the range of values for the rescission slope from 1 to 3 (e.g., Brutsaert and Nieber, 1977; Rupp and Selker, 2006b). This implies that the natural variability of recession parameters can be blurred by the artifacts of recession data analysis.

Our assessment of the sensitivity of individual recession analyses to the segment selection and parameter estimation methods is complementary to the work of Stoelzle et al. (2012), which shows the impacts of recession analysis methods on the resulting recession characteristics derived using multiple events collectively. Comparative recession analyses of both individual events in a watershed and characteristic recessions between watersheds have been used in the literature to make inferences about hydrologic processes. Interestingly, both studies have shown the sensitivity of the resulting recession models to the procedure of recession analysis. Therefore, cautions should be exercised when interpreting and comparing the results of recession analysis.

The systematic approach used here to assess the sensitivity of individual recession analysis to the methodological aspects is implemented by making simplifications. First, evapotranspiration and the combined error in streamflow estimated by means of rating curve were treated as noise for recession data. These two noise sources are different in nature that the first always tends to increase and the second can either increase or decrease the recession rate. Second, the noise in recession data were characterized using either multiplicative uncorrelated or multiplicative correlated AR(1) error models in this study because there is no generally accepted error models for streamflow data. Third, when selecting a complete recession curve starting from the peak and extending to the point at which the hydrograph begins to rise, we took the last peak as the hydrograph peak and omitted the short recession segments between multiple peaks. Lastly, for the variable time step parameter estimation method, a constant threshold was used in this study. Accounting for details of either of these simplifications would increase the accuracy of our sensitivity assessment, but would also make the assessment process more complex. The findings presented above would remain.

3.5 Conclusion

We used a systematic approach, similar to those designed by Tallaksen (1995), Hammond and Han (2006), and Stoelzle et al. (2012), to assess the sensitivity of individual recession analyses to the segment selection and parameter estimation methods. Our results draw from analyzing ~750 recession events observed at 25 USGS gauges suggested that: 1) the determination of the recession model $dQ/dt = -AQ^B$ for individual recession events is sensitive to the segment selection and parameter estimation methods used; 2) due to using different recession segments and calculation methods, the variations of the parameter estimates for the same recession event were comparable to the variations of *A* and *B* between different recession events; and 3) among the parameter estimation methods investigated in this study, the nonlinear direct fitting method proposed by Wittenberg (1999) tends to be most robust with respect to the uncertainty in streamflow data. The first two findings are consistent with Stoelzle and Stahl's (2012) conclusion that the results of examining multiple recession events collectively are sensitive to the recession extraction and parameterization methods.

Given the arbitrariness in the field of recession data analysis, our study complements the previous studies and raises cautions for comparative analyses of individual recessions. When investigating the causal relation between natural processes and the dynamics of recession behavior (e.g. the variability in recession parameters), the artifacts introduced by the calculation procedure should be recognized and reduced. To achieve this goal, we recommend using a consistent approach to select recession segments and using the nonlinear direct fitting method to estimate the recession parameters for individual events.

Table 3-1. Comparison of the estimates of recession parameters *A* and *B* at Clear Creek near Coralville, Iowa (USGS 454300) calculated using the CTS, VTS and the NDF methods. All recession segments have a starting point of 2 days and a length of 7 days.

Starting Date	A			B			Modeling error (%)		
Year/month/day	CTS	VTS	NDF	CTS	VTS	NDF	CTS	VTS	NDF
1995/07/06	0.22	0.19	0.20	0.30	1.41	1.94	54.63	9.82	0.41
1996/06/07	0.18	0.14	0.11	1.05	0.68	1.04	18.50	4.04	0.53
1997/05/08	0.20	0.16	0.21	0.42	1.20	2.08	41.51	5.71	0.68
1997/05/26	0.20	0.15	0.15	0.32	0.98	1.48	17.06	0.58	0.13
1998/10/05	0.26	0.13	0.13	1.42	2.17	2.52	15.49	3.38	0.51
1998/11/10	0.16	0.09	0.06	0.86	1.42	2.32	19.02	3.96	0.07
1999/04/23	0.17	0.06	0.06	1.13	2.32	1.84	21.00	5.66	0.23
2000/06/15	0.29	0.16	0.14	0.72	1.26	2.24	29.07	0.67	0.42
2000/07/10	0.32	0.18	0.18	1.13	1.76	2.08	29.54	0.17	0.96
2001/06/14	0.30	0.08	0.07	0.59	2.55	3.04	29.67	0.12	0.75
2001/10/23	0.29	0.53	1.48	0.54	1.92	3.78	47.87	11.45	3.49
2002/04/28	0.18	0.15	0.13	0.56	1.77	1.92	27.03	5.54	0.17
2002/08/23	0.30	1.33	1.84	0.37	2.23	2.54	60.57	3.31	0.40
2002/10/04	0.25	0.55	0.89	0.41	2.83	3.68	50.61	2.74	0.50
2004/05/31	0.21	0.13	0.12	1.23	1.66	2.12	20.19	2.82	0.46
2005/04/12	0.22	0.14	0.14	1.03	2.20	3.02	25.59	3.59	0.18
2007/04/13	0.17	0.12	0.09	0.88	1.92	2.92	18.31	5.45	0.77
2007/05/07	0.16	0.11	0.09	1.17	1.74	2.66	10.08	1.23	0.18
2007/06/24	0.26	0.14	0.14	1.02	1.36	1.60	16.17	7.28	0.07
2007/08/24	0.22	0.14	0.14	1.14	1.87	2.18	3.70	3.55	0.44
2007/10/02	0.23	0.22	0.24	0.31	3.00	3.72	37.19	1.92	0.11
2007/10/18	0.24	0.08	0.08	0.81	2.15	2.32	10.67	3.96	0.77
2008/07/22	0.27	0.10	0.09	0.69	1.46	1.66	23.47	0.41	0.16
2008/09/29	0.35	0.24	0.17	2.37	3.90	4.00	25.82	4.43	1.25
2009/06/24	0.10	0.08	0.08	1.70	2.15	2.20	1.47	3.16	0.06
2009/07/11	0.10	0.08	0.09	1.87	2.13	2.20	3.43	4.27	0.03
2009/07/25	0.13	0.13	0.15	0.49	1.83	2.64	16.19	2.51	0.18
2009/08/28	0.09	0.07	0.08	1.85	2.13	2.12	2.43	2.95	0.24
2009/10/30	0.04	0.04	0.03	2.30	2.54	2.80	2.21	3.01	0.25
2010/08/21	0.14	0.12	0.13	0.89	1.94	2.74	12.66	2.25	0.03
Median	0.21	0.14	0.13	0.88	1.92	2.28	19.61	3.35	0.33
Interquartile Range	0.10	0.07	0.08	0.62	0.69	0.71	16.06	2.08	0.36

Table 3-2. Comparison of the estimates of *B* at 25 gauges calculated with the CTS, VTS and NDF methods. All gauges are located within the HUC05 of the United States, and we use only the last six digits of their complete USGS gauge ID. NRec is the number of recession events analyzed; Median of *B* are the median values of *B* for multiple events at a gauge; IQR of *B* is the interquartile range of *B* estimates for multiple events at a gauge; Modeling error (%) is the median of the relative differences between the volumes of modeled and observed recession flows; *p* value is for the paired t-test; ΔB is the median value of absolute difference of *B* estimates given by two methods.

USGS Gauge No	Area (km^2)	NRec	Median of B			IQR of B			Modeling error (%)			*p*- value			ΔB		
			CTS	VTS	NDF	CTS	VTS	NDF	CTS	VTS	NDF	CTS-VTS	CTS-NDF	VTS-NDF	CTS-VTS	CTS-NDF	VTS-NDF
64942	7	14	0.55	1.31	2.06	0.80	0.88	0.70	31.21	11.39	0.83	0.15	0.01	0.00	1.31	1.75	0.76
464220	774	21	1.39	2.42	2.72	0.86	0.77	0.40	8.63	1.78	0.26	0.00	0.00	0.00	1.09	1.44	0.22
463500	784	18	2.03	2.38	2.63	0.73	0.71	0.82	0.69	0.87	0.39	0.00	0.00	0.00	0.32	0.62	0.20
458000	792	25	1.73	2.14	2.24	1.12	0.99	0.66	4.34	2.10	0.62	0.00	0.00	0.28	0.48	0.43	0.23
463000	898	30	1.78	2.20	2.48	1.09	0.75	1.02	1.25	1.19	0.56	0.00	0.00	0.01	0.33	0.41	0.23
457000	1033	12	1.45	1.96	1.89	0.30	0.77	1.18	4.15	1.32	0.26	0.00	0.00	0.05	0.55	0.62	0.24
459500	1362	38	1.19	1.45	1.62	0.81	0.85	1.17	4.03	1.26	0.37	0.02	0.00	0.01	0.26	0.58	0.15
458900	2190	24	1.93	2.27	2.13	0.94	1.29	1.43	1.96	1.38	0.87	0.00	0.00	0.45	0.16	0.39	0.20
457700	2729	22	1.47	1.65	2.08	0.70	1.05	1.43	8.21	3.19	0.52	0.00	0.01	0.25	0.37	0.68	0.27
458500	4300	13	1.76	1.82	2.14	0.82	0.62	0.90	1.76	1.19	0.31	0.00	0.00	0.20	0.53	0.74	0.23
462000	4520	33	1.19	1.59	1.66	0.62	0.63	0.84	1.60	0.83	0.24	0.00	0.00	0.25	0.23	0.33	0.13
464000	13322	25	1.77	2.04	2.22	0.68	0.64	0.48	2.60	0.88	0.59	0.00	0.00	0.00	0.31	0.54	0.30
464500	16854	9	1.54	1.67	2.18	1.15	1.23	1.54	5.60	1.42	0.30	0.07	0.06	0.08	0.47	0.98	0.51
454000	66	41	0.32	1.42	2.16	0.38	0.46	0.80	24.66	10.03	0.61	0.00	0.00	0.00	1.13	1.82	0.76
451900	145	41	0.73	2.11	2.70	0.48	0.90	0.90	29.52	5.51	0.45	0.00	0.00	0.00	1.31	1.85	0.64
454220	151	30	0.98	1.84	2.37	0.41	0.28	0.86	21.73	2.88	0.26	0.00	0.00	0.00	0.85	1.35	0.49
452200	184	35	0.67	1.51	2.14	0.49	0.39	0.69	28.45	4.36	0.40	0.00	0.00	0.00	0.81	1.47	0.62
454300	254	30	0.88	1.92	2.28	0.62	0.69	0.71	19.61	3.35	0.33	0.00	0.00	0.00	1.04	1.49	0.53

Table 3-2. Continued

451700	306	25	1.21	1.96	2.62	0.52	0.48	0.88	7.31	2.43	0.61	0.00	0.00	0.00	0.66	1.36	0.69
453000	489	39	1.13	2.17	2.62	0.77	0.86	0.99	18.93	1.98	0.62	0.00	0.00	0.00	0.78	1.18	0.38
452000	520	31	1.63	2.45	2.82	0.85	0.52	0.80	6.65	0.94	0.29	0.00	0.00	0.00	0.73	1.34	0.46
451210	580	34	1.47	2.03	2.20	0.58	0.55	0.75	10.55	1.77	0.56	0.00	0.00	0.00	0.45	0.69	0.18
455500	1486	43	1.74	2.07	2.14	0.43	0.37	0.60	2.00	1.56	0.72	0.00	0.00	0.00	0.22	0.35	0.14
451500	3966	21	1.20	1.56	1.46	0.58	0.75	0.78	2.54	1.58	0.53	0.00	0.02	0.58	0.29	0.33	0.20
453100	7233	21	1.75	2.17	2.18	0.91	0.80	1.18	1.04	1.16	0.57	0.01	0.22	0.23	0.17	0.30	0.20

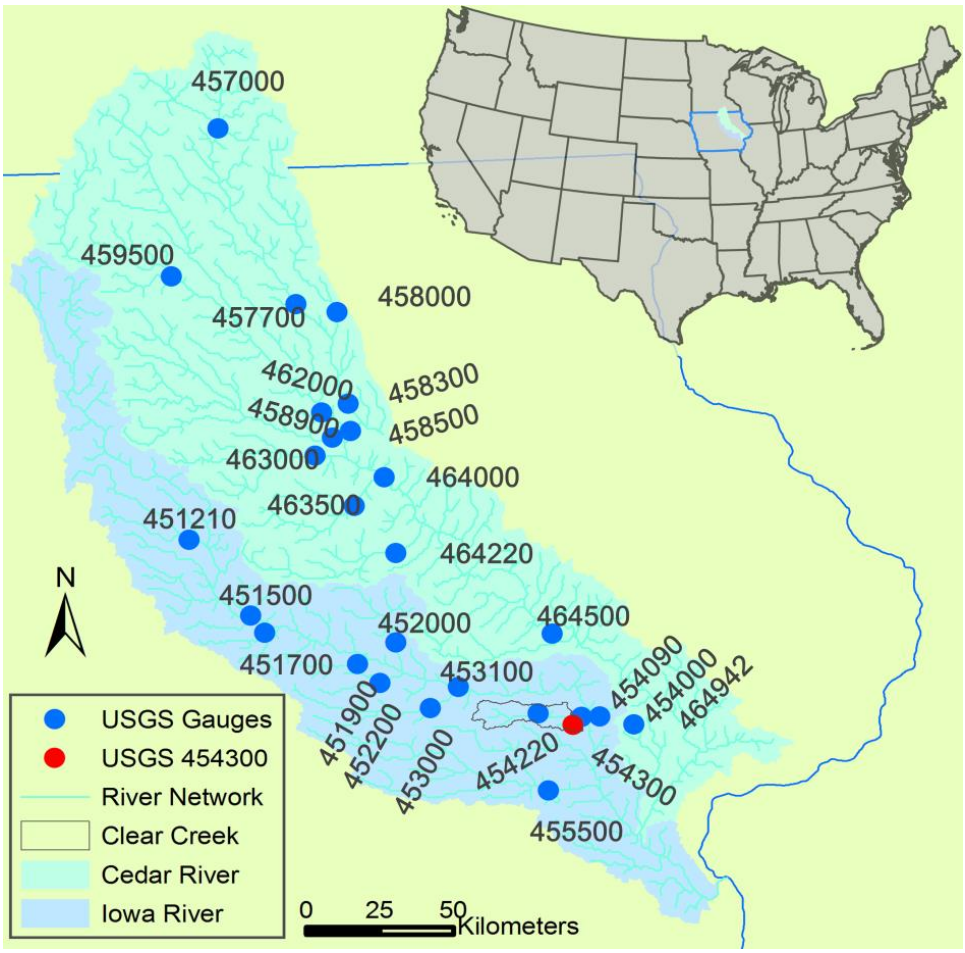

Figure 3-1. Location of the USGS stream gauges used in this study.

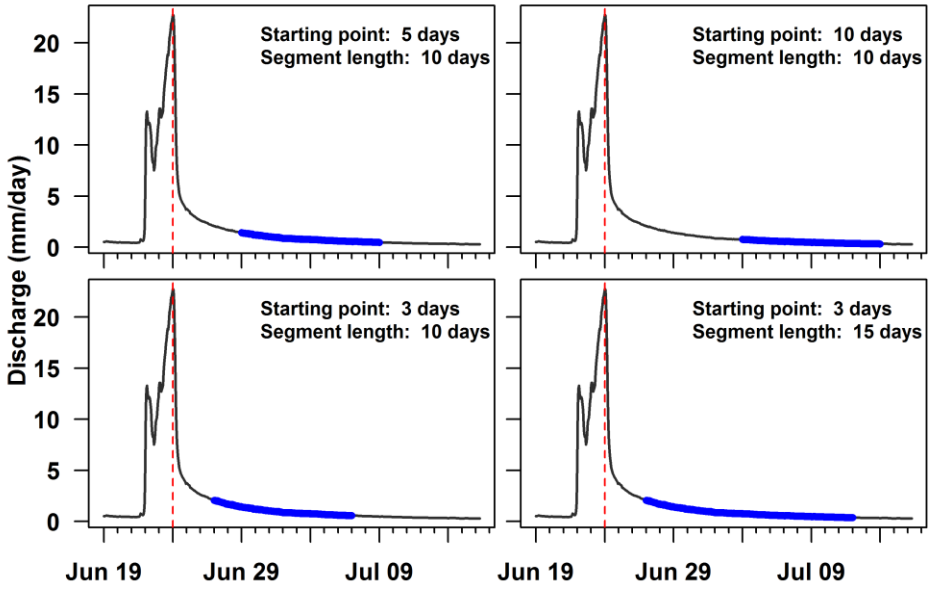

Figure 3-2. The schematic of selecting recession segments from a complete recession curve by fixing the length while varying the starting points (upper panels) and by fixing the starting point while varying the lengths (lower panels). The starting point of a recession segment is measured from the hydrograph peak that is marked by the red dashed-line. The blue curve is the recession segment used to estimate the recession parameters *A* and *B*. This is a 27-day long complete recession curve observed at Clear Creek near Coralville, Iowa (USGS 454300) and spanned from June 24, 2007 until July 19, 2007.

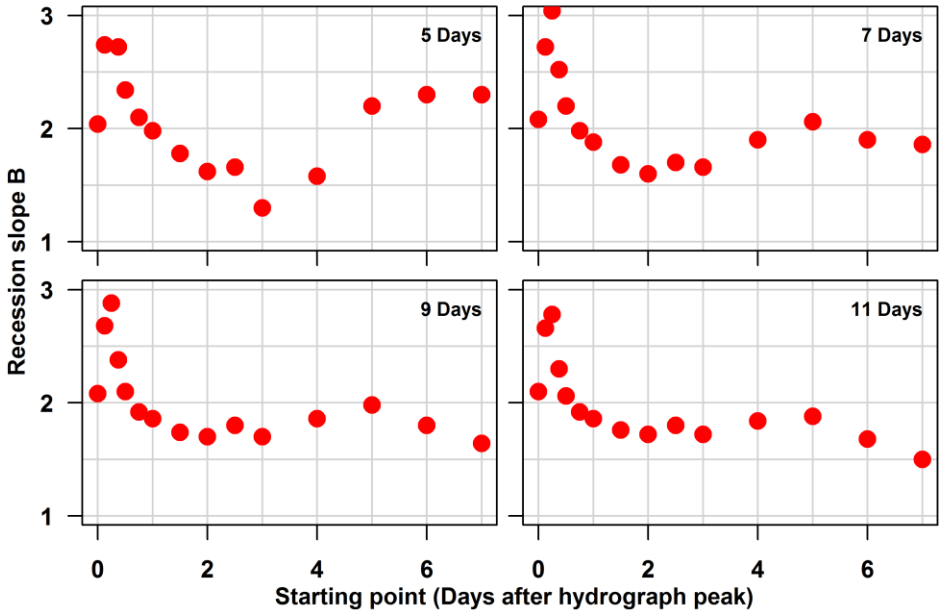

Figure 3-3. Variability of *B* estimates due to the change in starting points of recession segments (a single event). The same example recession event as in Figure 3-2 is used here. The text at the top right corner is the length of the recession segments used to estimate *B*. At each fixed recession length, we first extracted recession segments using different starting points (0~7 days after hydrograph peak) and then estimated the values of *B* using the NDF method. The range of *B* values (defined as $\Delta B = B_{max} - B_{min}$) due to the change in starting points is about 1.5 for this example event.

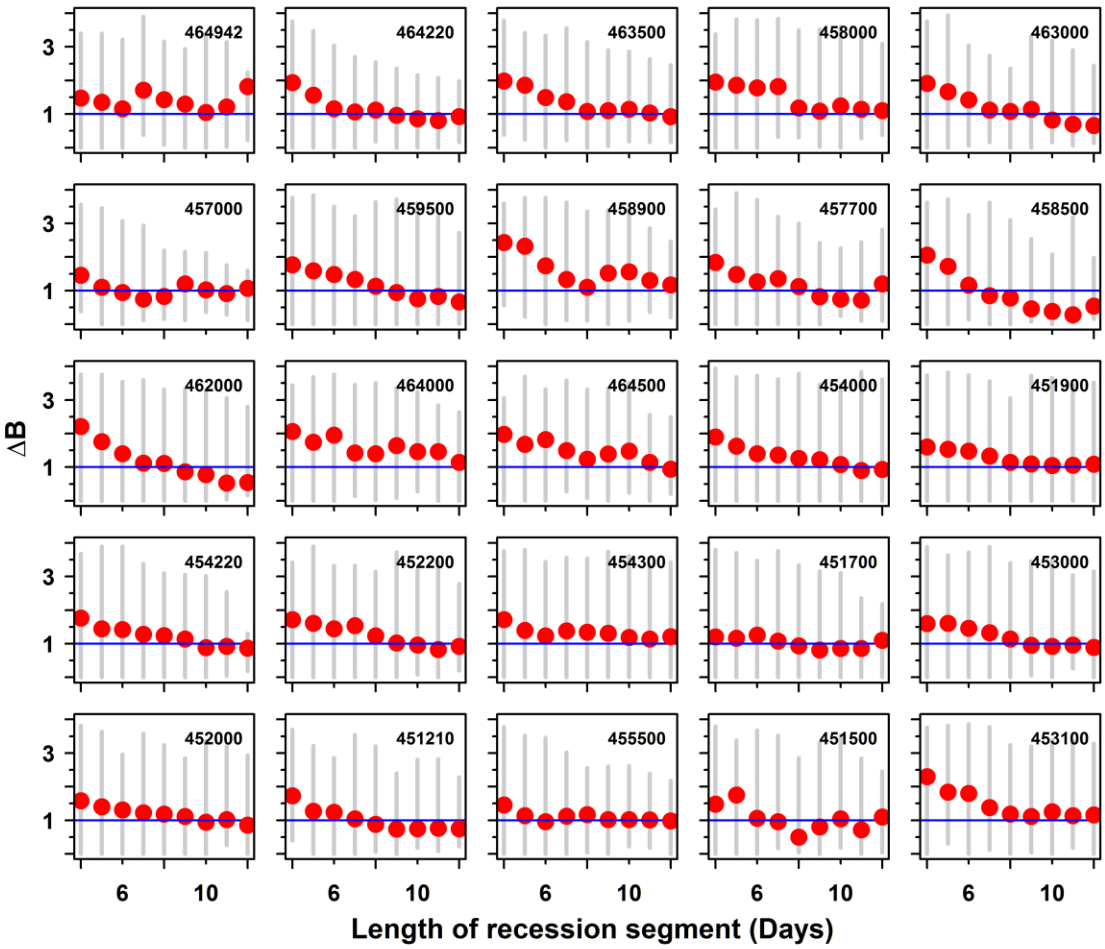

Figure 3-4. Variability of *B* estimates due to the change in starting points of recession segments (multiple events). For each USGS gauge (see gauge ID at the top right corner), we repeated the analysis in Figure 3-3 to obtain ΔB values for all of the recession events. Each red dot is the median value and each gray line segment represents the range of ΔB at a fixed recession length. The median values of ΔB for all gauges are around 1.0.

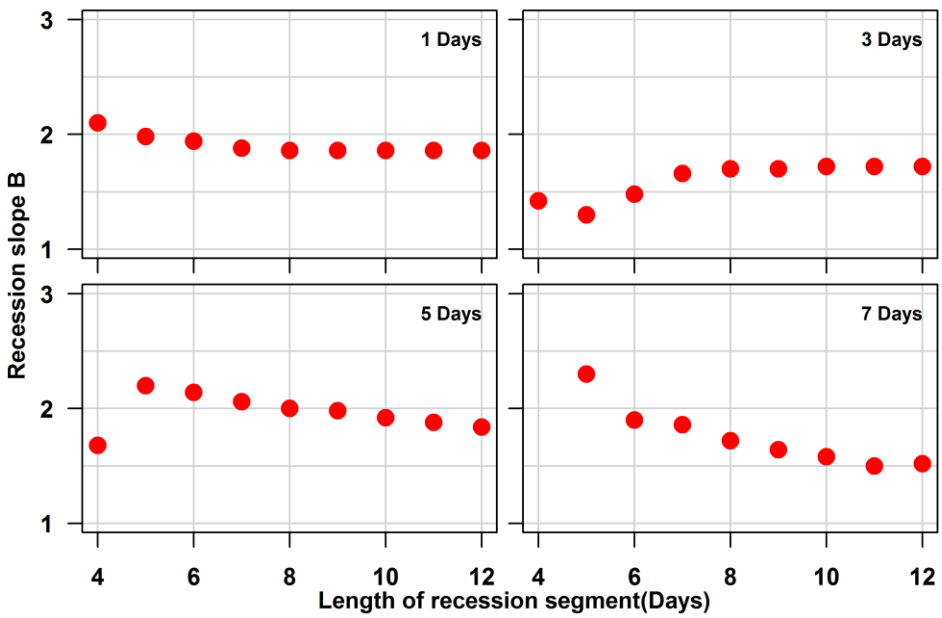

Figure 3-5. Variability of *B* estimates due to the change in lengths of recession segments (a single event). The same example recession event as in Figure 3-2 is used here. The text at the top right corner is the starting point (number of days after hydrograph peak) of the recession segments used to estimate *B*. At each fixed starting point, we first extracted recession segments using different lengths (4~12 days) and then estimated the values of *B* using the NDF method. The range of *B* values (defined as $\Delta B = B_{max} - B_{min}$) due to the change in recession lengths is about 0.5 for this example event.

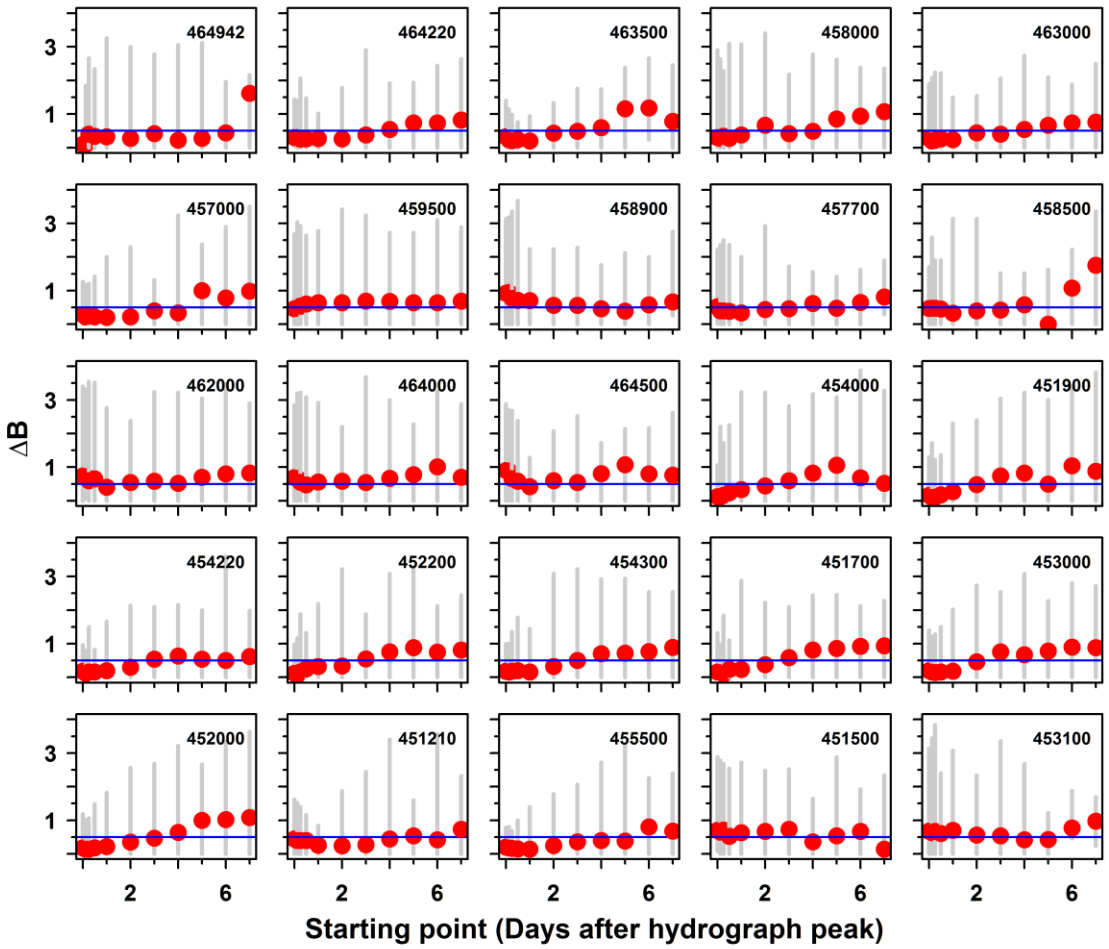

Figure 3-6. Variability of *B* estimates due to the change in lengths of recession segments (multiple events). For each USGS gauge (see gauge ID at the top right corner), we repeated the analysis in Figure 3-5 to obtain ΔB values for all of the recession events. Each red dot is the median value and each gray line segment represents the range of ΔB at a fixed starting point. The median values of ΔB for all gauges are around 0.5.

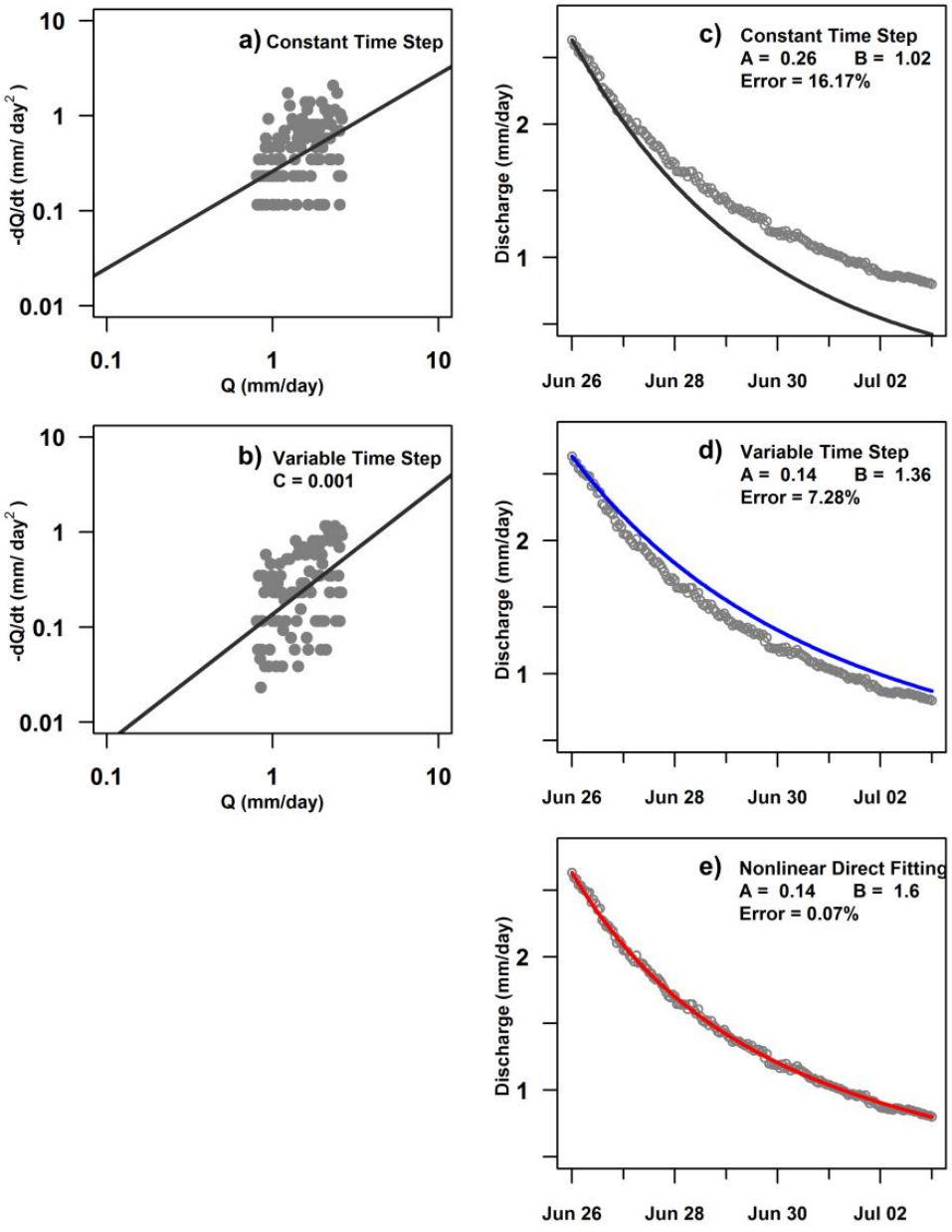

Figure 3-7. Variability of parameter estimates due to method choices. The same example recession event as in Figure 3-2 is used here. We extracted the recession segment from the complete recession curve using a starting point of 2 days and a length of 7 days. The parameters for the selected segment were estimated using the CTS ((a) and (c)), VTS ((b) and (d)) and NDF ((e)) methods. In (b), (d), and (e), the open circles are the measured streamflow values, and the lines are the modeled recession segments using the estimated parameters. For the VTS method, the value C = 0.001 was used to reduce the impact of the noise in streamflow data on the estimation of recession parameters. The modeling error was calculated as the relative difference between the volumes of modeled and observed recession flows.

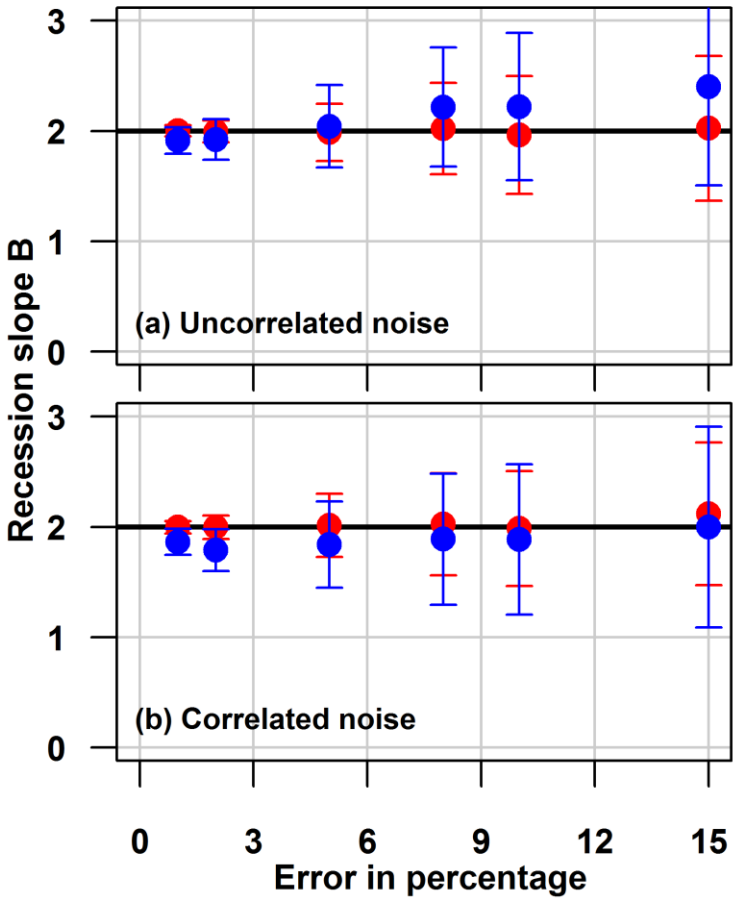

Figure 3-8. Robustness of the VTS (blue) and the NDF (red) methods to the noise in streamflow data. The true value of *B* is 2. Filled circles represent the mean values of *B*. Error bars show the standard deviation of *B* estimates at each magnitude of error. The mean and standard deviation were obtained based on the results of 1000 simulations. The length of the recession segment used is 7 days (168 hourly flow values). The uncorrelated noise are generated from a normal distribution $N(0, \sigma)$. The correlated noise are generated from the AR(1) model $E(t)= \rho E(t-1) + \varepsilon(t)$, where ρ is the correlation coefficient (ρ = 0.6 for this figure), $\varepsilon(t)$ is an i.i.d. random variable with mean 0 and standard deviation $\sqrt{1-\rho^2}\,\sigma$, and σ is the magnitude of data noise in percentage.

CHAPTER 4

DISSECTING RECESSION CURVES

4.1 Introduction

The hydrological response of a basin is determined by the flow paths of rainfall falling on each point within its boundary and the velocity of the water particles on their routes to the outlet. Hydrograph separation using a recession curve is one of the most frequently used techniques to identify flow sources which are strongly associated with flow paths (e.g., Pilgrim et al., 1979; Hooper and Shoemaker, 1986; Quinn et al., 1991; Tallaksen, 1995; Brown et al., 1999). The traditional multiple-reservoir hypothesis postulates that a basin partitions rainfall into different reservoirs, stores the water for various residence times, and ultimately releases the stored water at different rates in the forms of either evapotranspiration or streamflow (e.g., Griffiths and Clausen, 1997; Wagener et al., 2007). Therefore, the recession curve is a composite, i.e., different reservoirs dominate different stages of the outflow process, and it is often decomposed into fast near-surface flow, delayed soil matrix flow, and further delayed groundwater flow (e.g., Brutsaert and Nieber, 1977; Sivapalan, 2003; Sivapalan et al., 2003). The decomposition is commonly used to make inferences about hydrological processes in order to further assist basin storage estimation and enhance hydrological modeling (e.g., Brutsaert and Lopez, 1998; Wittenberg and Sivapalan, 1999; McDonnell et al., 2007; Spence, 2007; Kirchner, 2009; Seyfried et al., 2009; Biswal and Marani, 2010).

Many methods that have been proposed to decompose hydrographs are more or less subjective (e.g., Nathan and McMahon, 1990; Arnold et al., 1995; Tallaksen, 1995; Smakhtin, 2001; Eckhardt, 2005). The existing methods designed for hydrograph separation can be grouped into four general categories. The first entails graphical

techniques such as the straight line, fixed base, variable slope, and inflection point methods. These methods are based on a visual inspection of the recession curve's shape. The second entails digital filters, including methods developed by Nathan and McMahon (1990) and Eckhardt (2005), which filter out high-frequency fast flow while retain low-frequency base flow. The third group includes thresholding methods based on the empirical recognition of the natural process of hydrograph recession. These methods assume that fast flow ends either X-days ($X \geq 2$) after the hydrograph peak or when discharge drops below a certain threshold. Lastly, the fourth group consists of a chemical tracer-based approach that adopts the end member analysis (e.g., McDonnell et al., 1990; Genereux, 1998). The first three categories include various degrees of subjectivity: the graphic method depends on visual inspection; the digital filters eliminate some of the subjective elements but still rely on parameters which might be assigned subjectively; and the thresholding method is the most experience-based. The chemical tracer-based approach is usually used in hillslope hydrology but is technically challenging (due to the difficulty in determining the end members) and expensive to apply to large basins (e.g., Genereux, 1998; Uhlenbrook and Hoeg, 2003). These limitations weaken the reliability of the inferences made from hydrograph separation and hamper a wider use of the hydrograph separation technique.

To explore whether there is a more objective way to dissect a hydrograph recession into stages of the outflow process dominated by different storages, we analyzed the evolution path of the recession exponent B in equation (4-1) and related it to the outflow process,

$$\frac{dQ(t)}{dt} = -A[Q(t)]^B \qquad (4\text{-}1)$$

where $Q(t)$ is the total discharge (as the sum of flow from different reservoirs) at time t and A and B are parameters. The notion that different reservoirs can be characterized by different parameters, e.g., exponent B in equation (4-1) (Brutsaert and Nieber, 1977; Brutsaert and Lopez, 1998), implies that along with a recession process there is an associated evolution path of the recession exponent B. We followed this track to dissect hydrograph recession curves. Since there is no standard definition for streamflow components, in this study, fast flow refers to flow that vanishes in the first few hours after the peak discharge and contains both overland flow and quick subsurface flow. We assume that streamflow can be decomposed into fast flow, delayed soil water flow, and groundwater flow and that hydrograph recession can be separated into stages that are dominated by fast flow, soil water, and groundwater storages, accordingly.

The structure of this paper is as follows. Section 4.2 describes the data set used in the study. Section 4.3 introduces our method of recession analysis. Section 4.4 reports the results of the recession analysis, and section 4.5 provides an explanation of the observed phenomena. We close with a discussion and conclusions presented in sections 4.6 and 4.7, respectively.

4.2 Data

To increase the reliability of our analysis, we used recessions from multiple sites across scales under various weather conditions. We analyzed about 1000 recession curves over a period of around 15 years (1995-2010) from time-series of hourly discharge (USGS Instantaneous Data Archive streamflow data set) at 27 stream gauges in the Iowa and Cedar River basins in Iowa (Figure 3-1 and Table 4-1). The corresponding drainage areas at the gauge locations range from ~10 to 17000 km^2. The study region is fairly flat and has an average annual precipitation of 900 mm. Approximately three-fourths of the precipitation and 85% of the 45-65 thunderstorms occur from April through September (Villarini et al., 2011). Frozen soils near the surface last from late October to early April.

Considering the aforementioned facts, we selected only summer and autumn recessions. To limit the study to recessions following significant storms, we selected recessions corresponding to peak discharges greater than the 95% quantile of the streamflow of each gauge. Furthermore, to reduce the possible impacts of intervening rainfall and uncertainties carried by streamflow data, we analyzed only the recession segments with a monotonically decreasing trend. A complete recession begins with peak discharge and ends when the 24-hour moving average discharge begins to increase. We considered only recessions longer than five days as candidates.

4.3 Method

We assumed that each portion of a given recession curve represents the outflow process of a dominant reservoir (storage), and the reservoir can be characterized by parameter *B*. To examine the evolution path of the recession exponent *B* for an individual hydrograph recession, we selected recession segments, i.e., portions from the entire hydrograph recession, by keeping the recession length constant and systematically changing the starting point, and calculated the corresponding recession exponent *B* (see Figure 4-1). We repeated this analysis for all hydrographs included in the study. The pattern seen in Figure 4-1 is a systematic feature of the recession process, as we demonstrate in subsequent sections. There are tens of unique recession events for each basin; therefore, we needed a way to synthesize the evolution paths of *B* for all the hydrograph recessions. We selected the sample median as the characteristic evolution path of recession exponent *B* to represent the recession behavior of a basin. This is similar to the characteristic recession concept summarized by(Tallaksen, 1995).

4.3.1 Selection of recession segments

Since the calculation of *B* depends on both the recession's starting point and length, Tallaksen (1995) suggests selecting recession segments with the same starting

point and length in a consistent way. However, there is no standard guideline for when to start and end an analysis segment. To examine the evolution path of *B*, i.e., how *B* changes with the starting points of recession segments, the potential impact of changing recession lengths should be considered. We investigated the evolution paths of *B* at multiple recession lengths and checked for consistent patterns. Figure 4-2 shows the procedures we used to construct the evolution paths of *B* for an individual recession event and for a basin. In this study, we varied the starting points systematically from 0, 2, 4, 6, 9, 12, 18, 24, 48, 72, and 96 hours after the hydrograph peak (hereafter we call it "time lag") and the recession lengths from 1, 2, 3,… up to 10 days if the recession was long enough (i.e., not interrupted by a following storm event). For the selected recession segments, we calculated the corresponding values of *B* using the method described below in Section 4.3.2.

4.3.2 Method to calculate event-based recession exponent

For a given recession segment, we employed the iterative least-squares method suggested by Wittenberg (1999) to estimate the recession exponent *B*. We varied exponent *B* systematically from 0 to 5 with a step size of 0.01. For each value of *B*, value *A* was calculated using equation (4-2)

$$A = \frac{\sum_{t=1}^{n}[Q(t-1) - Q(t)]}{\Delta t \sum_{t=1}^{n}[\frac{Q(t) + Q(t-1)}{2}]^{B}} \tag{4-2}$$

where *n* is the length of the recession curve, and $\Delta t = 1$ hour is the time step. Solving equation (4-1) for *Q(t)* gives

$$Q(t) = Q(0)[1 - \frac{(1-B)At}{[Q(0)]^{1-B}}]^{1-B} \tag{4-3}$$

where *Q(0)* is the discharge at the starting point of the recession segment used to calculate exponent *B*, and $\boldsymbol{t}$ is the number of hours elapsed from the starting point. Using values of *A*, *B*, and *Q(0)*, equation (4-3) provides a simulated hydrograph and the associated relative prediction error *RE* in volume (time-integrated discharge) is calculated as

$$RE = \frac{V_{obs} - V_{pred}}{V_{obs}} \times 100\% \qquad (4\text{-}4)$$

We selected the optimal pairs of *A* and *B* when the relative error in equation (4-4) was at the minimum.

4.4 Results of data analysis

We examined hydrograph data from 27 sub-watersheds in the Cedar and Iowa River basins in Iowa following the method presented in Section 4.3. Figure 4-3 presents the evolution path of *B* for four representative events observed at the USGS gauge Clear Creek near Coralville, Iowa. Each panel of Figure 4-3 is similar to the lower portion of Figure 4-1 and shows how recession exponent *B* changes with recession start (i.e., lag from hydrograph peak) when recession length (labeled in the upper right corner) is fixed. For example, the panel in the second row and first column in Figure 4-3 shows that, for the recession event occurring on June 24, 2007, when the length of the recession segment is fixed as 4 days, the recession exponent *B* first increases, then decreases, and finally tends to remain approximately constant as the starting point of recession segment moves away from the hydrograph peak. To determine whether this pattern is independent of the recession lengths used to calculate *B*, we repeated the procedure described in Figure 4-2 for different recession lengths. We summarize the results in Figure 4-3(a). To further test if this pattern holds across recession events, we repeated the process used to create Figure 4-3(a) in order to produce Figure 4-3(c) ~ (d).

Our investigation of individual recession events shows that recession exponent *B* varies in three distinct ways as recession continues: (i) *B* increases, then decreases, and then finally remains roughly constant (Figure 4-3(a) and (c)); (ii) *B* increases and stays roughly constant (Figure 4-3(b)); and (iii) *B* increases at the beginning and then decreases (Figure 4-3(d)). Generally, we observe more consistent patterns in the evolution of *B* when the recession length is greater than 5 days. This is probably because the method used to estimate *B* is sensitive to uncertainties carried in the streamflow series, undetected light rainfall, and the neglect of evapotranspiration. It is also interesting that the turning points of the evolution of *B* in Figure 4-3 do not change significantly with recession lengths. This has practical significance of avoiding concerns about how to select a recession length to construct the evolution path of *B*, as long as the recession length is greater than 5 days.

We followed the method described in Section 4.3 to further test whether the observed pattern is statistically significant across events in a specific basin. We examined all of the 70 recession events observed at the USGS gauge at Clear Creek near Coralville, Iowa. In Figure 4-4, we superimpose the characteristic evolution path of *B* onto its individual evolution paths. At each combination of recession length and start, we calculated the *B* values (black dots along the same vertical line in each panel) for all of the recession events and selected the sample median as the characteristic recession exponent *B* (the red dots). Each panel of Figure 4-4 shows how the characteristic recession exponent *B* changes with recession start (i.e., lag from hydrograph peak) when recession length (labeled in the upper right corner) is fixed. For instance, the fourth panel in Figure 4-4 shows that, for the basin that drains through the outlet at the USGS gauge at Clear Creek near Coralville, Iowa, when the length of the recession segment is fixed as 4 days, the characteristic recession exponent *B* first increases, then decreases, and finally tends to remain approximately constant as the starting point of the recession segment moves away from the hydrograph peak. We explored the dependency of this pattern on

recession length and produced the rest panels of Figure 4-4. Apparently in Figure 4-4, there are significant scatter along each vertical line. This scatter shows that recession processes varied across time even in the same basin. These differences in recession processes might be caused by discrepancies in spatiotemporal characteristics of rainfall fields, antecedent soil moisture condition, seasonality, and possibly the uncertainties embedded in streamflow observations.

Figure 4-5 displays further investigation about how this pattern changes across basins. In Figure 4-5, we show the characteristic evolution of *B* at 25 USGS gauges with drainage areas ranging from 7 to about 17000 Km^2. Examination of the characteristic evolution of basins shows that: (i) for small and medium size basins with drainage area less than ~1000 km^2, the median values of *B* increase at the beginning, then decrease, and then finally remain roughly constant as the time lag increases; and (ii) for large basins, exponent *B* increases at the beginning then stays roughly constant.

4.5 A theoretical explanation

To study the evolution path of recession exponent *B*, we split a recession process into two stages, i.e., recession before and after fast flow ends. We first explore mathematically how recession exponent *B* changes as recession continues before fast flow ends, and then we summarize how recession exponent *B* varies after fast flow ends by using meta-analysis.

Our mathematical explanation begins with showing that the values of *B* calculated using the original and the peak-discharge normalized recession segment are the same. We define the peak-discharge normalized series $Q(t)^*$ as

$$Q(t)^* = \frac{Q(t)}{Q_p} \tag{4-5}$$

where $Q_p = \max(Q(t))$, which is the peak discharge. By analogy to equation (4-1),

$$\frac{dQ(t)}{dt} = -A[Q(t)]^B \tag{4-6}$$

and substituting equation (4-5) into (4-6) gives

$$\frac{dQ(t)}{dt} = -A' Q_p^{\,1-B'} [Q(t)]^{B'} \tag{4-7}$$

Comparing equation (4-1) and (4-7) indicates that *B'* equals *B* and, for convenience, we use the normalized series for further mathematical analysis. We decompose discharge $Q_t(t)$ at the basin outlet into fast flow $Q_f(t)$ and slow flow $Q_s(t)$

$$Q_t(t) = Q_f(t) + Q_s(t) \tag{4-8}$$

Fast flow includes overland flow and quick subsurface flow, while slow flow consists of soil water and groundwater flow. We assume that

$$Q_f(t) = r(t) Q_s(t) \tag{4-9}$$

where $r(t)$ is the ratio between fast and slow flow and that it decreases monotonically from r_{max} at peak discharge to 0 at zero fast flow. We further assume that before fast flow ends, $Q_s(t)$ remains approximately constant. This assumption is reasonable since the rate of change in slow flow is expected to be much smaller than that of fast flow. Substituting equation (4-9) into (4-8) gives

$$Q_t(t) = [1 + r(t)] Q_s(t) \tag{4-10}$$

and dividing both sides of (8) by $Q_p = (1 + r_{max}) Q_s(t)$ yields

$$Q_t^*(t) = Q_s^*(t) + Q_f^*(t) \tag{4-11}$$

where

$$Q_t^*(t) = \frac{Q_t(t)}{Q_p} = \frac{1+r(t)}{1+r_{max_s}}$$

$$Q_s^*(t) = \frac{Q_s(t)}{Q_p} = \frac{Q_s(t)}{(1+r_{max})Q_s(t)} = \frac{1}{1+r_{max}}, \text{ and}$$

$$Q_f^*(t) = \frac{Q_f(t)}{Q_p} = \frac{r(t)Q_s(t)}{(1+r_{max})Q_s(t)} = \frac{r(t)}{1+r_{max}}$$

Taking the derivative for both sides of equation (4-11) with respect to *t* gives

$$\frac{dQ_t^*(t)}{dt} = \frac{1}{1+r_{max}}\frac{dr(t)}{dt} \tag{4-12}$$

Combining equation (4-6), (4-11), and (4-12) yields (note that we showed *B'* = *B*)

$$\frac{1}{1+r_{max}}\frac{dr(t)}{dt} = -A'\left(\frac{1+r(t)}{1+r_{max}}\right)^B \tag{4-13}$$

and solving it for *B* gives

$$B = \frac{\ln\left(\frac{-dr(t)}{dt}\right) - \ln(A') - \ln(1+r_{max})}{\ln\left(\frac{1+r(t)}{1+r_{max}}\right)} \tag{4-14}$$

We make three observations from equation (4-14):

(i) Since *r(t)* decreases monotonically from r_{max} at peak discharge to 0 at zero fast flow, it is apparent that $0 < \frac{1+r(t)}{1+r_{max}} < 1$, and therefore, $\ln\left(\frac{1+r(t)}{1+r_{max}}\right) < 0$;

(ii) Considering that recession exponent *B* takes only positive values, and given our observation (i), the numerator in equation (4-14) has to be negative;

(iii) It is apparent that as recession continues, both $\ln(\frac{1+r(t)}{1+r_{ma}x})$ and $\ln(\frac{-dr(t)}{dt})$ decrease, with the later decreasing faster (approaching $-\infty$ from 0); therefore, *B* increases monotonically until $Q_f(t) = 0$.

As demonstrated above, exponent *B* at early recession (before fast flow diminishes) increases as recession continues. How exponent *B* changes after fast flow recedes can be explained as follows. After fast flow ends, the streamflow is fed by soil water and groundwater sources, and these storages release water at various rates (Griffiths and Clausen, 1997). According to equation (4-1), each of the storages can be characterized with different exponent *B* values. The three well-known solutions of the Boussinesq equation under the scenarios of short, intermediate, and long time after hydrograph peak show that the corresponding exponent *B* values reduce from 3 to 1.5 and then to 1(e.g., Brutsaert and Nieber, 1977; Brutsaert and Lopez, 1998; Szilagyi and Parlange, 1998; Rupp and Selker, 2006a). This theoretical result indicates that if both soil water and groundwater storages function actively after fast flow ends, we should observe exponent *B* decreasing as recession continues. The evolution of exponent *B* depends on the duration over which each storage dominates. Ideally, when a recession lasts long enough, exponent *B* would converge to a pseudo-constant recession exponent (with the gradient of *B* becoming approximately zero) characterizing the groundwater reservoir with the slowest response rate (Blume et al., 2007).

In summary, from the theoretical perspective, a certain pattern in the plot of exponent *B* against time lag from hydrograph peak should be expected. The evolution path of exponent *B* throughout an entire recession (starting from hydrograph peak) begins with a common increasing trend that is followed by a decreasing tendency that may or may not converge to a pseudo-asymptote. Discussion of the evolution paths of recession exponent *B* will be covered in section 4.6.2. For now, we conclude that exponent *B*

reaches the maximum and starts to stay roughly constant when fast flow ends and the groundwater flow begins to dominate streamflow response.

4.6 Discussion

The consistent patterns of the evolution paths of recession exponent *B* can serve as the foundation for many applications in hydrologic analysis. It can be extended to an objective method to dissect a hydrograph recession, i.e., to determine the turning points of outflow processes dominated by various flow sources. This is essential for base flow analysis, modeling, and management. It can also be used to separate hydrographs and to help identify flow sources (and thus flow paths) and evaluate their relative contributions. The potential for these applications to deepen our understanding of hydrologic processes at the basin scale will be discussed in detail in the following sections.

4.6.1 Ideal vs. real evolution paths of recession exponent

The evolution paths of recession exponent *B* do not always include the increasing, decreasing, and pseudo-constant components, which is inconsistent with the concept we introduce in Figure 4-6. We refer to such conceptual cases as ideal recession evolution. An ideal evolution path of *B* would be observed if a basin is effectively recharged and the recession continues long enough before a new storm event occurs. Under these circumstances, the dominances of all of the three processes including fast response (i.e., overland flow and quick subsurface flow), soil water depletion to streams, and groundwater contribution would be observable and distinguishable. These three processes correspond to the increasing, decreasing, and pseudo-constant parts of the evolution path of *B*, respectively (Figure 4-6). If these conditions are not satisfied, we will not be able to obtain a complete evolution of the recession exponent. Based on the ~1000 recession events analyzed in this study, we found that the second or the last portion of an ideal evolution was frequently not observed for reasons which we discuss below.

We hypothesize that the duration over which a reservoir provides significant contribution to streamflow is determined by the amount of water stored in the respective storage and its release rate. For a specific reservoir, the larger the actual storage it has, the longer it contributes to streamflow and the longer the duration that the recession process can be represented by a corresponding exponent *B*. Note that actual storage is different from storage capacity (Spence, 2007; Spence, 2010). Storage capacity is controlled by geological, topographic, soil, land use, and cover conditions, while actual storage is subject to recent historical rainfall characteristics including the total amount and the spatiotemporal variability. This hypothesis leads to three scenarios of how exponent *B* would vary as recession continues after fast flow ends.

Scenario 1. Exponent *B* decreases monotonically as recession goes on (Figure 4-3(c)). This scenario appears when the basin is effectively recharged (therefore a longer soil depletion process) and the recession is interrupted by a new storm event before groundwater flow begins to dominate streamflow.

Scenario 2. Exponent *B* decreases monotonically at the beginning and then stays pseudo-constant (Figure 4-3(a) and (d)). This is primarily because the reservoirs with smaller residence times have small actual storages. The small actual storages could be result from limited storage capacities or insufficient recharges during the storm events. In contrast, the reservoir characterized by the pseudo-constant of *B* stores a large amount of water and is therefore able to support the streamflow for a longer duration. This scenario happens when the basin is relatively dry and soil depletion can only support streamflow for a short duration.

Scenario 3. Exponent *B* remains pseudo-constant (Figure 4-3(b)). This occurs when all the reservoirs with shorter response times have small actual storages. This scenario is most probable when the basin is very dry and rainfall is ineffective to recharge the soil storages; therefore, the streamflow is dominated by groundwater after fast flow recedes.

In all, the real evolutions of recession exponent usually are incomplete. On the one hand, ideally, if a recession lasts long enough, exponent *B* would converge to a pseudo-asymptote characterizing the groundwater reservoir with the slowest response speed. However, in reality, for wet and semi-arid basins (e.g., Hammond and Han, 2006), streamflow is forced to rise before it is controlled dominantly by groundwater due to frequent rainfall, and thus the last portion of the evolution of *B* will not be easily observable (Figure 4-3(c)). And on the other hand, for arid basins or dry periods, it is possible that soil water plays a very limited role in supporting streamflow, therefore, the decreasing portion of the evolution of *B* is missing (Figure 4-3(b)). As we explain in the following sections, these incomplete evolution paths offer great opportunities to explore the mechanism of basin hydrological response under various circumstances.

4.6.2 Application: dissecting recession curves

To obtain reliable recession analysis results, the first question to answer is what flow source is of interest and when should we assign the beginning and end of the associate recession process (Tallaksen, 1995). This question is strongly related to the segmentation of a recession curve. There are many proposals to separate hydrograph recessions, including graphical, threshold, digital filter, and isotope-based methods (e.g., Nathan and McMahon, 1990; Arnold et al., 1995; Tallaksen, 1995; Smakhtin, 2001; Eckhardt, 2005). However, for decades, there has been no consistent theory-based methodology to select recession segments for recession analysis. The flexibilities in selecting the starting and ending point of recession analysis make it difficult to compare results within or between basins from different studies. Based on physical and mathematical reasoning, and as is borne by intensive data analysis, we propose to dissect a recession to different stages of release of stored water in a basin by examining the evolution path of exponent *B*. As concluded at the end of Section 4.5, exponent *B* reaches the maximum and starts to remain roughly constant when fast flow ends and the

groundwater flow begins to dominate streamflow response. We use these two turning points to divide a hydrograph recession.

Once the dissection of a recession curve is complete, we can conduct recession analysis for each of the segments to make inferences about the associated hydrologic processes. For example, to analyze groundwater recession, groundwater storage, and recharge, we start from the time that the recession exponent begins to stay approximately constant until the end of the recession. To analyze soil water recession, we start from the point where the recession exponent reaches its maximum and continue until the time that the recession exponent begins to remain a pseudo-constant (Halford and Mayer, 2000; Brutsaert, 2008). This method can also help with base flow separation and event-based runoff coefficient calculation. We can work backwards to calculate the contributions of water to the total streamflow by each of the flow sources using the estimated recession parameters and the discharge at the turning points (e.g., Szilagyi and Parlange, 1998; Wittenberg and Sivapalan, 1999; Blume et al., 2007).

Compared to traditional methods, the method presented herein tends to reduce the dependency on human judgment. Instead, the streamflow data indicates the turning points. This is advantageous because it provides a strategy to reduce the arbitrariness in recession analysis. Our method can be used as a consistent criterion to select segments for recession analysis and promote comparative recession analysis (Figure 4-6).

In addition, our approach allows investigations of the entire recession limb rather than merely the recession tails typically used by traditional recession analysis. There is an increasing need to understand how a basin responds to storms across scales and to further advance event-based hydrological modeling and forecasting (e.g., Sivapalan, 2003; Sivapalan et al., 2003). Hydrograph recession, as a result of continuous release of water from various natural storages, has the potential to provide unique insight into basin hydrological response. However, the information it carries has been partially decoded, i.e., traditional recession analysis with goals of estimating the amount of groundwater

stored in a basin or studying base flow uses only recession tails to avoid the noise introduced by fast flow as a result of storm events (e.g., Wittenberg and Sivapalan, 1999; Brutsaert, 2008; Brutsaert and Sugita, 2008). By expanding the analysis to the earlier portion of a hydrograph recession, our method can be used not only to obtain knowledge about groundwater response but also to decode information about the fast response and delayed soil response(e.g., Brutsaert and Lopez, 1998; Wittenberg and Sivapalan, 1999; McDonnell et al., 2007; Spence, 2007; Kirchner, 2009; Seyfried et al., 2009; Biswal and Marani, 2010).

4.6.3 Application: within- and between- basin comparisons

In the long history of exploring the mechanism of streamflow generation, there have been many attempts to produce generalizations or theories that might be widely accepted through comparative analyses of catchment responses (e.g., Wagener et al., 2007; Sivapalan, 2009). These studies use short-term based indices (e.g., event runoff coefficient), long-term based indices (e.g., mean monthly variation of runoff, annual runoff coefficient), and long-term representative curves (e.g., flow duration curves) to characterize basin hydrologic responses. However, in these studies, the hydrologic response is either described by a single number that obscures details or by metrics that cannot be used for comparison at different temporal scales. To fill this gap, we propose to use evolution paths of the recession exponent as a metric for hydrological comparison. This metric is process-based in the sense that it provides some information about the contribution history and magnitude of streamflow sources, while also being useful for both an event-based comparison of the individual evolution paths and a long-term comparison of the characteristic evolution paths. On one side, future efforts can be made to investigate how rainfall fields interact with initial basin conditions across events by comparing the evolution paths of the recession exponent within individual basins (as shown in Figure 4-3) (e.g., Zehe and Blöschl, 2004; Zehe et al., 2005; Hammond and

Han, 2006; Blume et al., 2007). And on the other, it will be interesting to explore how climate, together with basin characteristics, determines the representative (or the average) hydrologic response behavior across basins by comparing their characteristic evolution paths of the recession exponent (as shown in Figure 4-5) (e.g., Merz et al., 2006; Berthet et al., 2009). For example, Figure 4-5 shows that the evolution of the recession exponent for all of the basins converged to approximately 2. This indicates that these basins have similar groundwater releasing behavior, which makes sense because they are all from the same region. With these advantages, comparison of the evolution paths of the recession exponent might assist the paradigm shift in hydrology research by providing a consistent way to learn from data and to develop new hypotheses for more advanced hydrological process understanding (e.g., Dooge, 1986; Beven, 1989; Sivapalan et al., 2003; Troch et al., 2009; Spence, 2010).

4.6.4 Application: importance of groundwater contribution to streamflow

It is generally recognized that groundwater is the most important contributor to streamflow under dry conditions. The lengthy and widespread 2012-2013 North American drought provides us a good opportunity to test this recognition. We selected nested sub-basins in the Iowa River basin and their associated recession curves starting from early May to late August. Figure 4-7 shows the evolution of the recession exponent across nested basins obtained using the method introduced in Section 4.3 but using daily streamflow data. The recession length used was 90 days. There are some fluctuations around unit in the evolution paths of the recession exponent of theses basins. Nevertheless, the recession exponent tends to remain around unit across scales. This scale-invariance in recession exponent indicates that, during the drought, streamflow for all of the investigated nested basins originates from the same groundwater storage. We explain the pseudo-asymptote of the recession exponent to be unit, rather than 2 as shown

earlier, by arguing that the basins were under severe drought in 2012 so their streamflow was fed by deep groundwater with a slower release rate.

Groundwater contribution to streamflow is important not only during dry periods, but also during high flows in some cases. It is also widely recognized that the temporal variability of streamflow decreases with spatial scales, i.e., the discharge response for large basins is less sensitive to individual storm events. A straightforward explanation might be because the water fluxes induced by storm events are much smaller compared to storages for large basins, while the opposite is true for small to medium size basins. This shows the importance of basin storage in streamflow generation. Interestingly, a similar inference can be made by investigating the characteristic evolution paths of the recession exponent. On the one hand, Figure 4-5 shows that the contribution from soil water storage decreases as basin scale increases, and it diminishes when a basin drains an area larger than ~1000 km^2 (the decreasing portion of the evolution of B is missing). On the other hand, Figure 4-5 specifies that the groundwater contribution to streamflow becomes more important as spatial scale increases, and it starts to dominate when the spatial scale is greater than some threshold. This is consistent with the findings that streamflow generation at large basins is not just the aggregation of responses from hillslopes and small catchments (e.g., Shaman et al., 2004; Uchida et al., 2005a; Frisbee et al., 2011). Through this example, it seems that we can study the characteristic evolution path to infer the importance of groundwater in supporting streamflow for a basin. This inference can be valuable in determining the hydrological model structure for a basin which is in the spirit of a top-down approach to hydrological modeling.

4.6.5 Limitations

The proposed method for dissecting recession curves eliminates the arbitrariness in determining the starting point for recession analysis. However, it is subject to some

limitations. First, we observed diurnal cycles in daily streamflow during low flow periods due to evapotranspiration, which may impact the rate of recession (e.g., Federer, 1973; Weisman, 1977; Wittenberg and Sivapalan, 1999; Gribovszki et al., 2010) . Second, land use and tile drainage in Iowa have been shown to increase the volume of baseflow (e.g., Schilling and Libra, 2003; Schilling, 2005; Zhang and Schilling, 2006; Schilling and Helmers, 2008). The impact of evapotranspiration and human activities on the shape of the recession curve warrant further investigation. Another challenge is the uncertainty in streamflow measurements (Harmel et al., 2006; McMillan et al., 2012), which is more severe under extreme low flow conditions. Regulations of water resources may also fail our method. The most significant challenge might be applying this method to basins in which streamflow may originate from interconnected subsurface storages with different depletion speeds, and this problem could be even worse for large basins with significant heterogeneity in geological configurations. We see a consistent evolution path of the recession exponent in the Iowa and Cedar River basins. This is because the diurnal cycle in streamflow is not significant due to the humid climate, and more importantly, the subsurface geological structure and soil are relatively homogeneous. However, this does not mean that we can generalize this phenomenon to other regions without inspection due to the reasons discussed above. Nevertheless, this method can be used to test if the streamflow for a basin is controlled by simple or complex configuration of subsurface reservoirs, and the first case is more likely for most of the small to median sized basins because of the relative smooth change in geology.

4.7 Conclusions

Recession curves, resulting from the continuous release of water from various natural storages, carry a wealth of information about basin hydrological response. Isolating different flow sources, such as fast flow, delayed soil water flow, and base flow, is essential to decode this information but has long been hindered by subjectivity. The

notion that a hydrograph recession can be dissected into stages of the outflow process dominated by different storages and that different reservoirs can be characterized by functions in the form of $dQ/dt = -AQ^B$ (Brutsaert and Nieber, 1977) implies that along with a recession process there is an associated evolution path of the recession exponent *B*. We followed this approach and developed an objective method to dissect a recession curve into stages of different outflow processes. The method allows the analysis of the evolution path of the recession exponent *B* in $dQ/dt = -AQ^B$ and relates it to the outflow process. Both data-based and theoretical analysis indicates that as recession continues, recession exponent *B* first increases, then decreases, and finally remains approximately constant. Occasionally, one of the last two portions is missing due to the negligible contribution from soil water storage or the interruption of following storm events. The points where recession exponent *B* reaches its maximum and begins to level off are the times that fast response and soil water response end, respectively.

Table 4-1. Description of the USGS stream gauges investigated in this study

USGS Gauge No.	Gauge Name	Drainage Area (km^2)
464942	Hoover Cr at Hoover Nat Hist Site, IA	7
464220	Wolf Creek near Dysart, IA	774
463500	Black Hawk Creek at Hudson, IA	784
458000	Little Cedar River near Ionia, IA	792
463000	Beaver Creek at New Hartford, IA	898
457000	Cedar River near Austin, MN	1033
459500	Winnebago River at Mason City, IA	1362
458900	West Fork Cedar River at Finchford, IA	2190
457700	Cedar River at Charles City, IA	2729
458300	Cedar River at Waverly, IA	4005
458500	Cedar River at Janesville, IA	4300
462000	Shell Rock River at Shell Rock, IA	4520
464000	Cedar River at Waterloo, IA	13322
464500	Cedar River at Cedar Rapids, IA	16854
454090	Muddy Creek at Coralville, IA	22
454000	Rapid Creek near Iowa City, IA	66
451900	Richland Creek near Haven, IA	145
454220	Clear Creek near Oxford, IA	151
452200	Walnut Creek near Hartwick, IA	184
454300	Clear Creek near Coralville, IA	254
451700	Timber Creek near Marshalltown, IA	306
453000	Big Bear Creek at Ladora, IA	489
452000	Salt Creek near Elberon, IA	520
451210	South Fork Iowa River, IA	580
455500	English River at Kalona, IA	1486
451500	Iowa River at Marshalltown, IA	3966
453100	Iowa River at Marengo, IA	7233

All of these gauges are located within the HUC05 of the Unite States, and we use only the last six digits of their complete USGS gauge numbers.

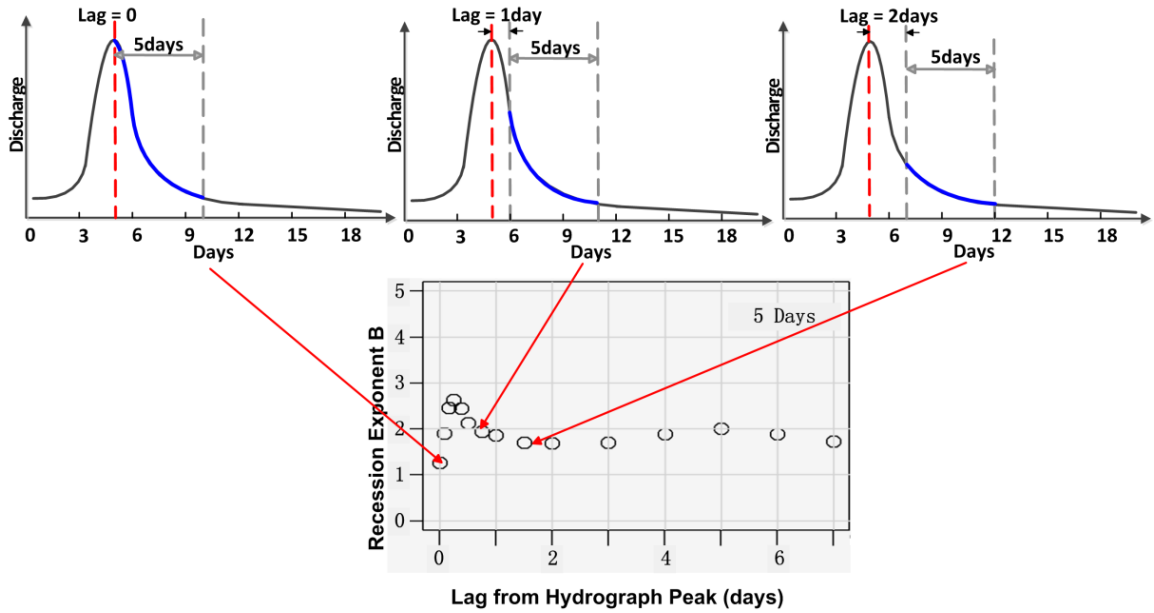

Figure 4-1. Schematic of the evolution path of an individual recession event. The lag represents the starting point of a recession segment, and it is measured from the hydrograph peak marked by the red dashed-line. The blue curve is the recession segment used to estimate the recession exponent *B*. In the lower panel of Figure 4-2, each circle represents the *B* value that is calculated using a specific starting point (horizontal axis) and recession length (the text at the upper right corner.). For example, the first circle in the lower panel represents the value of exponent *B* calculated using the selected recession segment starting from the hydrograph peak with a recession length of 5 days.

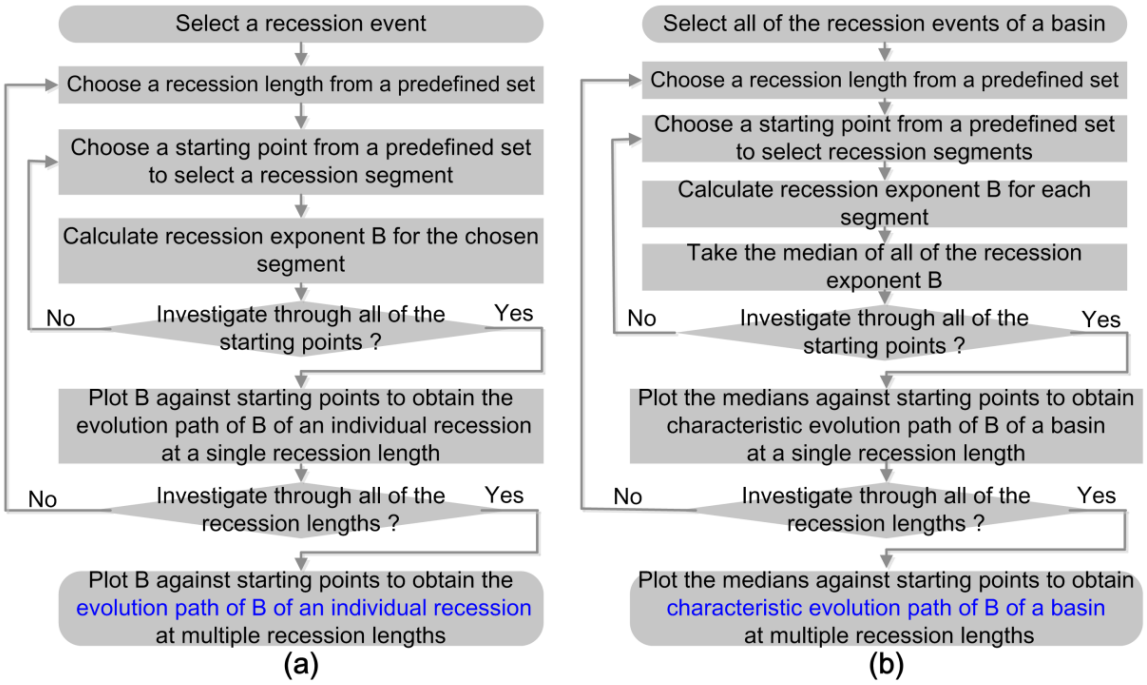

Figure 4-2. Flowchart of constructing the evolution path of the recession exponent *B* for an individual recession event (a) and a basin (b).

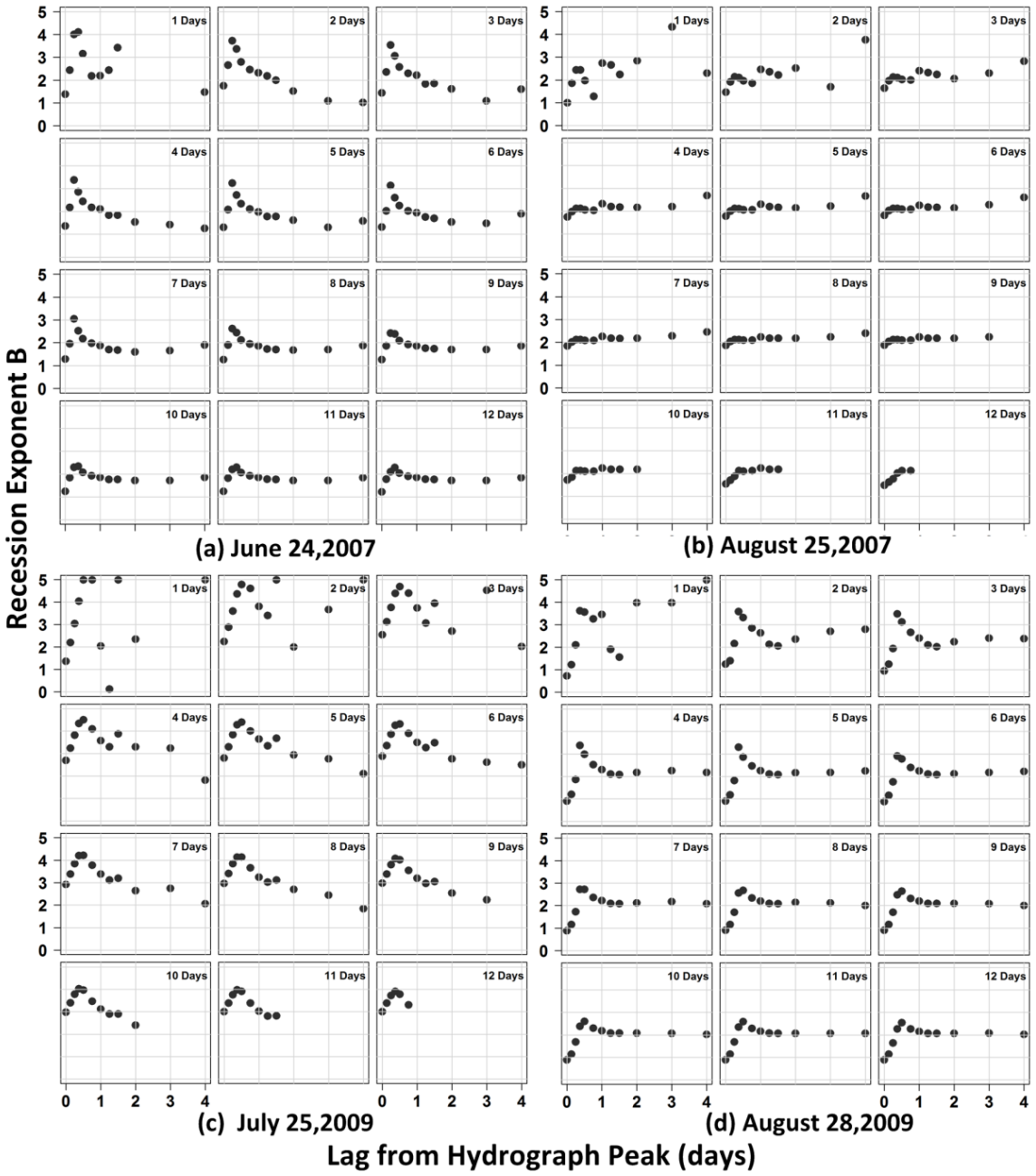

Figure 4-3. Evolution paths of recession exponent *B* for individual recession events: June 24, 2007 (a), August 25, 2007 (b), July 25, 2009 (c), and August 28, 2009 (d) at USGS454300, Clear Creek near Coralville, area = 254.0 km^2. Each panel in this figure is similar to the lower panel in Figure 4-2.

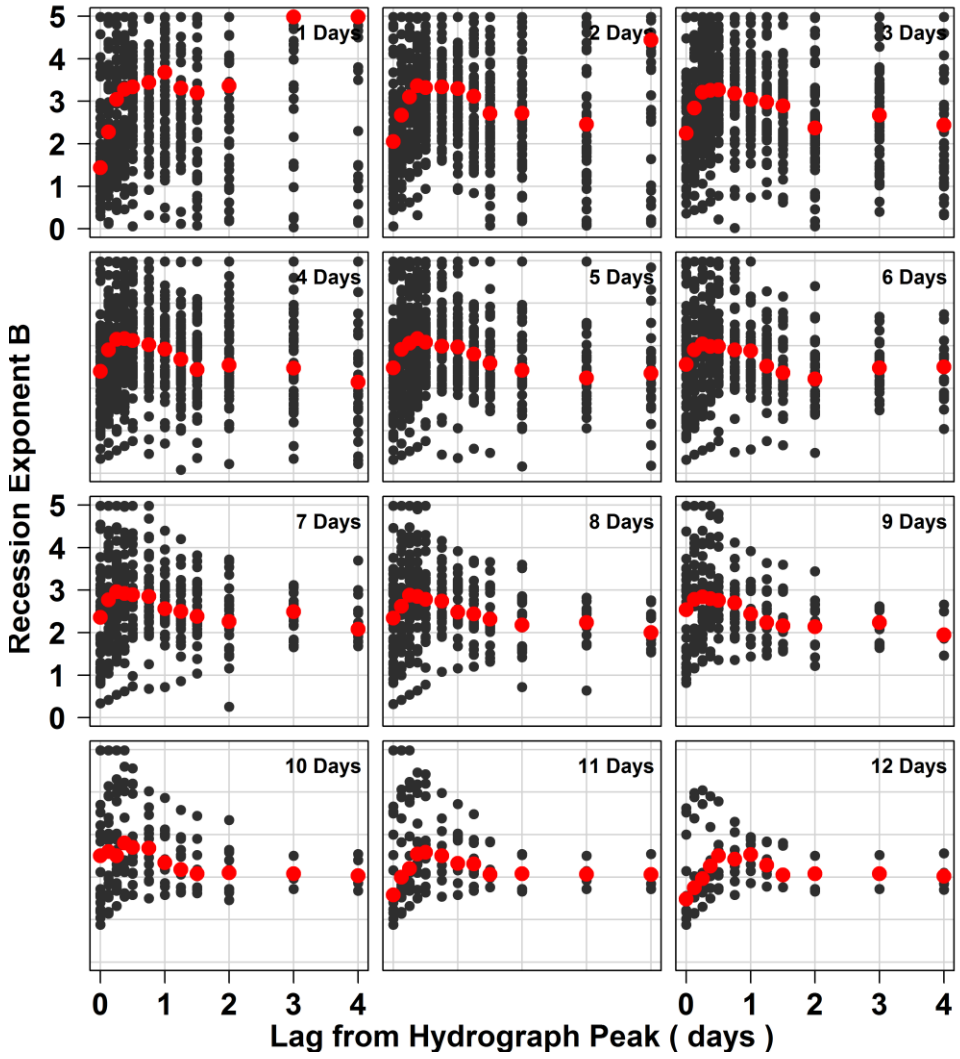

Figure 4-4. The characteristic evolution path of recession exponent *B* at USGS454300, Clear Creek near Coralville, area = 254.0 km^2. Each gray dot is the exponent *B* calculated from a recession segment with a certain starting point and recession length. Gray dots along the same vertical line represent *B* values calculated using different recession segments that are selected with the same starting point and recession length. The red dots are the medians of the *B* values along the same vertical line. The text at the upper right corner is the length of the recession segment used to estimate exponent *B*. For example, the first red dot in the first panel represents the median value of exponent *B* calculated for all of the selected recession segments starting from the hydrograph peak with a recession length of 1 day.

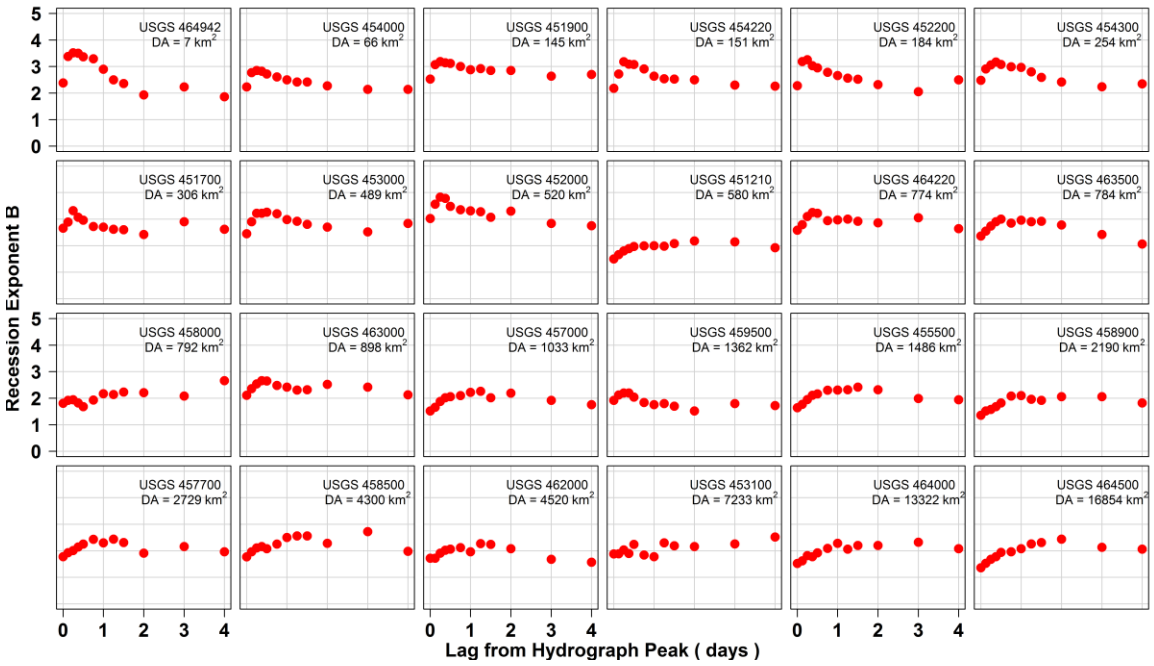

Figure 4-5. Characteristic evolution paths of recession exponent *B* for USGS streamflow gauges in the Iowa and Cedar River basins, Iowa. Two out of 27 gauges are not shown here because of the small numbers of recession events available. The explanation of the plot is the same as that for Figure 4-5. For simplicity and clarity, we do not plot the gray dots as in Figure 4-5. The lengths of recession segments used are 5 days.

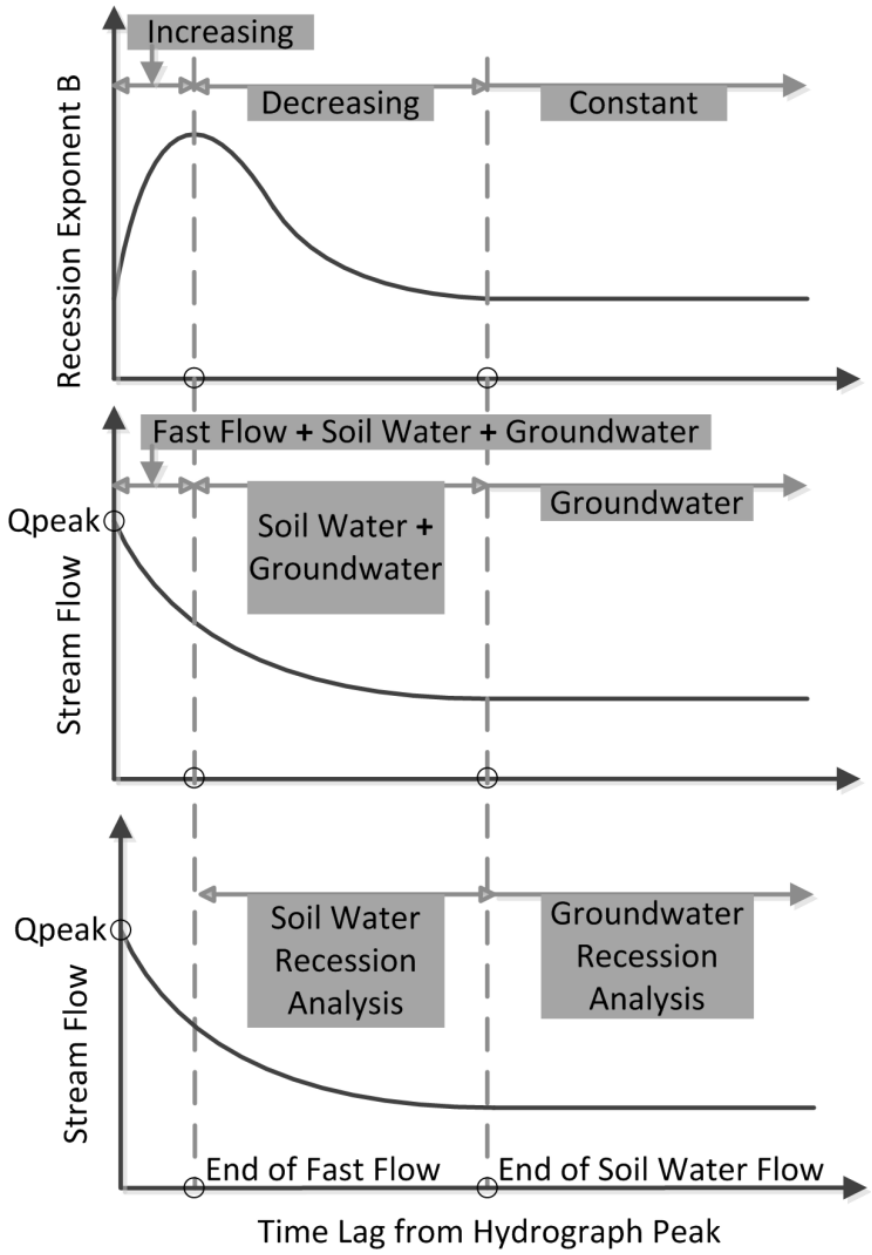

Figure 4-6. Dissecting hydrograph recessions according to the evolution path of *B*. Upper panel: evolution of the recession exponent *B*; Middle panel: contributors to streamflow for different periods of recession; Bottom panel: periods for soil water and groundwater recession analysis. The periods are identified according to the evolution path of *B*.

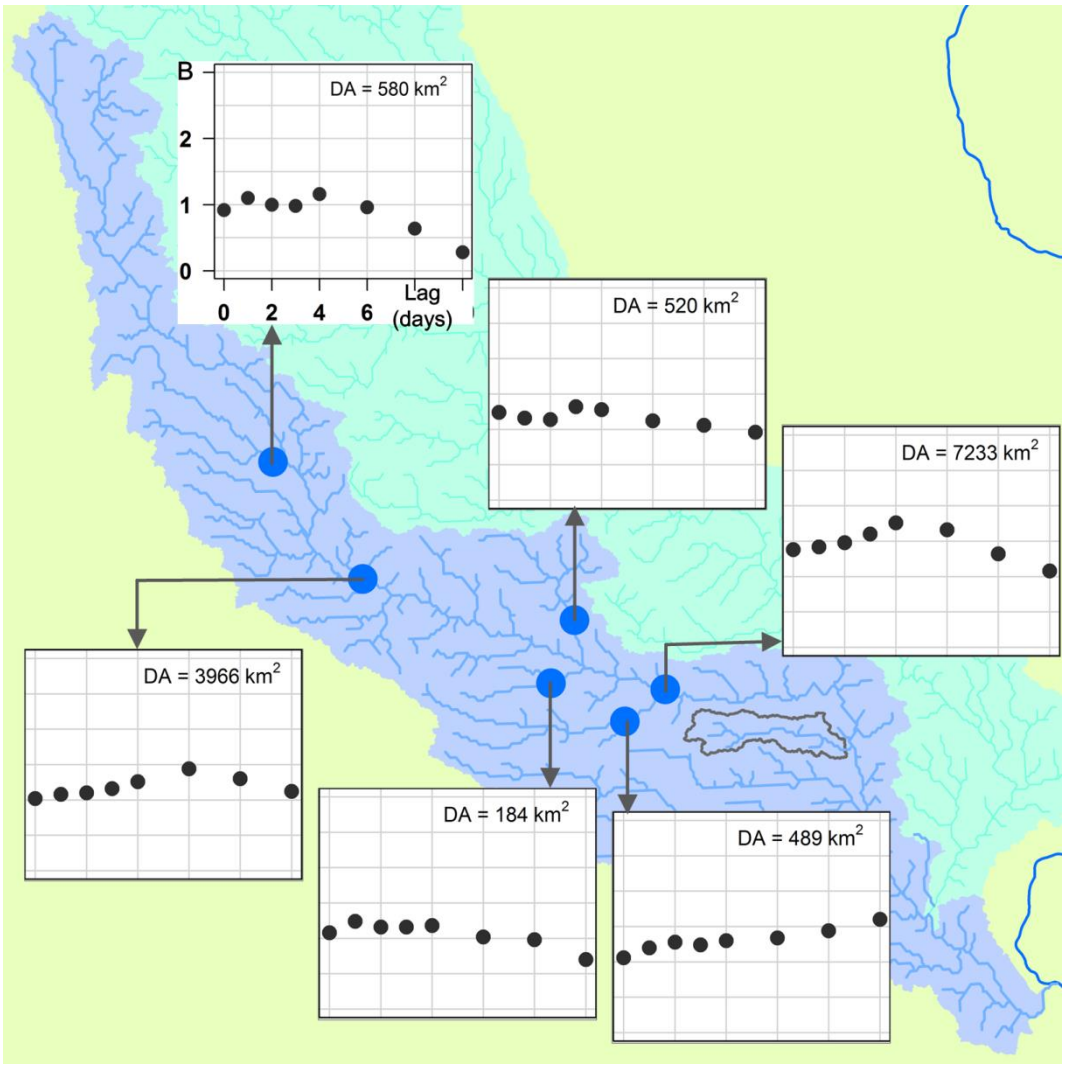

Figure 4-7. Characteristic evolution paths of recession exponent *B* for nested USGS streamflow gauges in the Iowa River basin, Iowa during the lengthy and widespread drought in 2012. The recession lengths used were 90 days for each basin. The horizontal and vertical axes are the same as that for the plot at USGS gauge 451210.

CHAPTER 5
RECESSION ANALYSIS ACROSS SCALES: IMPORTANCE OF ORGANIZED-RANDOM SPATIAL VARIABILITY FOR AGGREGATING HYDROLOGIC RESPONSES

5.1 Introduction

Catchments are categorized as complex systems with some degree of organization (Dooge, 1986), indicating that both aspects of organization (spatial pattern) and randomness of smaller-scale process are important for hydrologic response at larger scales. In the practice of aggregating hydrologic processes across spatial scales, the effect of the randomness of variability represented by statistical distributions has been extensively studied (e.g., Dagan and Bresler, 1983; Moore, 1985; Mantoglou and Gelhar, 1987; Bierkens et al., 2000; Harman et al., 2009; Troch et al., 2009). Meanwhile, the importance of the organization of variability represented by spatial distribution functions has been recognized (e.g., Beven and Kirkby, 1979; Moore and Grayson, 1991; Grayson et al., 1997; McGlynn et al., 2003; Schulz et al., 2006; Jencso et al., 2009; Van Nieuwenhuyse et al., 2011). However, the influence of the intersection of the random and organized small-scale variability on aggregating hydrologic processes across spatial scales remains poorly understood.

Recession process, as an important portion of hydrologic response, has been widely used to provide insights for hydrologic understanding and modeling (e.g., Hall, 1968; Zecharias and Brutsaert, 1988; Vogel and Kroll, 1992; Troch et al., 1993; Tallaksen, 1995; Szilagyi et al., 1998; Smakhtin, 2001; Chapman, 2003; Rupp and Selker, 2006a; Brutsaert, 2008; Kirchner, 2009; Shaw et al., 2013; Troch et al., 2013). Among these applications, recession analyses across spatial scales have been used to understand

the role of variability of landscape properties in the upscaling of hydrologic processes. By analyzing the early-time recessions for three nested catchments in the Panola Mountain Research Watershed, Clark et al. (2009) found that the early stage recession process was approximately linear for the hillslope and became more nonlinear with increasing spatial scale (from 0.1 to 10, and 41 ha). Different approaches were used to reproduce and explain this observed change of recession behavior with scale. Clark et al. (2009) delineated the watersheds into three landscape classes including hillslopes, ephemeral riparian aquifers, and permanent stream aquifers. They assumed that the variations of recession behavior were substantial between landscape classes and there was no difference between elements within each landscape class. Their delineation of the watersheds with similar recession behavior implies the organization of the between-element variability of recession processes, i.e., the major difference in recession process is between landscape classes rather than between each element. In contrast, Harman et al. (2009) divide the watersheds into hillslopes and used statistical distributions to represent the between-hillslope variability of recession processes. Additionally, Harman et al. (2009) presumed that the recession behaviors at the hillslopes were randomly distributed in space. This representation of the watersheds suggests the randomness of the between-hillslope variability of recession processes.

The works of Clark et al. (2009) and Harman et al. (2009) only investigated early-time recession processes at the small scales ranging from 0.1 to 10, and to 41 ha due to data limitations. However, a larger range of scales is of interest to practical applications. Also, Clark et al. (2009) and Harman et al. (2009) demonstrated the individual effects of the organization and randomness of small-scale recession behavior on the spatial aggregation of recession process, respectively. It is a more realistic representation of the natural recession processes to account for both. Lastly, the functioning of the stream network in transferring the outflows from local areas to the watershed outlet is not important at the small scales investigated by Clark et al. (2009) and Harman et al. (2009),

while it is of great importance for aggregating hydrologic processes to larger scales (e.g., Rodr ́guez-Iturbe and Vald ́s, 1979; Gupta and Mesa, 1988; Biswal and Marani, 2010; Mutzner et al., 2013).

In this study, we extend the works of Clark et al. (2009) and Harman et al. (2009) to explore the recession process across spatial scales ranging from ~70 to 17000 km^2. We analyzed recession curves from 25 nested USGS stream gauges located in the Iowa and Cedar River basins over a period of about 150 days with negligible precipitation during the 2012-2013 North American drought. Focus on these long individual recessions in nested basins over the same time period reduces confounding factors typically encounter when comparing recessions across space and time. These recession processes all occur at basins with similar geophysical characteristics and have similar wetting and drying history. Differences in recession behaviors are therefore related to the change in spatial scales, if such exist. We ask the following questions in this study: 1) How do late-time recession characteristics change across spatial scales? 2) What is the effect of the organized and random variability of small-scale recession behaviors on the spatial aggregation of recession process? We address the first question by analyzing observed recession data and the second question through diagnostic simulation using a distributed drainage model.

5.2 Recession data analysis for the 2012-2013 drought

5.2.1 Site description

We analyzed recession curves that were observed over the period from early May to late September of 2012 at 25 USGS stream gauges in the Iowa and Cedar River Basins in Iowa, USA (Figure 3-1 and Table 4-1). The corresponding drainage areas at the gauge locations range from ~70 to 17000 km^2. These gauges are free from reservoir regulation and notable water withdraws for agricultural or municipal use. The agricultural practices are rain fed and the region has a small number of farm ponds. For this region that has a

rather flat terrain, approximately three-fourths of the 900 mm average annual precipitation and 85% of the 45-65 thunderstorms occur from April through September. Frozen soils and snow melting near the surface last from late October to early April. The recession data used in this study are daily streamflow data downloaded from USGS National Water Information System (http://waterdata.usgs.gov/nwis.sw).

5.2.2 Recession analysis using individual events

Long recession curves would be preferred for examining late-time recession process for a catchment if they are available. However, short recession curves, which contain limited information about late-time recession process, are more often in reality. To overcome this problem, the master recession curve method (Nathan and McMahon, 1990) and the Brutsaert-Nieber method (Brutsaert and Nieber, 1977) have been most commonly used for quantifying the late-time recession characteristics of a catchment. The former method increases the information needed by merging multiple recession curves, while the later by studying the lower envelopes of the cloud plot of *log(dQ/dt)* against *log(Q)*that ensembles multiple recessions. Though these methods partially solve short length problem by mixing information from multiple recession events, they neglect the substantial between-event variation of recession processes due in part to different wetting and drying histories. There has been discussion about analyzing recession curves individually instead of collectively (e.g., Biswal and Marani, 2010; Shaw and Riha, 2012).

The extreme 2012-2013 drought provides us a unique opportunity to rigorously investigate recession process across scales. On one hand, the long period with negligible precipitation started from late April of 2012 and persisted until late November of 2012 during the drought event. This long-duration drought provides recession curves with lengths much longer than the characteristic recession timescale of shallow groundwater aquifers (around 45 ± 15 days (Brutsaert, 2008)), thus allowing for examining late-time recession events individually. On the other hand, the nested Iowa and Cedar River basins

experienced similar wetting and drying history during the widespread 2012-2013 drought, thus isolating the effect of catchment size on late-time recession process. Overall, we use these long recession curves (about 150 days) observed during the individual extreme 2012-2013 drought event to explore how the late-time recession process depend on spatial scales.

5.2.3 Quantifying late-time recession characteristics

Mathematical expression for recession modeling

Modeling recession curve consists of two steps: (1) choosing a suitable functional form, and (2) determining the model parameters. The hydraulic groundwater theory suggests that the outflow from the groundwater storage in a basin can be approximated by a power function (Brutsaert and Nieber, 1977; e.g., Rupp and Selker, 2006b)

$$S = KQ^b \tag{5-1}$$

where S (mm) is the groundwater storage in the basin, Q (mm/day) is the discharge measured at the basin outlet, and K and b are parameters. Both S and Q are averaged over the catchment area. The parameters K and b could be directly determined if measurements of both S and Q were available. However, it is difficult to measure groundwater storage S for a basin and thus the most commonly adopted method to estimate K and b is through combining the storage-discharge relation with the mass conservation equation

$$\frac{dS}{dt} = P - Q - E \tag{5-2}$$

where P (mm) and E (mm) are the precipitation and evapotranspiration averaged over the basin, respectively. To study recession process, usually a period with the absence (or at least negligible amount) of recent precipitation and evapotranspiration is chosen such that

$$\frac{dS}{dt} = -Q \tag{5-3}$$

Taking the derivative of equation (5-1) with respect to time *t* and combining it with equation (5-3) yields

$$\frac{\mathrm{dQ}}{\mathrm{dt}} = \frac{-1}{\mathrm{Kb}}\mathrm{Q}^{2-\mathrm{b}} = -\mathrm{AQ}^{\mathrm{B}} \tag{5-4}$$

where $A = \frac{1}{\mathrm{Kb}}$ and $B = 2 - b$. Parameters *A* and *B* are named as recession intercept and recession slope, respectively, in the plot of *log(-dQ/dt)* against *log(Q)*. The recession intercept *A* and recession slope *B* represent two characteristics of a recession event, i.e., the linearity and the recession rate, respectively. We will investigate these two in this study. Under the scenario of $B = 1$, i.e., a linear reservoir, $K=1/A$ is named as recession timescale (has a unit of time). Note that the linear late-time recession process is not an assumption but a hypothesis to be tested in this work. We will use the widely adopted Equation (5-4) in the literature as our mathematical expression to describe the observed recession data.

Consistent approach to estimate recession parameters

The estimation of recession parameters has been documented to depend on the calculation procedure, i.e., the selection of recession segment (e.g., Vogel and Kroll, 1992; Vogel and Kroll, 1996; Hammond and Han, 2006) and parameter estimation methods (e.g., Wittenberg, 1994; Tallaksen, 1995; Stoelzle et al., 2012). However, there is no precise guidance on how to reduce the inconsistency in determining recession parameters.

To lessen the artifacts introduced by the calculation procedure, thereby allowing reliable between-catchment comparison of the recession characteristics, we use a

consistent selection of recession segments and use the same method to estimate the recession parameters. We use the same starting point of 12 days after hydrograph peak and the same segment length of 120 days to select late-time recession segments from both the observed and simulated hydrographs. The large lag after hydrograph peak helps to limit the contribution from sources other than the groundwater reservoir and the long recession segments provides rich information about the groundwater drainage process. Then for each of the selected recession segment, we adopt the nonlinear direct fitting method recommended by Wittenberg (1999) to estimate the late-time recession parameters. Accordingly, we varied *B* systematically, e.g., from 0 to 5 with a step size of 0.01, and calculated the value of *A* at each value of *B* using equation

$$A = \frac{\sum_{t=1}^{n}\left(Q_{t-1} - Q_t\right)}{\Delta t \sum_{t=1}^{n}\left(\frac{Q_{t-1} + Q_t}{2}\right)^B} \tag{5-5}$$

where n is the length of the recession segment, and Δt is the observational interval. Solving equation (5-4) for Q (here we explicitly express Q as a function of t) gives

$$Q_t = Q_0\left[1 + \frac{(1-B)At}{Q_0^{1-B}}\right]^{\frac{1}{1-B}} \tag{5-6}$$

where Q_0 is the discharge at the starting point of the recession segment used to calculate B, and t is the number of days elapsed from the starting point. All recession segments are modeled using their initial discharges Q_0, the values of A and B, and equation (5-6). Following Wittenberg (1999), the modeling error E is defined as

$$E = \frac{V_{\mathrm{mod}} - V_{obs}}{V_{obs}} \times 100\% \tag{5-7}$$

where V_{obs} and V_{mod} are the volume of the observed and modeled hydrographs, respectively. The optimal paired values of A and B were selected by minimizing the modeling error.

5.3 Results of data analysis

For each basin, we used different combinations of starting points (10, 12, 14 days after hydrograph peak) and lengths (90, 100, 110, 120 days) to extract recession segments and then to estimate its late-time recession parameters. The estimates obtained for each basin are similar probably because the information provided by these long segments are representative for the late-time recession process. We present only the results obtained using a starting point of 12 days after hydrograph peak and a segment length of 120 days. Figure 5-1 displays the performances and parameter estimates of the $dQ/dt = -AQ^B$ model for the observed recessions during the 2012-2013 drought for all 25 gauges, as a function of drainage area. The low values of modeling error (<6%) shown in the top panel of Figure 5-1 indicate that the power law (Equation (5-4)) model provides good fits to the observed recession curves, and thus allowing us to infer how the two important characteristics of late-time recession process vary with spatial scale.

The first is the linearity/nonlinearity of the late-time recession process represented by the parameter B. The values of B, shown in the middle panel of Figure 5-1, appear to be scattered around $B = 1$. The estimated B values tend to be more variable for relatively smaller basins than for larger ones. The larger variability at the smaller scales might be caused by the noise in the streamflow data. Smaller streams tend to have smaller flow rates and thus may subject to more uncertainties in the flow measurements. Nevertheless, the estimates of B at 16 out of the 25 sites investigated remain within the interval of [0.75, 1.25] and the median value of B for all 25 sites is 1.05. This indicates that the linear reservoir hypothesis is a reasonable approximation to the late-time recession behavior in the Iowa Cedar River basins during the 2012-2013 drought.

The second characteristic is the recession timescale of the late-time recession process represented by the parameter *A*. Given the linearity of the late-time recession process, the reciprocal of *A* has the physical interpretation of recession timescale and a unit of time (days in this study). The values of *A*, shown in the bottom panel of Figure 5-1, appear to be scattered around the median value of 0.029/day. This indicates that the late-time recession timescales tend to be relatively invariant (34 days) for the Iowa Cedar River basins during the 2012-2013 drought. Similar analyses for the 1988 drought of these basins also indicate a relatively invariant recession timescale of 36 days (Appendix C). Similarly to the case of parameter *B*, the variation of the estimates of *A* tends to decrease with increasing spatial scales.

Overall, analyses of observed recession data suggest that the late-time recession process at the large scale (70 ~ 17000 km^2) in the Iowa and Cedar River basins tend to be linear ($B = 1$) and homogeneous (constant $A = 0.029$/day) during the 2012-2013 drought. To more rigorously test this hypothesis of linearity and homogeneity, we reproduced these late-time recession curves for all 25 gauges during the 2012-2013 drought with the median values of $A = 0.029$/day and $B = 1$. The overall good fit as shown in Figure 5-2 supports our hypothesis.

5.4 Diagnostic drainage experiment

The linearity and homogeneity of late-time recession processes at the catchment scale (70 ~ 17000 km^2) raises the question: what is the connection between the process linearity and homogeneity at the catchment scale and the process variability at the hillslope scale? Two types of explanation to the recession behavior at the catchment scale are the hydraulic interpretation (e.g., Brutsaert and Nieber, 1977; Rupp and Selker, 2006b; Troch et al., 2013) and the landscape interpretation (e.g., Clark et al., 2009; Harman et al., 2009). We follow the later in this paper to explore our question

We adopt diagnostic drainage experiment for this purpose, as Clark et al. (2009) and Harman et al. (2009) did in their studies. Diagnostic experiment (Weiler and McDonnell, 2004) is a comment instrument in hydrology and it does not attempt to model the hydrologic system, but serves as a tool to understand the effects of essential elements under consideration (Van Nieuwenhuyse et al., 2011) and test hypotheses (Weiler and McDonnell, 2006). However, different from the hypothesis testing on the basis of hypothetical models (Pappenberger and Beven, 2006), our diagnostic experiment does refer to observations.

5.4.1 Conceptual design of the simulation study

Our diagnostic simulation is inspired by empirical observations and the widely accepted fact that the catchment-scale hydrologic response is the manifestation of the self-similarity of the river network (Rodriguez-Iturbe and Rinaldo, 1997) and the variability of the small-scale hydrologic processes (Blöschl and Sivapalan, 1995). We empirically observed the spatial organization of basin drainage process. As a basin drains, hillslopes attached to the tips of the river network become first disconnected from the permanent stream aquifers. This disconnection becomes more pronounced from hillslopes to larger catchment scales as the basin drainage continues without recharge. This observation suggests that hillslopes feeding small streams (small Strahler orders) have shorter recession timescales, indicating a spatially organized sequential drainage process. Our observation is consistent with two independent lines of study. The first argues that landscape organization is the first-order control on the mean residence time of water in a basin (e.g., McGlynn et al., 2003; McGuire et al., 2005; Jencso et al., 2009) and that residence time increases with the ratio between riparian and hillslope area (Jencso et al., 2010). The second line of study reveals the effect of the sequential shrinkage of the river network (from smaller to larger streams) on catchment recession behavior (e.g., Biswal and Marani, 2010; Biswal and Nagesh Kumar, 2013; Mutzner et

al., 2013). Overall, our observation and the literature suggest the releasing of water from catchment storage is hierarchical, i.e., is sequential and spatially organized. Accordingly, we pursue our goal by using a distributed drainage model with capabilities to explicitly consider the randomness and organization of the recession variability at the hillslope scale.

5.4.2 Structure of the distributed drainage model

In our model, a basin is decomposed to hillslopes that are interconnected by the river network. Each channel link and the associated hillslope (drainage area on the two sides of the channel link) are assigned a Strahler order. For more information about this hillslope-link based representation of the landscape, please refer to our previous papers (e.g., Mantilla, 2007; Mandapaka et al., 2009; Small et al., 2013). As done in the works of Clark et al. (2009) and Harman et al. (2009), our model assumes linear drainage process at the hillslope scale

$$Q_{h,i,t} = Q_{h,i,0} e^{-t/K_i} \tag{5-8}$$

where $Q_{h,i,t}$ (mm/day) is the outflow at time t (days), $Q_{h,i,0}$ (mm/day) is the initial outflow, and K_i (days) is the recession timescale of i^{th} the hillslope. The recession processes at the hillslope scale are aggregated to that at larger scales through channel routing (e.g., Mantilla, 2007; Small et al., 2013)

$$\frac{dQ_{c,i,t}}{dt} = \frac{v_{c,r} A_i^{-0.1} Q_{c,i,t}^{0.25}}{L_i} \left(\sum_{k=1}^{n} Q_{c,k,t} + Q_{h,i,t} - Q_{c,i,t}\right) \tag{5-9}$$

where $Q_{c,i,t}$ and $Q_{c,k,t}$ (mm/day) is the outflow from the i^{th} and k^{th} channel link, $v_{c,r}$ is universe reference flow velocity with a value of 0.3 m/s for low flows, A_i (km^2) and L_i (km) are the accumulative upstream drainage area and the length of the i^{th} channel link, and n is the number of links that drain into the i^{th} link. The actual channel flow velocity

at each channel link is locally adjusted according to its accumulative upstream drainage area and flow rate as shown in Equation (5-9).

5.4.3 Parameterization of the distributed drainage model

We follow the works of Clark et al. (2009) and Harman et al. (2009) to represent the spatial organization and randomness of the hillslope-scale drainage processes, respectively. The organization is represented by classifying the landscape into three categories, such as areas drain into ephemeral, intermittent, and perennial streams. The randomness is represented by randomly assigning parameter values in space regardless of the differences between landscape categories.

We assigned recession timescales *(K)* over the hillslopes with three schemes (Table 5-1). The first is the organized scenario, under which hillslopes are classified to three categories according to their Strahler orders. Each category has the uniform value of *K* (0.5, 5, 30 days for the three categories), indicating the recession processes at the hillslope scale are hierarchical and only the between-category variability is important and propagates to larger scales. This scenario is similar to that explored by Clark at al. (2009), but we implicitly assign the fractional area according to the Strahler order. The second scheme represents the random scenario, under which there is no classification of hillslopes. We generate random numbers of *K* from Gamma distributions and randomly distribute them over the hillslopes regardless of their Strahler order. Therefore, the between-hillslope variability has no order. This scenario is similar to that investigated by Harman et al. (2009). The last scheme represents the organized-random scenario, which is the mixture of the former two scenarios. Under the last scenario, hillslopes are classified to three categories according to their Strahler orders. However, we generate *K* values from Gamma distributions with a different mean value (0.5, 5, 30 days for the three categories) for each category and assign them over the hillslopes from this category. This scenario considers both the between-category variability and the between-hillslope

variability within each category, and thus allows aggregating both the organized and random variability at the hillslope scale to larger scales. Note that we assume that the coefficient of variation of *K* reduces with the Strahler order for the organized-random scenario and we will discuss about this assumption in Section 5.4. The mean values of *K* for each category are similar to those used by Clark (2009) and to those found by Jencso et al. (2010) through their field surveys.

5.4.4 Steady-state drainage experiment for the Cedar River basin

We run the designed simulations in the Cedar River basin, which has been divided to around 305,000 hillslope-link pairs. This basin has the highest stream order of 9 and a median hillslope area of 0.041 km^2. Figure 5-3 describes the structure of the Cedar River basin. Of the total drainage area of about 17000 km^2, the hillslopes of order 1 cover ~50%, the order 2 hillslopes cover ~20%, and the remainder covers about 30%. For each stream order, we selected 100 channel links randomly and saved their simulated hydrographs for further analysis (900 hydrographs in total for each simulation scenario).

Similar to Clark's (2009) and part of Harman's (2009) work, we first drove the entire basin to a steady state (when recharge equals discharge) by applying 180 days recharge with constant low intensity of 2.4 mm/day. The recharge duration and intensity are selected such that each hillslope reaches its steady state and the flow rates are similar to that observed during the 2012-2013 drought. We then stopped the recharge to let the basin drain for 180 days.

5.4.5 Analyses of the simulated recession curves

For each simulation run, we conducted recession analysis for the simulated hydrographs using exactly the same procedure as described in Section 5.2. For each sampled channel link, we used different combinations of starting points (10, 12, 14 days after hydrograph peak) and lengths (90, 100, 110, 120 days) to extract recession segments and then to estimate its late-time recession parameters. The estimates obtained for each

channel link were similar for different combinations and therefore we consistently use a starting point of 12 days after hydrograph peak and a segment length of 120 days to extract recession segments. The early recession processes are nonlinear, which is consistent with the findings of Clark et al. (2009) and Harman et al. (2009). Figure 5-4 displays the performance and parameter estimates of the $dQ/dt = -AQ^B$ model for simulated recessions for all 900 links sampled, as a function of upstream drainage area. The low values of modeling error (<8%) shown in the top panel of Figure 5-4 indicate that the power law model provide a good fit to the simulated recession curves. Note that we generated many realizations and redid the same analysis and obtained similar results. We present only the results obtained by analyzing hydrographs sampled from a randomly selected realization.

Results show that, for each of the three scenarios, the late-time recession processes for basins larger than 10 km^2 can be approximated by the same recession model (middle and bottom panel of Figure 5-4). This may due to the spatial averaging of the small-scale recession processes through the river network. However, the values of *B* level off at about 1 for the organized and organized-random scenarios and at values far from 1 for the random scenario. For example, we found that the level-off value of *B* is 1.23 when the coefficient of variation of *K* is 0.5 for the random scenario (middle panel of Figure 5-4) and it increases (and thus deviates more from 1) with increasing coefficient of variation of *K*. This is consistent with the finding of Harman et al. (2009) that for the random scenario: 1) the exponent *B* depends only on and increases with the coefficient of variation of *K* and 2) the coefficient of variation of *K* increased from 0.31 in the 0.1 ha hillslope to 1.20 in the 41 ha catchment. These results indicate that it is necessary to account for the spatial organization of recession processes at the hillslope scale to reproduce the approximate linearity of the late-time recession behavior at the large scale (>10 km^2). Apparently, all of these three scenarios are able to reproduce the nonlinear early-time recession behavior.

Compared to the organized scenario, the organized-random scenario provides the flexibility to account for between-hillslope variability of the drainage processes within each landscape category. Figure 5-4 shows that considering the within-category variability of *K* allows presenting the variation of late-time recession characteristics at the scale smaller than 10 km^2. Though we do not have observed data in this study to show this variation at smaller scales, the literature documented that probably larger variation exists at small scales (e.g., Savenije, 2001). Also, at the scales less than 10 km^2 (contain less than 250 hillslopes), the spatial averaging of the hillslope processes is not sufficient and therefore more rigorous variation present at the scales less than 10 km^2.

The analyses of the simulated recession curves are not sensitive the routing scheme, magnitude and spatial variability of recharge rate. We investigated the effect of channel velocity and found that the constant channel velocity of 0.3m/s and the variable channel velocity (see Equation (5-9)) have negligible impact on the shape of the recessions. Regarding recharge rate, we found that different mean values of recharge rate only affect the amount of runoff but have no effect on the shape of the recessions, which is consistent with the findings of Clark et al.(2009). Furthermore, spatial uniform or variable recharge rates produce almost the same shape of the recessions.

5.5 Discussion

The individual influence of the organized and random spatial variability of the hillslope scale hydrologic processes on the catchment scale hydrologic response is of intense interest. However, the combined influence of the random and organized between-hillslope process variability on the spatial aggregation of hydrologic response remains poorly understood. We attempted to gain insight regarding this aspect by analyzing drainage processes for individual recession event in nested basins. We first quantified the late-time recession characteristics of the 25 nested basins ranging in size from 70 to 17000 km^2 in the Iowa and Cedar River basins during the 2012-2013 drought. We then

developed a distributed drainage model with three parameterization schemes to investigate how the spatial aggregation of hydrologic processes is affected by the intersection of the randomness and organization of the between-hillslope variability.

5.5.1 On the Linearity and homogeneity of recession processes

The result of data analyses presented in Section 5.2 suggests that the late-time recession process is approximately linear ($B = 1$) and homogeneous ($A = 0.029$/day, i.e., a recession timescale of 34 days) for the Iowa and Cedar River basins (70 ~ 17000 km^2) during the long-duration 2012-2013 drought. This linearity is consistent with the previous data analyses based studies, which showed that the late-time recession behavior can be described by the linear reservoirs (e.g., Vogel and Kroll, 1992; Brutsaert and Lopez, 1998; Eng and Brutsaert, 1999). It is also consistent with the analytical solutions to the linearized one-dimensional Boussinesq equation (Brutsaert and Nieber, 1977) and the two-dimensional Laplace equation (van de Giesen et al., 2005). A more complete overview can be found in the articles by Rupp and Selker (2006b) and Troch et al. (2013) and the references therein. This homogeneity at the large scale is consistent with the findings that late-time recession timescale becomes more stable (Savenije, 2001) and converges to 45 ± 15 days as the catchment size increases (Brutsaert, 2008). Overall, these studies indicate that the late-time recession behavior for large basins, in at least some regions, can be described by a linear and homogeneous groundwater reservoir.

Meanwhile, data analysis (e.g., Troch et al., 1993; Szilagyi et al., 1998; Wittenberg, 1999; Biswal and Marani, 2010; Aksoy and Wittenberg, 2011; Mutzner et al., 2013; Shaw et al., 2013) and analytical derivation (Brutsaert and Nieber, 1977; Rupp and Selker, 2006b) both indicate that the early-time recession process is nonlinear ($B > 1$). It is also interesting that Cark et al. (2009) and Harman et al. (2009) found that the early-time recession process becomes more nonlinear, i.e., B deviates more from 1, with increasing spatial scales.

5.5.2 A random or organized representation of watersheds?

Spatial aggregation of hydrologic process depends on the watershed representation. Watershed representation in distributed hydrologic models consists of two components, which are model parameters and mathematical equations describing the runoff generation and transportation mechanisms. Given a similar runoff generation mechanism, the spatial variability of hydrologic process is characterized by the spatial distribution functions of model parameters. On the one hand, the spatial distribution function of parameters may often be conveniently viewed as identical to statistical distributions, i.e., the model parameters is assumed to be randomly distributed or variable in a certain sense (e.g., Dagan and Bresler, 1983; Moore, 1985; Mantoglou and Gelhar, 1987; Bierkens et al., 2000; Harman et al., 2009). This is a random representation of a catchment. On the other hand, the spatial distribution function of parameters may be regarded as deterministic, i.e., the model parameters are functions of state variable of hydrologic systems and/or characteristics of catchments (Beven and Kirkby, 1979; e.g., Wood et al., 1990; Moore and Grayson, 1991; McGlynn et al., 2003; Jencso et al., 2009). This is an extremely organized (or actually deterministic) representation of a watershed. Both types of watershed representations have shown some success, raising the question: which one should be chosen?

We show through our diagnostic simulations (Section 5.5.3) that, at least for recession process, it is necessary to use the combination of the two to represent watersheds and therefore to appropriately aggregate hydrologic response in space. Our simulation study show that the nonlinearity of recession behavior at the larger scale increases with the degree of the random between-hillslope variability of drainage processes (see Section 5.3.5). This is consistent with the finding of Harman et al. (2009) and implies that small and sufficient between-hillslope variability is needed to produce the linear and nonlinear recession behavior, respectively, at the larger scales. This can be used, as Harman et al. (2009) did, to provide an explanation to the increasing nonlinearity

of early-time recession behavior with increasing spatial scales by assuming that the variability of recession timescales increases with spatial scales. However, this configuration cannot explain the linear late-time recession process at the larger scales. We worked around this problem by adding some degree of organization to the between-hillslope variability of drainage processes. We classified hillslopes to three categories according to their Strahler orders, and used three Gamma distributions with increasing mean values (0.5, 5, 30 days) and decreasing coefficient of variation (0.75, 0.5, 0.125) to characterize the spatial variability of the recession timescales (Table 5-1). With this hierarchical configuration, we were able to simultaneously reproduce 1) the increasing nonlinearity of early-time recession behavior with increasing spatial scales by introducing sufficient between-hillslope variability; and 2) the linear late-time recession process at the large scale by embracing small between-hillslope variability.

Our argument of an organized-random representation of watersheds is consistent with the notion that catchments are complex systems with some degree of organization and randomness (Dooge, 1986). We use the Strahler order and Gamma distribution to simultaneously address both the organization and randomness of hillslope-scale variability. This approach can be viewed as a simple implementation of the hierarchical representation of watersheds (e.g., McGlynn and McDonnell, 2003; McGlynn and Seibert, 2003; McDonnell et al., 2007; Clark et al., 2009), in the sense that it jointly contrasts the organized variability between classes and limits the random variability within each class. It allows us to identify the dominant process controls that should be considered in aggregating hydrologic processes across scales. This approach can be used as a starting block for distributed recession modeling.

Though in this study we have extended the works of Clark et al. (2009) and Harman et al. (2009) to larger spatial scales, to the late-time recession behavior, and to examine how the spatial aggregation of recession process is affected by the intersection of the randomness and organization of the between-hillsope variability, we still simplified

our approach by making assumptions. For our data analyses of late-time recessions, we neglect the impact of evapotranspiration and other noise in the data (see the hydrographs for 45700 and 45770 in Figure 5-2). Probably this negligence will not significantly bias the results of data analyses because we use long segments and the basins were extremely dry and the plants had difficulty in extracting water from deeper aquifers. For our diagnostic drainage experiment, we assume that the hillslope drainage process is linear, though supported by the data analysis of Clark et al. (2009), this assumption needs to tested or can be relaxed. Also, we only investigate the recession process after steady state recharge in our simulations and it may be worthwhile to include other cases of recession process after more realistic recharge scenarios. Lastly, we classify the landscape into three categories according to the Strahler order, aiming to connect to the common classification of landscape units into areas drain into ephemeral, intermittent, and perennial streams. This classification metric might be replaced by other surrogates (Van Nieuwenhuyse et al., 2011).

5.6 Conclusion

This study shows that the intersection of the organization and randomness of the processes variability at the hillslope scale is important for the spatial aggregation of hydrologic response. While other data analysis shows that the early-time recession process becomes more nonlinear as spatial scale increases at relatively smaller scales (Clark et al., 2009), the data analyses of individual and concurrent recession events in nested basins here suggest that the late-time recession behavior tends to be linear with homogeneous recession timescale at the large scale. Our diagnostic simulation study show that these observations can be simultaneously reproduced using a distributed drainage model with a hierarchical description of the recession processes at the hillslope scale. This suggests that under the template of the self-similar structure of the river network(Rodr ́guez-Iturbe and Vald ́s, 1979), the hierarchical representation of

watersheds (Blöschl and Sivapalan, 1995; Sivapalan, 2003), which simultaneously considers the organized (between-category) and random (within-category) variability of process at the hillslope scale, provides an approach for the spatial aggregation of hydrologic response.

Table 5-1. Parameterization schemes of the recession timescales *K* over hillslopes

Parameterization schemes	Mean value of *K* (days)	Coefficient of variation of *K*
Organized scenario	Order 1: 0.5	0
	Order 2: 5	0
	Others: 30	0
Random scenario	All: 30	0.5
Organized-random scenario	Order 1: 0.5	0.75
	Order 2: 5	0.5
	Others: 30	0.125

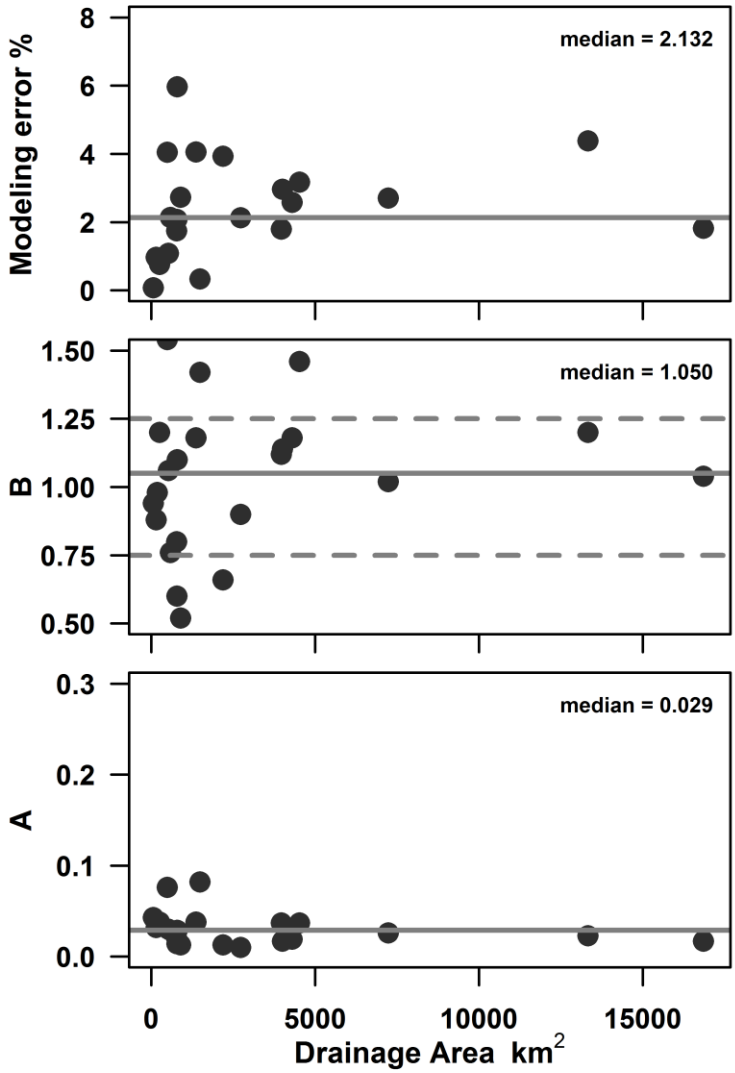

Figure 5-1. Performance and parameters of the $dQ/dt = -AQ^B$ model plotted as a function of the drainage area top: modeling error of reproducing the observed recession curves; middle: parameter *B*; and bottom: parameter *A*. The horizontal gray lines represent the corresponding median values. The result is obtained by analyzing the observed recession curves (late-time) in the Iowa and Cedar River basins during the 2012-2013 drought. The starting point used is 12 days after hydrograph peak and the recession length is 120 days.

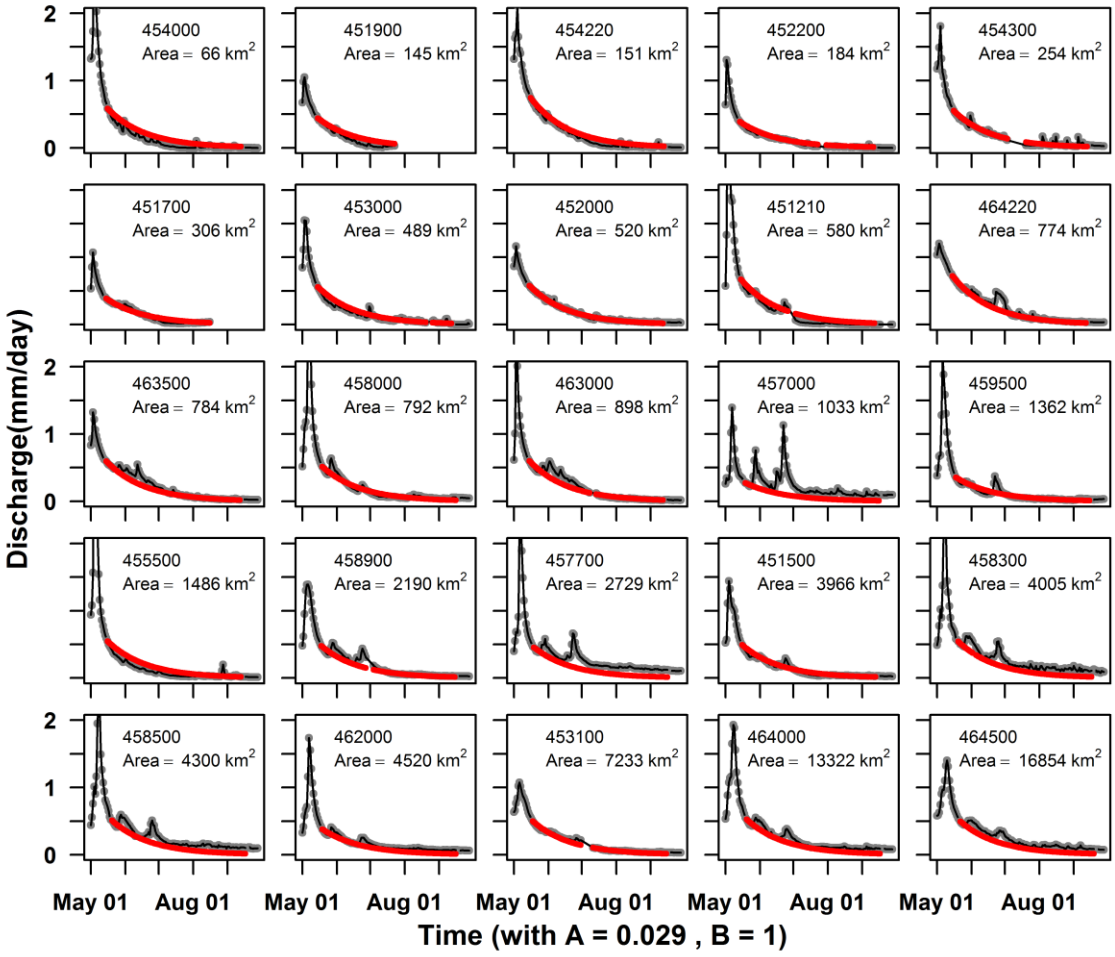

Figure 5-2. Comparison between the observed (gray) and modeled (red) recession curves. Constant values of *A = 0.029* and *B = 1*are used for modeling recession curves at all gauges.

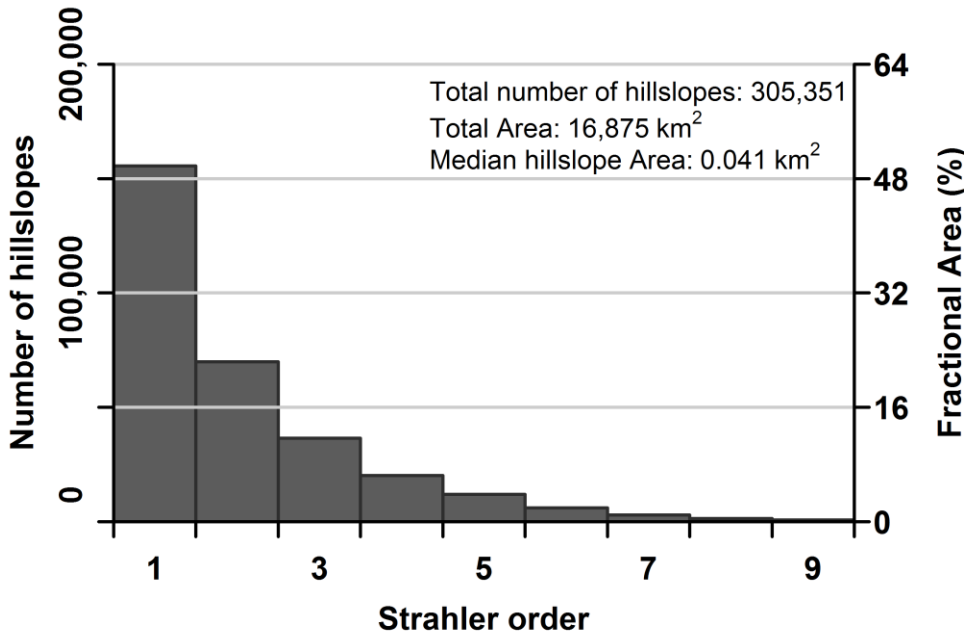

Figure 5-3. Structure of the Cedar River basin.

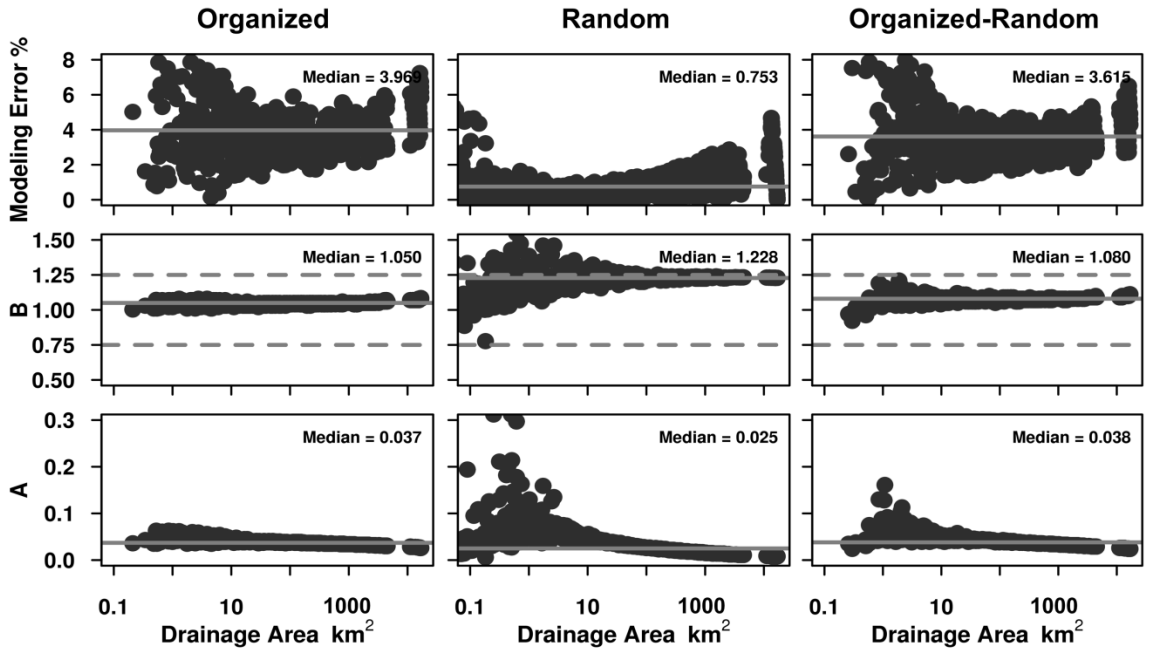

Figure 5-4. Parameters and performance of the dQ/dt = -AQB model versus drainage area. In the vertical direction, top: parameter A; middle: parameter B; and bottom: relative error of reproducing the simulated recession curves. In the horizontal direction, left: the organized scenario; middle: the random scenario; right: the organized-random scenario. The solid gray lines represent the corresponding median values. The dashed lines represent the value of B = 0.75 and B = 1.25. This result is obtained by analyzing simulated recession curves (late-time) for the Cedar River basin. The starting point used is 12 days after hydrograph peak and the recession length is 120 days.

CHAPTER 6

SUMMARY AND FUTURE RESEARCH

6.1 Conclusions

The results of data analysis show that patterns of hydrologic processes can be identified both at the small (<1 km^2) and the large spatial (>~10 km^2) scales. This is supported by:

1) The results from Chapter 2 show that the surface runoff responses from areas with spatial proximity (in the range of distance about 0~2 km) are spatially variable in magnitude while being similar in shape (the sequence of high and low flows). This spatial patter persists in time;

2) Chapter 4 shows that as a recession continues, the recession exponents associated with the stages of water being released from various storages tend to show some temporal evolution paths. Investigation of the characteristic evolution paths suggests that recession processes that occur 2-3 days after the hydrograph peak tend to be homogeneous with respect to the recession exponent (convergent to the value of 2) in the Iowa and Cedar River basins. It also indicates that subsurface drainage processes becomes more important as the spatial scale increases from 7 to 17000 km^2;

3) The data analyses in Chapter 5 suggests that the late-time recession processes over the 1988 and 2012 periods of severe drought in the Iowa and Cedar River basins can be approximated by a linear reservoir with a constant recession timescale of about 35 days.

The results of diagnostic simulations using recession in the Cedar River Basin as an example suggest that hydrologic processes at larger scales bear the spatial patterns of hydrologic processes at the small-scale:

4) The diagnostic simulation study in Chapter 5 shows that, at least for recession process, it is necessary to consider both the randomness and organization of small scale process variability in order to appropriately aggregate the hydrologic response in space. By introducing a hierarchical representation of watersheds, which jointly contrasts with the organized variability between classes and limits the random variability within each class, we were able to simultaneously reproduce 1) the increasing nonlinearity of early-time recession behavior with increasing spatial scales by introducing sufficient between-hillslope variability and 2) the linear late-time recession process at the large scale by embracing small between-hillslope variability.

The results of data analyses and diagnostic simulation study together show that while analysis of hydrologic systems at multiple spatial scales can provide useful insight into the spatial aggregation of hydrologic processes,

5) Thoughtful data collection (such as the experimental design in Chapter 2) and careful data analysis (as illustrated in Chapter 3) are the basis for the attempts made in this thesis.

6.2 Limitations

I simplified my study by making some assumptions. For the study of the spatial pattern of the surface runoff processes across neighboring hillslopes in Chapter 2, I assumed that the precipitation and soil moisture data from a NOAA weather station that is about 1~3 km away were representative for the 12 hillslopes of interest. The Iowa Flood Center is collaborating with colleagues from Iowa State University to enhance the monitoring network at these experimental sites. A more thorough analysis of more

detailed precipitation and soil moisture data collected at the hillslopes may help deepen our understanding of the controls of the pattern. When analyzing recession curves, I followed many other studies that neglect the impact of evapotranspiration on recession process. It seems reasonable to assume that the influence of evapotranspiration on the late-time recession processes during the server 1988 and 2012 droughts are negligible, while it is not true in the case of early-time recession processes under normal conditions. Contrasting recession processes at late-time during periods of severe drought (nearly no evapotranspiration) with those at the early-time may facilitate assessment of how the zero evapotranspiration assumption affects the results presented in this study. In the diagnostic simulation study, the interactions between neighboring hillslopes are not considered and warrant enhancement in future work.

I centered my exploration of hydrologic processes in Iowa for four reasons. First, Iowa is representative of the U.S. Midwestern watersheds subject to agricultural land use and a humid climate. Second, the landscape in Iowa is relatively uniform and the regulation due to such as big reservoirs and lakes is rare. Third, the topic of this thesis follows the mission of the Iowa Flood Center, which is to develop physically-based hydrologic models for flood prediction to better serve the communities in the state of Iowa. Lastly, I have superior knowledge about this region. It would be interesting to test the validity of the results found in Iowa in other regions in order to assess the universality of the characteristics of hydrologic processes.

Lastly, increasing my knowledge of the physiography and geology of the study region and being exposed to more field work would enhance my interpretation of the results of data analysis in the thesis.

6.3 Future research

I discuss two aspects of future research including the short-term plans to refine the work that has been done in this thesis and the long-term more broad research perspectives.

Using the lagged regression method to analyze rainfall time series measured at sites with spatial proximity may provide insights for the understanding of the observed spatial patterns of the surface runoff presented in Chapter 2. This proposed approach may help to understand how small-scale rainfall characteristics affect the magnitude, overall shape, and timing of spatial runoff fields. The 12 hillslopes studied are nested in two nearby USGS gauges, providing us the opportunity to investigate how this small-scale runoff patterns scale up.

It would be interesting to investigate the sources of the water consumed by vegetation and thus to assess the impact of evapotranspiration on various stages of the recession processes. This can be pursued by comparing the amount of soil moisture depletion with the evapotranspiration data available. Attacking this problem may also shed light on the estimation of evapotranspiration using streamflow data.

Groundwater dominates baseflow recession processes during extreme drought periods. Examining the concurrent hydrograph recessions of streamflow and groundwater levels have the potential to provide a more comprehensive and reliable characterization of the subsurface drainage processes.

The results of this thesis offer insight into the connection between the patterns of hydrologic processes at multiple spatial scales and foster the aggregation of hydrologic processes in space. However, the challenge to find a simple yet effective representation of small scale process variability remains. Catchments are categorized as complex systems with some degree of organization (Dooge, 1986), which indicates that both aspects of organization (spatial pattern) and randomness of smaller-scale process are important for the hydrologic response at larger scales. This inspires many potential approaches to represent watersheds. One approach is to adopt the representative

elementary volume concept (e.g., Hubbert, 1957; Wood et al., 1988; Reggiani et al., 1998), which is still open to debate. A second approach is to look for emergent spatial patterns and consider them in the context of hydrologic modeling (e.g., Beven and Kirkby, 1979; Moore and Grayson, 1991; Blöschl and Sivapalan, 1995; Grayson et al., 1997; McGlynn et al., 2003; Sivapalan, 2003; Schulz et al., 2006; Jencso et al., 2009; Van Nieuwenhuyse et al., 2011). This thesis follows the second method. Identifying patterns of hydrologic processes at various spatial scales is limited by the innovative data collection. The explosive development of new technologies, such as the application of tracers, ground penetrating radar, electrical resistance tomography, and remote sensing techniques, together with thoughtful experimental designs such as the nested basin and paired basin approaches, have the potential to identify spatial patterns in the future. Quantitative consideration of the identified small scale spatial patterns using simple indices (e.g., Beven and Kirkby, 1979; McGlynn et al., 2003; Jencso et al., 2009; Van Nieuwenhuyse et al., 2011) also warrants further investigation. Therefore, measuring, identifying, and accounting for spatial patterns of hydrologic processes to enhance the capability of distributed hydrologic models, and thus providing useful information for water resources management under the changing climate and environment, is an emerging area of interest for hydrologists.

APPENDIX A

CONTROLS OF THE SCALING FACTOR

For each individual runoff event, we explored the spatial variation of the scaling factor by plotting the scaling factor of each hillslope against the structural characteristics of the hillslope including 1) width of prairie strip at footslope; 2) maximum slope length; 3) slope; 4) and drainage area. High shape similarity persists across hillslopes for all of the events showed in Figure A-1 to A-3. These figures suggest that the spatial variation of the scaling factor for individual events is weakly related to and cannot be consistently explained by the individual structural characteristics of the hillslopes we investigated in this study. However, the combined effects of these structural characteristics of the hillslopes on the spatial variation of the scaling factor cannot be detected through the analysis presented here.

We also explored the relationship between the temporal variation of the scaling factor and the rainfall and runoff characteristics for each hillslope. For most of the hillslopes, the scaling factors are weakly related to the total amount of rainfall (Figure A-4), indicating that the effect of the total amount of rainfall on the scaling factor is masked by other factors that are more important. Figure A-5 shows that for most of the hillslopes, the scaling factor increases towards unity with the increase in the peak runoff rate, implying that the more runoff generated, the more similar the hillslopes are in producing runoff.

These analyses suggest exploring how other factors, such as the rainfall intensity, antecedent soil moisture, and seasonality influence the spatiotemporal variability of the scaling factor. This was done in Chapter 2.

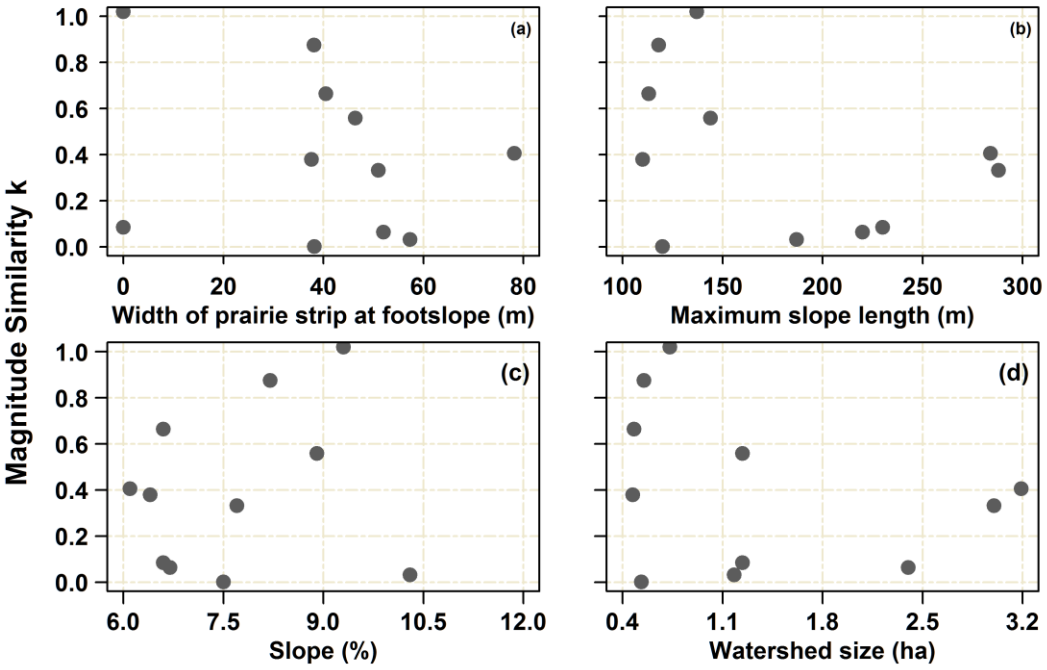

Figure A-1. Scatterplots of scaling factor *k* versus width of prairie strip widths at footslope (a), maximum slope lengths (b), slopes (c), and sizes (d) of the hillslopes for the event on May 25 of 2008.

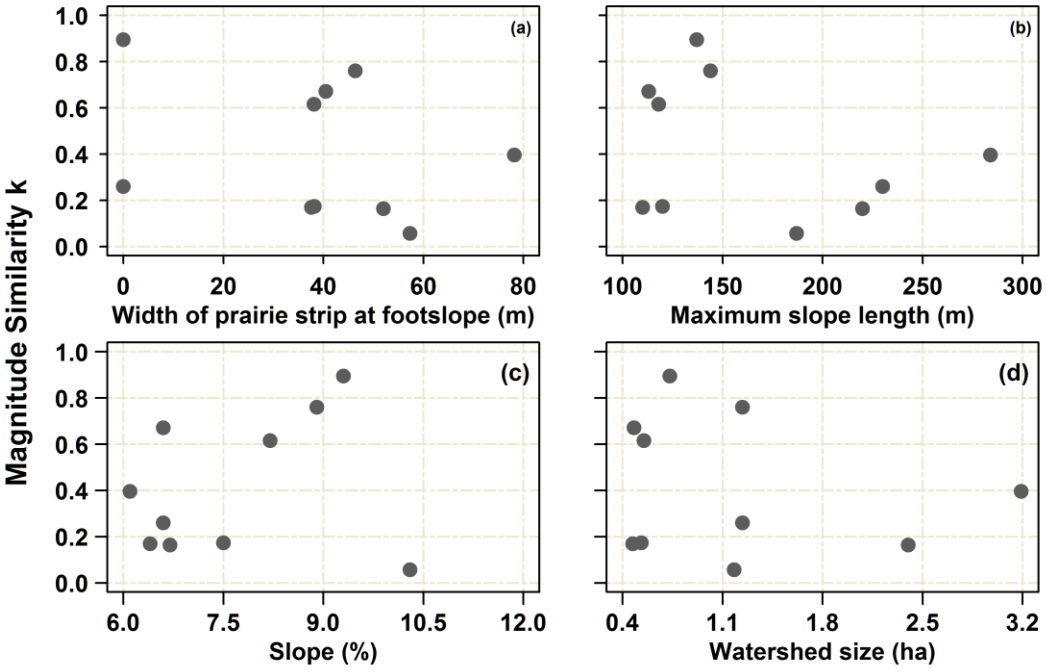

Figure A-2. The same as Figure A-1but for the event on April 26 of 2009.

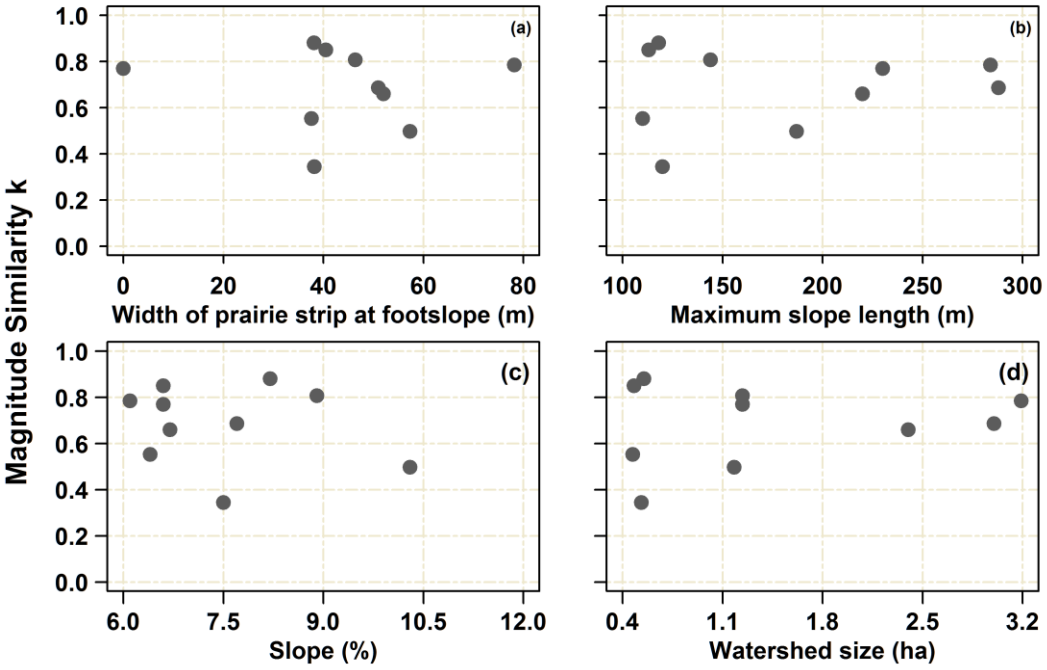

Figure A-3. The same as Figure A-1but for the event on June 10 of 2011.

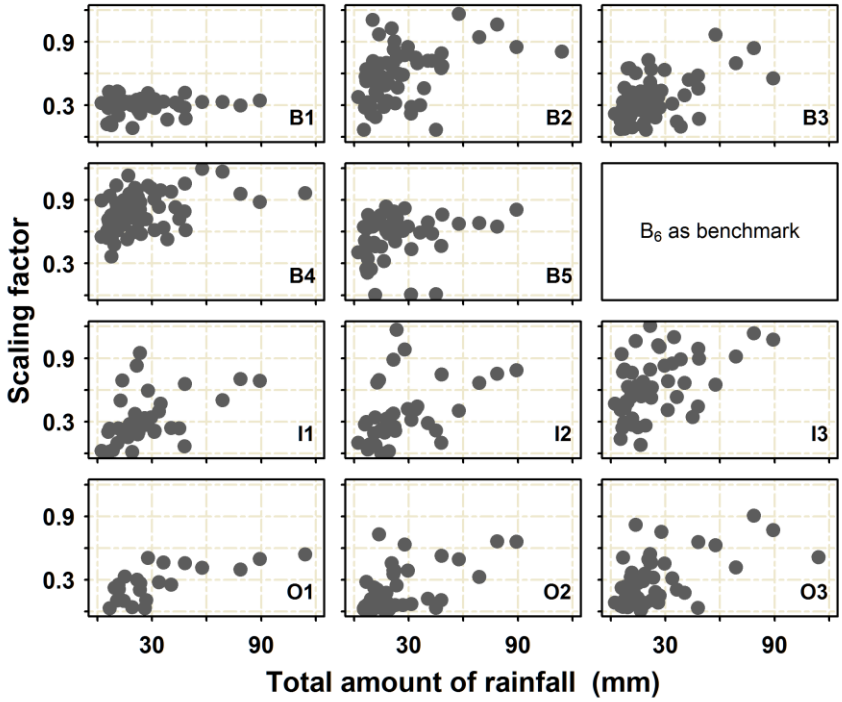

Figure A-4. Relationship between the scaling factor and the total amount of rainfall of each storm event.

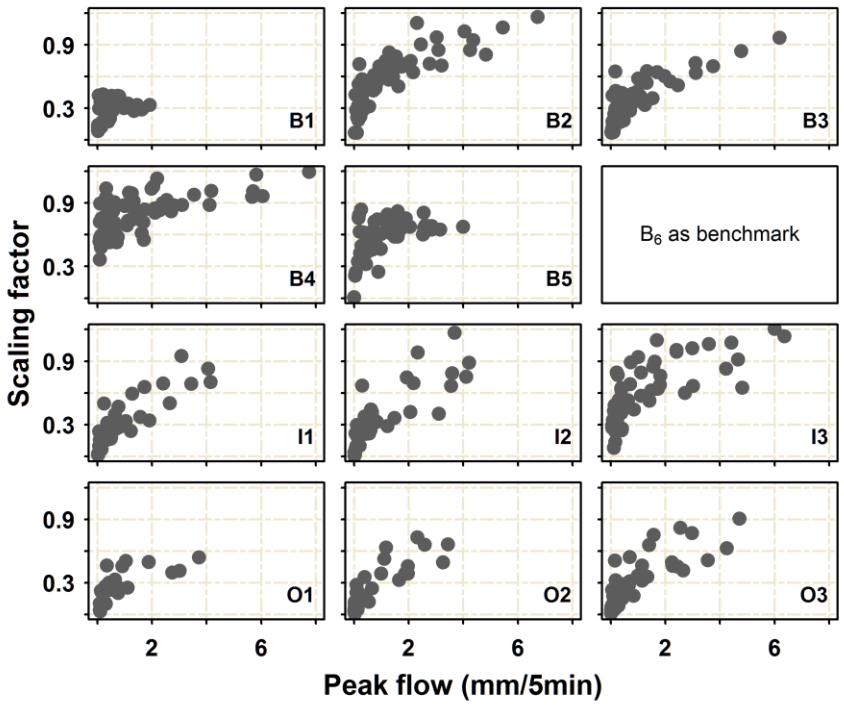

Figure A-5. Relationship between the scaling factor and the peak flow at each hillslope for each storm event.

APPENDIX B

SENSITIVITY OF RECESSION ANALYSIS TO THE CHOICE OF ΔT

The most widely used approach for analyzing recession curve, which is proposed by Brutsaert and Nieber, examines the rate of change of discharge *dQ/dt* as a function of discharge *Q*, thus eliminating the need of determining a time reference:

$$-\frac{dQ}{dt} = f(Q) \tag{B-1}$$

where *f* is the characteristic function for a recession event. Since *Q* is the discharge observed at the basin outlet, equation (B-1) is a lumped recession model. As suggested by Brutsaert and Nieber and has been validated by extensive recession analyses across geographical and climate regions, *f* typically takes the form of the power law relationship:

$$-\frac{dQ}{dt} = AQ^{B} \tag{B-2}$$

where *A* and *B* are parameters. Parameters *A* and *B* are named as recession intercept and recession slope, respectively, in the plot of *log(-dQ/dt)* against *log(Q)*. The recession intercept *A* and recession slope *B* represent two characteristics of a recession event, i.e., the linearity of recession process and the recession rate, respectively. Under the scenario of $B = 1$, i.e., a linear reservoir, *1/A* is named as recession timescale (has a unit of time).

The terms in equation (B-2) can be calculated using the backwards difference and average as $dQ/dt = (Q_t - Q_{t-\Delta t})/\Delta t$ and $Q = (Q_t + Q_{t-\Delta t})/2$ for a given recession segment, where the time step Δt can be constant or variable. The constant time step can be chosen to be 1 day (e.g., Brutsaert and Nieber, 1977; Vogel and Kroll, 1992), 1 hour (e.g., Clark et al., 2009), or 15 minutes(e.g., Rupp and Selker, 2006b). Rupp and Selker (2006a) showed that the constant time step method may bias the estimates of *A* and *B*, and they recommended the use of variable time steps to calculate *dQ/dt* in order to remove this

limitation. The terms in equation (B-2) can also be numerically expressed using other schemes, such as the central difference and average.

The optimal choice of the time step Δt is determined from the consideration of the drainage process of interest, the observational frequency, and the magnitude of noise of streamflow data. Using a too small Δt may suffer from the noise in the streamflow data, i.e., $\Delta Q = (Q_t - Q_{t-\Delta t})$ may become comparable to the magnitude of data uncertainty, while choosing a too large Δt may lose the capability to capture the temporal evolution of the different drainage processes for a single recession event. Two ways can be used to tackle this problem: 1) using a shorter time step for the early stages and a longer time step for the late stages of the recession process (variable Δt); and 2) using a method that is not sensitive the choice of Δt. Rupp and Selker (2006a) pursued the along the first direction and we chase the second in the following.

The recession segment that observed at the USGS gauge at Clear Creek near Coralville over the 7-day period from June 26 to July 3 of 2007 is used as an example to investigate the sensitivity of recession analysis to the choice of Δt. We first aggregated the streamflow data originally observed at the interval of 15 minutes to hourly and daily data by averaging over the aggregation intervals, and then estimated the recession parameters A and B using the constant time step (CTS), variable time step (VTS), and the nonlinear direct fitting (NDF) method.

Comparison shows that the nonlinear direct fitting method is not sensitive to the choice of time step Δt (Figure B-1). Consistent with the literature, our result indicates that the constant time step method is most sensitive the choice of time step (the same as the temporal resolution of the data) and the variable time step method greatly reduces this sensitivity. Interestingly, the estimates given by the nonlinear direct fitting method are almost identical when data with different temporal resolutions are used. Furthermore, the differences in the parameter estimates decrease with the degradation of the temporal resolution of streamflow data and are negligible at the daily scale. The similar values of

A and *B* showed in the bottom and rightmost panels indicate that the nonlinear direct fitting method is most capable among the three to deal with data noise, allowing for analyzing both the early- and the late-time recession data with high temporal resolution. The variable time step method can also be used for this purpose, while more information is needed to determine the threshold value *C*.

We provide more details about our data analysis to explain the significant differences between the estimates and the data in Figure B-1. We discuss three aspects of the model fitting that logically demonstrate the correctness of the results:

1) Theoretical aspects: regression in the log-log and the original scales

Both the CTS and the VTS methods estimate *A* and *B* in the log-log scale using the least squares linear regression. Therefore, the goal is to maximize the amount of variation in $log(-dQ/dt)$ rather than the variation in $-dQ/dt$ that is explained by the power-law recession models. In contrast, the NDF method uses iterative direct curve fitting to estimate *A* and *B* in the original units. This leads to different optimal solutions for *A* and *B*, especially when significant noise (such as measurement error in stages, errors due to the rating curves, and evapotranspiration) exists in the recession data.

2) Theoretical aspects: handling data noise

Mathematically, the CTS and the VTS methods calculate $-dQ/dt$ using forward or backward differences, which are subject to numerical errors. This indicates that the estimates of *A* and *B* given by these two methods may be sensitive to the local noise in the recession data. In contrast, the NDF method estimates the parameters using

$$A = \frac{\sum_{t=1}^{n}[Q(t) - Q(t-1)]}{\Delta t \sum_{t=1}^{n}[\frac{Q(t) + Q(t-1)}{2}]^{B}} \tag{B-3}$$

by systematically varying *B*. The summations in the equation make the estimation more robust with respect to local errors in the recession data due to the smoothing effect.

3) Practical aspects: Code checking

There is always a possibility that we made errors in our codes. We carefully checked our code. In addition, using the event shown in Figure B-1 as an example, we also compared the results given by our code and Excel. A comparison of the middle panel of Figure B-1 to Figure B-2 shows that the results given by our code and Excel are consistent. It is difficult to check the NDF method using Excel, but we do not think that its result is questionable. Also, our simulation shows that the method performs well in the limit of "low noise" (the rightmost panel in Figure B-1).

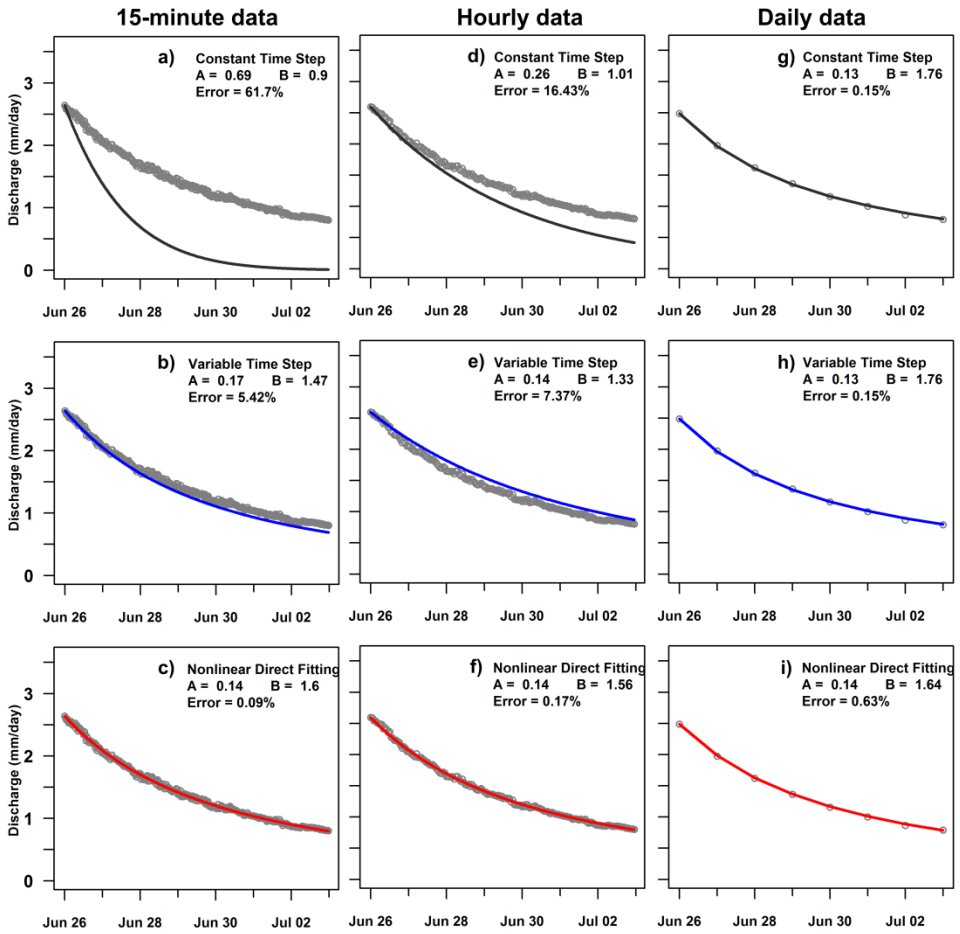

Figure B-1. Comparison of *A* and *B* estimated using three methods and streamflow data with three temporal resolutions. This 27-day long recession segment was observed at the USGS gauge at Clear Creek near Coralville (USGS05454300) with an observational interval of 15 minutes. We extracted the recession segment from the complete recession curve using a starting point of 2 days and a length of 7 days. We aggregated the 15-minute streamflow data to hourly and daily data by taking the mean values. The open circles are the observed streamflow values, and the lines are the modeled recession segments using the estimated parameters. For the variable time step method, the value $C = 0.001$ was used to reduce the impact of the noise in streamflow data on the estimation of recession parameters. The modeling error was calculated as the relative difference between the volumes of modeled and observed recession flows.

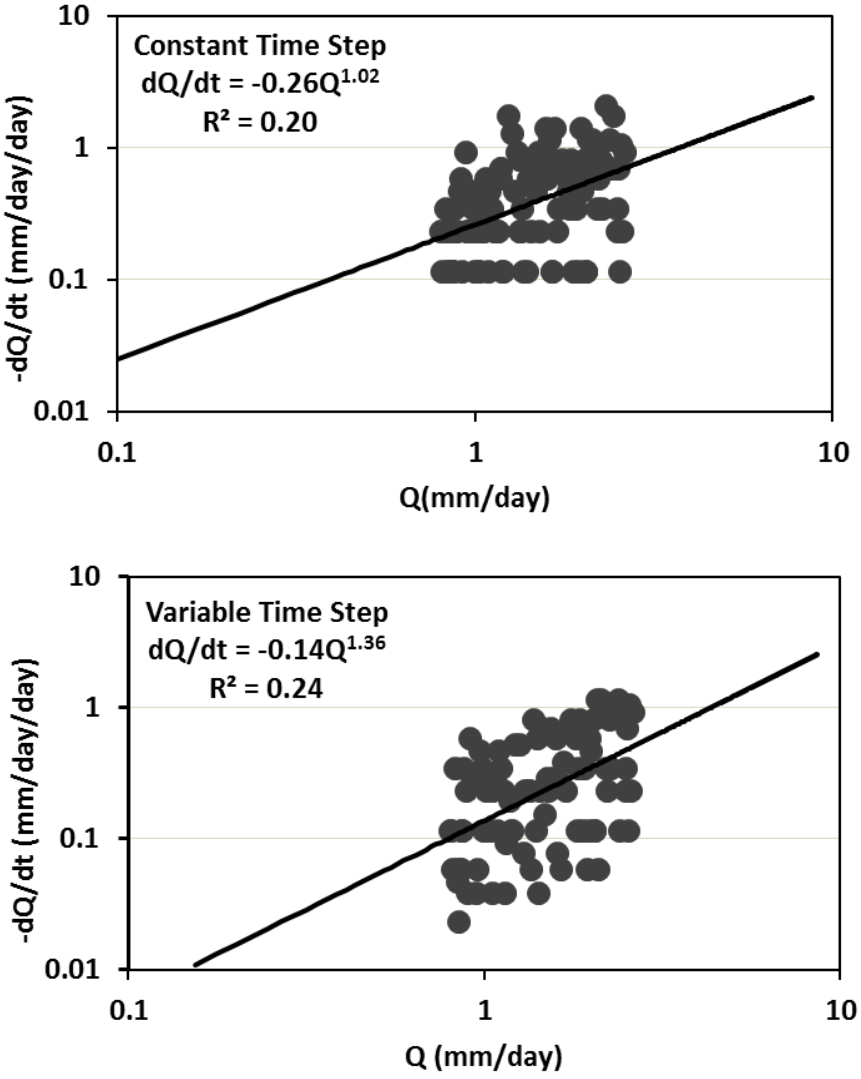

Figure B-2. Estimating the recession parameters using the CTS and the VTS methods in Excel. The same hourly data as that in the middle panel of Figure B-1 is used here. This figure is used to verify the results given by our code.

APPENDIX C

ANALYSIS OF LATE-TIME RECESSIONS DURING SEVERE DROUGHT EVENTS

We compare the characteristics of late-time recession behaviors for the nested basins in the Iowa and Cedar River basins during the 1988 and 2012 severe droughts. Since our goal is to investigate the effect of spatial scales on the late-time recession behavior for a relatively homogeneous region, long periods over which all the basins experience similar wetting and drying history will be our targets. Though there are many other drought years since 1970, the 1988 and 2012 drought events similarly last for long periods and cover wide areas, allowing for an apple-to-apple comparison. Daily streamflow data are used here.

Stability of the results of analyzing recessions during the 2012 drought

We first show the stability of the results of analyzing 2012 drought recessions using our carefully designed calculation procedure. The result of recession analysis is sensitive to the calculation procedure, i.e., the selection of recession segment and parameter estimation methods (see Chapter XXX). This sensitivity originates from the complex temporal evolution of the dominant drainage processes for each recession event and the noise in the recession data. It is not unreasonable to assume that the dominant drainage process is the releasing of water from the unconfined aquifers during the late-time (10 days after hydrograph peak) recession processes. Therefore, data noise in the recession data is of our major concern that may impact the results of our analyses. The major sources of noise in streamflow data are the stage measurement inaccuracies and the transformation of stage to discharge using rating curves. We assume that the impact of evapotranspiration on recession process is negligible during the severe drought periods, such as the 1988 and 2012 droughts. We note that the magnitude of data error is more pronounced for during the periods of floods and droughts, and thus we use long recession

segments and noise-robust method (the nonlinear direct fitting method) to estimate the recession parameters for this analysis.

The parameter estimates for the 2012 drought are stable. Figure C-1, Figure C-2, and Figure C-3show that the values of A and B are around 0.03 and 1, respectively, when different starting points and recession lengths are used. This indicates that the late-time recession behaviors for the Iowa and Cedar River basins during the 2012 drought can be approximated by a linear reservoir with a recession timescale (equals *1/A*) of about 33 days.

Stability of the results of analyzing recessions during the 1988 drought

We now analyzing the recessions in the Iowa and Cedar River Basins during the 1988 drought. Though the 1988 drought might be a good candidate to study the late-time recession behaviors across scales, the quality of the recession data is poor. The flow rates at the beginning of the recessions for most gauges are around or below their 25% quintiles. This makes the accurate measurement of streamflow difficult, which can partly explain the high data noise. The data noise together with other factors such as small amount of precipitation make the usable duration for late-time recession analysis to be around 45 days.

The parameter estimates for the 1988 drought are stable. Figure C-4 and Figure C-5 show that the estimated recession timescales are around 35 days (*A = 0.028*), respectively, when different recession lengths (30 and 45 days) are used. Figure C-6 illustrates that the recession segments that are effective for our data analysis at all gauges can be reasonably modeled with fixed parameters, indicating that the late-time recession behaviors for the Iowa and Cedar River basins during the 1988 drought can be represented by a linear reservoir with a recession timescale of about 35 days (i.e., *A = 0.028*). Since the usable lengths of recession segments are limited and the flows are too

low, we fixed the starting point of the recession segments to be 5 days after hydrograph peak and constrained the value of *B* to be 1 for this analysis.

Comparison between the 1988 and the 2012 recessions

As summarized in Figure C-7, the results of analyzing the 1988 and 2012 drought are consistent, suggesting that the late-time recession processes in the Iowa and Cedar River basins tend to be linear and homogeneous. The recession timescale of late-time drainage processes tends to be constant (~ 33 days) at the spatial scales ranging from about 70 to 17000 km^2. This is consistent with the findings that late-time recession timescale becomes more stable (e.g., Savenije, 2001) and converges to 45 ± 15 days as the catchment size increases (Brutsaert, 2008). Overall, our analysis supports the hypothesis that the late-time recession behavior for large basins, in at least some regions, can be described by a linear and homogeneous groundwater reservoir.

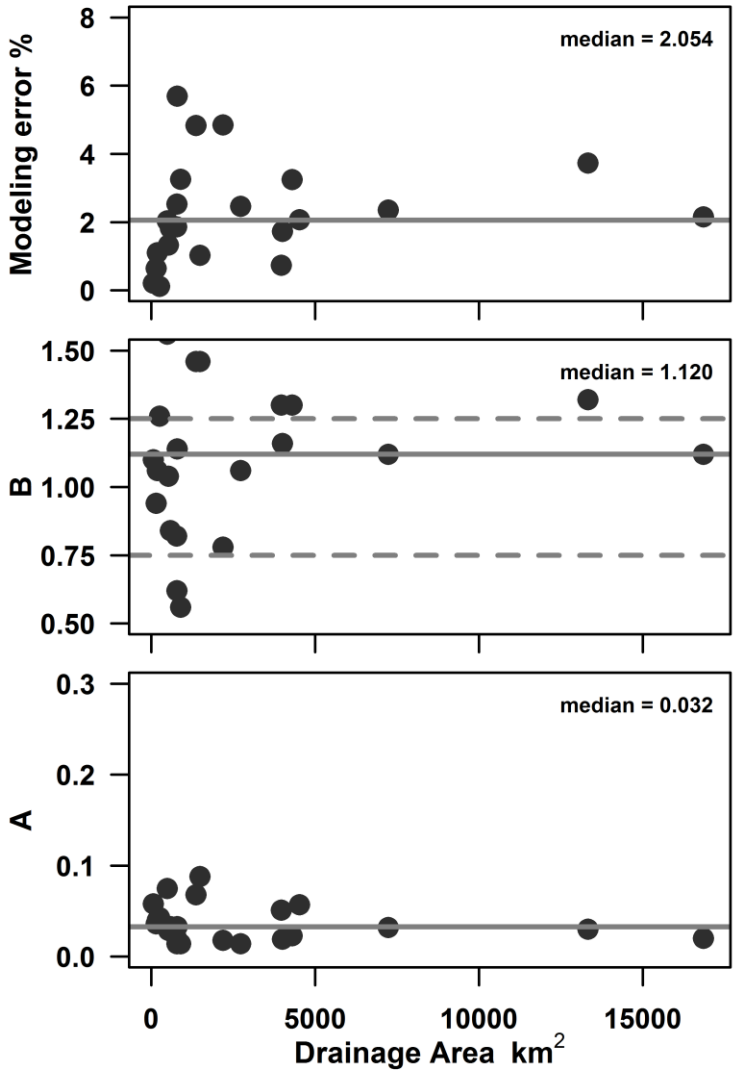

Figure C-1. Performance and parameters of the $dQ/dt = -AQ^B$ model plotted as a function of the drainage area top: modeling error of reproducing the observed recession curves; middle: parameter *B*; and bottom: parameter *A*. The horizontal gray lines represent the corresponding median values. The result is obtained by analyzing the observed recession curves (late-time) in the Iowa and Cedar River basins during the 2012-2013 drought. The starting point used is 10 days after hydrograph peak and the recession length is 120 days.

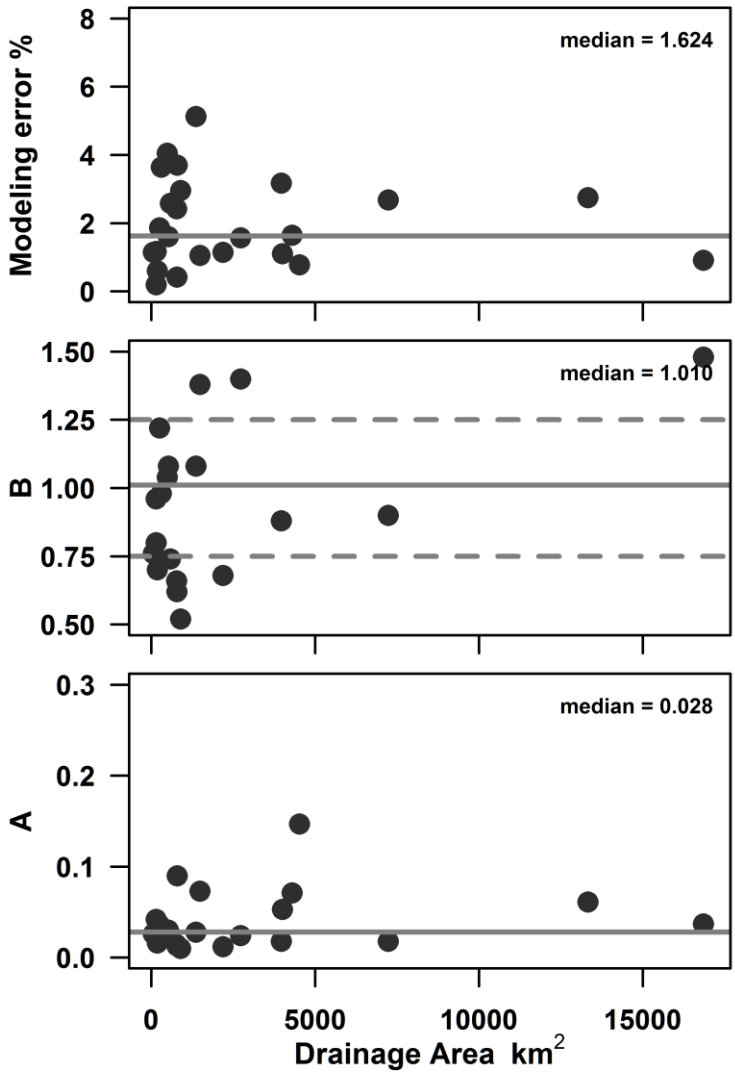

Figure C-2. Similar to Figure C-1 but the starting point used is 20 days after hydrograph peak and the recession length is 120 days.

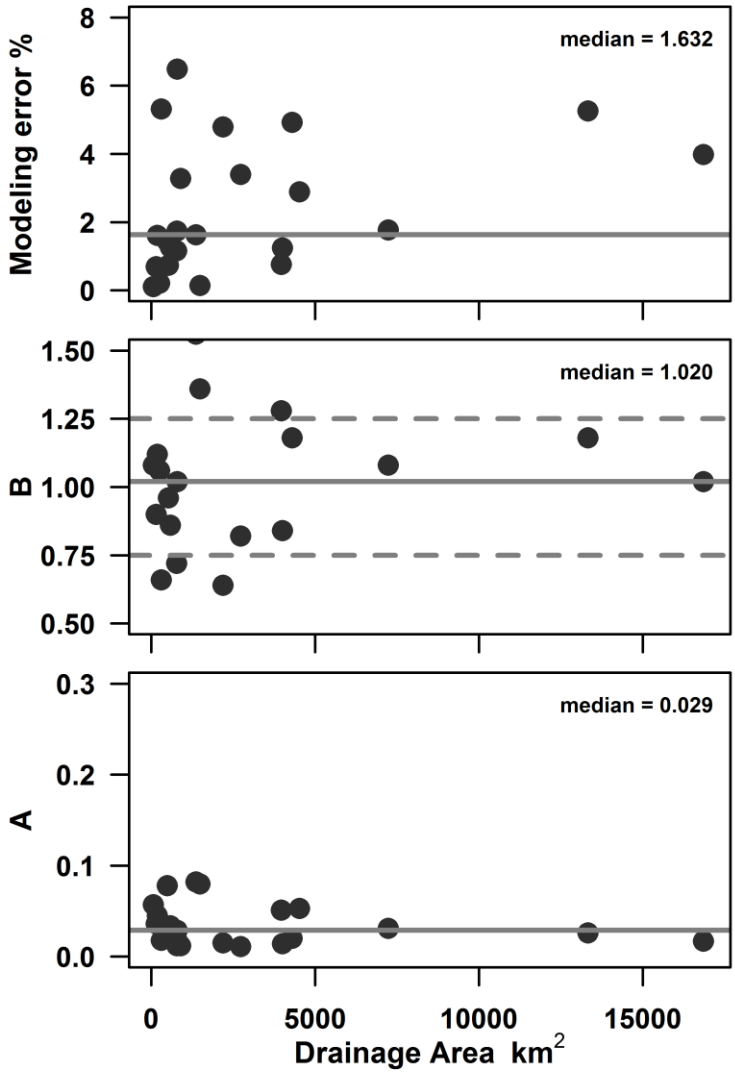

Figure C-3. Similar to Figure c-1 but the starting point used is 10 days after hydrograph peak and the recession length is 90 days.

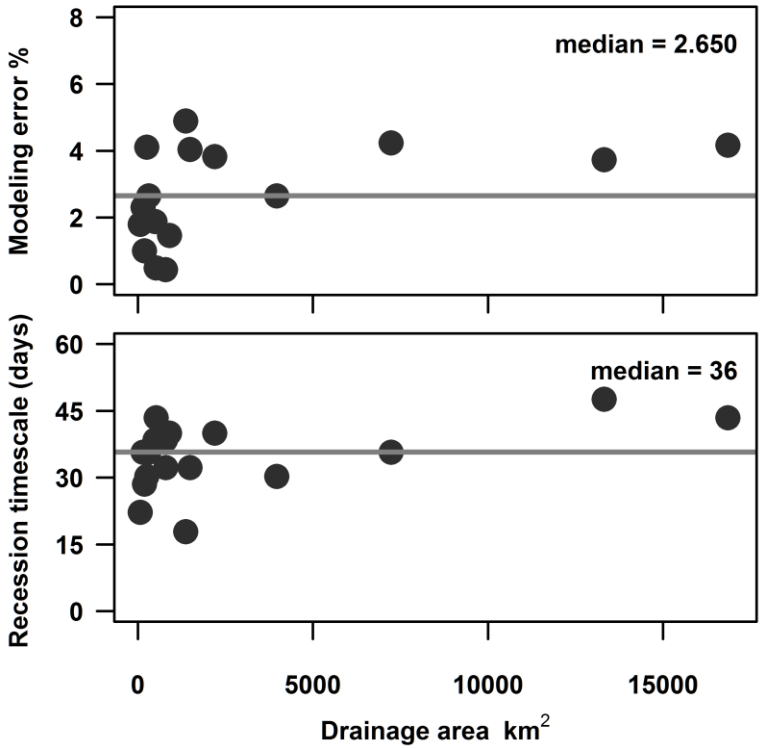

Figure C-4. Performance and parameters of the $dQ/dt = -AQ^B$ model plotted as a function of the drainage area top: modeling error of reproducing the observed recession curves; and bottom: recession timescale ($1/A$). The horizontal gray lines represent the corresponding median values. The result is obtained by analyzing the observed recession curves (late-time) in the Iowa and Cedar River basins during the 1988 drought. The starting point used is 5 days after hydrograph peak and the recession length is 30 days.

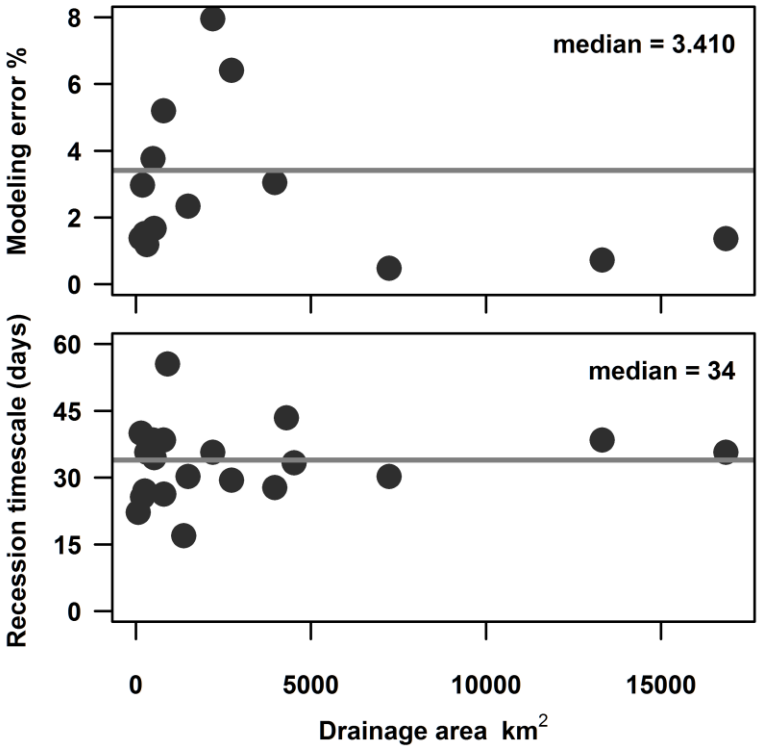

Figure C-5. Similar to Figure C-4 but the starting point used is 5 days after hydrograph peak and the recession length is 45 days.

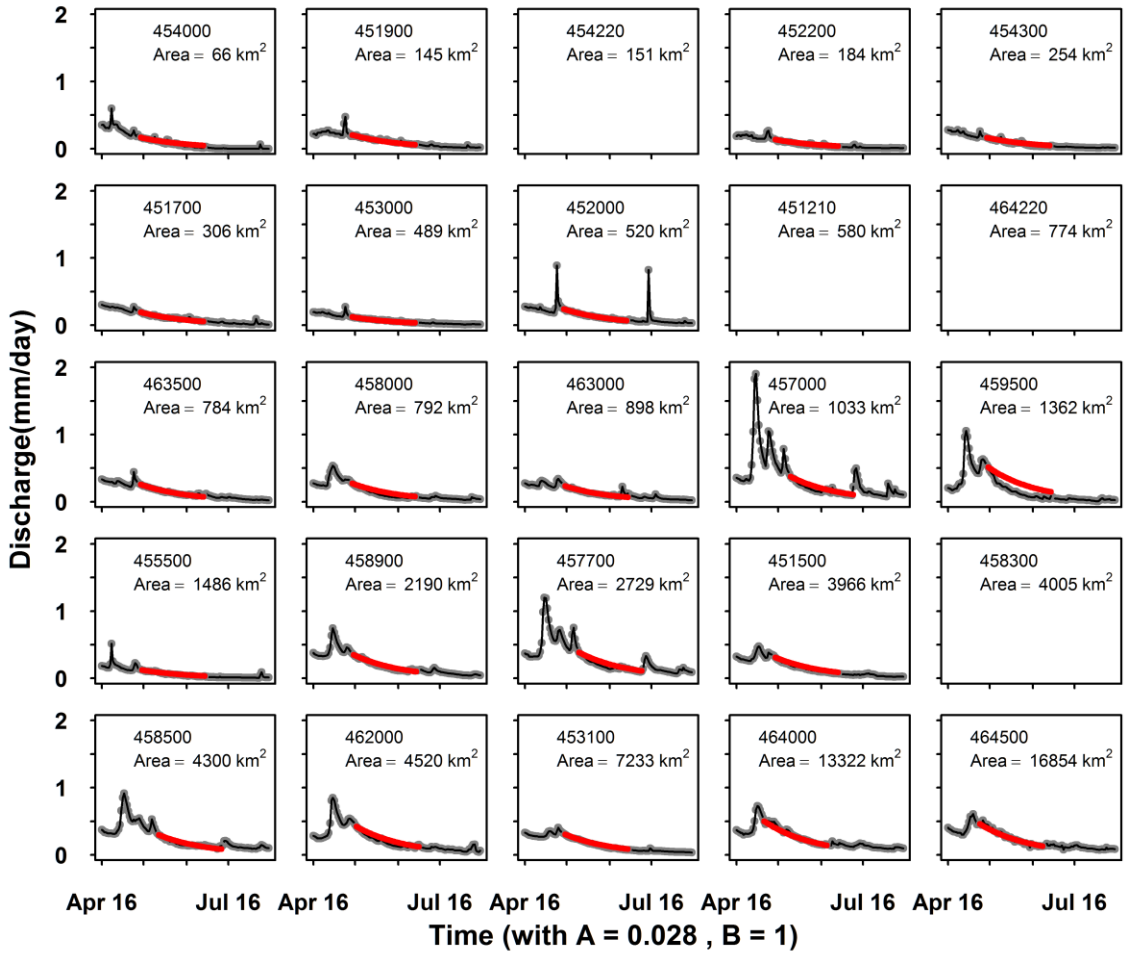

Figure C-6. Comparison between the observed (gray) and modeled (red) recession curves during the 1988 drought. Constant values of $A = 0.028$ (recession timescale of 36 days) and $B = 1$ are used for modeling recession curves at all gauges.

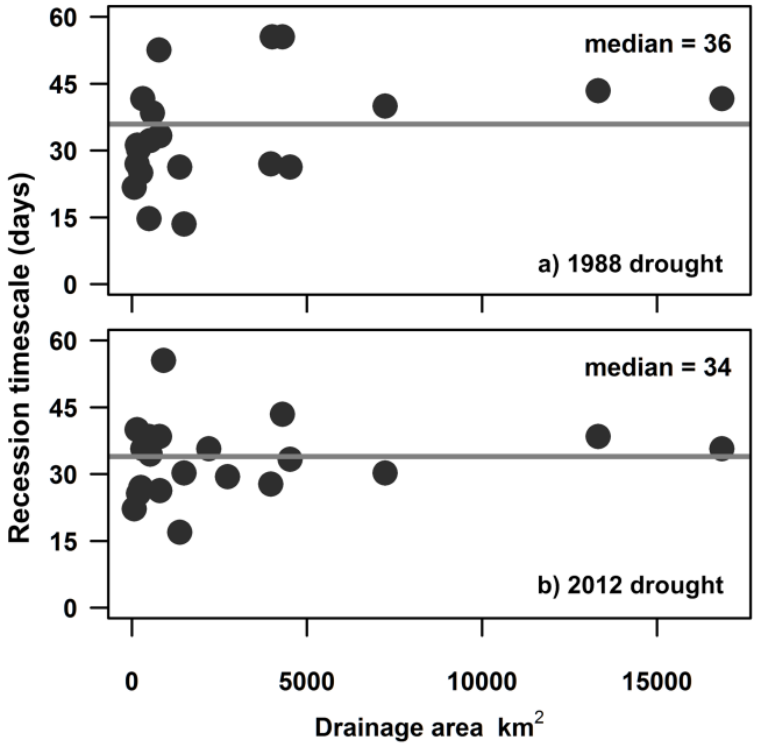

Figure C-7. Recession timescales of late-time drainage processes plotted as a function of the drainage area for a) the 1988 drought; and b) the 2012 drought. The horizontal gray lines represent the corresponding median values. The result is obtained by analyzing the observed recession curves (late-time) in the Iowa and Cedar River basins.

REFERENCES

Abaci, O., Papanicolaou, A.N.T., 2009. Long-term effects of management practices on water-driven soil erosion in an intense agricultural sub-watershed: monitoring and modelling. Hydrological Processes, 23(19): 2818-2837. doi: 10.1002/hyp.7380.

Aksoy, H., Wittenberg, H., 2011. Nonlinear baseflow recession analysis in watersheds with intermittent streamflow. Hydrological Sciences Journal, 56(2): 226-237. doi: 10.1080/02626667.2011.553614.

Andréassian, V., Lerat, J., Le Moine, N., Perrin, C., 2012. Neighbors: Nature's own hydrological models. Journal of Hydrology, 414–415(0): 49-58. doi: http://dx.doi.org/10.1016/j.jhydrol.2011.10.007.

Archfield, S.A., Vogel, R.M., 2010. Map correlation method: Selection of a reference streamgage to estimate daily streamflow at ungaged catchments. Water Resour. Res., 46(10): W10513. doi: 10.1029/2009wr008481.

Arnold, J.G., Allen, P.M., Muttiah, R., Bernhardt, G., 1995. Automated Base Flow Separation and Recession Analysis Techniques. Ground Water, 33(6): 1010-1018. doi: 10.1111/j.1745-6584.1995.tb00046.x.

Arnold, J.G., Srinivasan, R., Muttiah, R.S., Williams, J.R., 1998. Large area hydrologic modeling and assessment part I: Model development. JAWRA Journal of the American Water Resources Association, 34(1): 73-89. doi: 10.1111/j.1752-1688.1998.tb05961.x.

Asano, Y., Uchida, T., 2010. Is representative elementary area defined by a simple mixing of variable small streams in headwater catchments? Hydrological Processes, 24(5): 666-671. doi: 10.1002/hyp.7589.

Avants, B.B., Epstein, C.L., Grossman, M., Gee, J.C., 2008. Symmetric diffeomorphic image registration with cross-correlation: Evaluating automated labeling of elderly and neurodegenerative brain. Medical Image Analysis, 12(1): 26-41. doi: http://dx.doi.org/10.1016/j.media.2007.06.004.

Bachmair, S., Weiler, M., Troch, P.A., 2012. Intercomparing hillslope hydrological dynamics: Spatio-temporal variability and vegetation cover effects. Water Resources Research, 48(5): W05537. doi: 10.1029/2011wr011196.

Band, L.E., 1986. Topographic Partition of Watersheds with Digital Elevation Models. Water Resources Research, 22(1): 15-24. doi: 10.1029/WR022i001p00015.

Bautista, S., Mayor, Á., Bourakhouadar, J., Bellot, J., 2007. Plant Spatial Pattern Predicts Hillslope Runoff and Erosion in a Semiarid Mediterranean Landscape. Ecosystems, 10(6): 987-998. doi: 10.1007/s10021-007-9074-3.

Benda, L.E.E. et al., 2004. The Network Dynamics Hypothesis: How Channel Networks Structure Riverine Habitats. BioScience, 54(5): 413-427. doi: 10.1641/0006-3568(2004)054[0413:TNDHHC]2.0.CO;2.

Berne, A., Krajewski, W.F., 2013. Radar for hydrology: Unfulfilled promise or unrecognized potential? Advances in Water Resources, 51(0): 357-366. doi: http://dx.doi.org/10.1016/j.advwatres.2012.05.005.

Berthet, L., Andréassian, V., Perrin, C., Javelle, P., 2009. How crucial is it to account for the antecedent moisture conditions in flood forecasting? Comparison of event-based and continuous approaches on 178 catchments. Hydrol. Earth Syst. Sci., 13(6): 819-831. doi: 10.5194/hess-13-819-2009.

Beschta, R.L., Pyles, M.R., Skaugset, A.E., Surfleet, C.G., 2000. Peakflow responses to forest practices in the western cascades of Oregon, USA. Journal of Hydrology, 233(1–4): 102-120. doi: 10.1016/s0022-1694(00)00231-6.

Betson, R.P., 1964. What is watershed runoff? Journal of Geophysical Research, 69(8): 1541-1552. doi: 10.1029/JZ069i008p01541.

Beven, K., 1989. Changing ideas in hydrology — The case of physically-based models. Journal of Hydrology, 105(1–2): 157-172. doi: http://dx.doi.org/10.1016/0022-1694(89)90101-7.

Beven, K., 1997. TOPMODEL: A critique. Hydrological Processes, 11(9): 1069-1085. doi: 10.1002/(sici)1099-1085(199707)11:9<1069::aid-hyp545>3.0.co;2-o.

Beven, K., 2012. Rainfall-runoff modelling : the primer. Wiley-Blackwell: Chichester.

Beven, K., Binley, A., 1992. The future of distributed models: Model calibration and uncertainty prediction. Hydrological Processes, 6(3): 279-298. doi: 10.1002/hyp.3360060305.

Beven, K., Freer, J., 2001a. A dynamic TOPMODEL. Hydrological Processes, 15(10): 1993-2011. doi: 10.1002/hyp.252.

Beven, K., Freer, J., 2001b. Equifinality, data assimilation, and uncertainty estimation in mechanistic modelling of complex environmental systems using the GLUE methodology. Journal of Hydrology, 249(1-4): 11-29. doi: 10.1016/s0022-1694(01)00421-8.

Beven, K.J., 2011. Rainfall-runoff modelling: the primer. Wiley. com.

Beven, K.J., Kirkby, M.J., 1979. A physically based, variable contributing area model of basin hydrology / Un modèle à base physique de zone d'appel variable de l'hydrologie du bassin versant. Hydrological Sciences Bulletin, 24(1): 43-69. doi: 10.1080/02626667909491834.

Beven, K.J., Wood, E.F., Sivapalan, M., 1988. On hydrological heterogeneity — Catchment morphology and catchment response. Journal of Hydrology, 100(1–3): 353-375. doi: http://dx.doi.org/10.1016/0022-1694(88)90192-8.

Bierkens, M.F., Finke, P.A., Willigen, P.d., 2000. Upscaling and Downscaling Methods for Environmental Research. Developments in Plant and Soil Science, 88. Kluwer Academic, Dordrecht, Boston, London, 190 pp.

Birkhoff, G.D., 1931. Proof of the ergodic theorem. Proceedings of the National Academy of Sciences of the United States of America, 17(12): 656.

Biswal, B., Marani, M., 2010. Geomorphological origin of recession curves. Geophysical Research Letters, 37(24): L24403. doi: 10.1029/2010gl045415.

Biswal, B., Marani, M., 2014. 'Universal' recession curves and their geomorphological interpretation. Advances in Water Resources, 65(0): 34-42. doi: http://dx.doi.org/10.1016/j.advwatres.2014.01.004.

Biswal, B., Nagesh Kumar, D., 2013. A general geomorphological recession flow model for river basins. Water Resources Research: n/a-n/a. doi: 10.1002/wrcr.20379.

Biswal, B., Nagesh Kumar, D., 2014. Study of dynamic behaviour of recession curves. Hydrological Processes, 28(3): 784-792. doi: 10.1002/hyp.9604.

Blöschl, G., Grayson, R.B., Sivapalan, M., 1995. On the representative elementary area (REA) concept and its utility for distributed rainfall-runoff modelling. Hydrological Processes, 9(3-4): 313-330. doi: 10.1002/hyp.3360090307.

Blöschl, G., Sivapalan, M., 1995. Scale issues in hydrological modelling: A review. Hydrological Processes, 9(3-4): 251-290. doi: 10.1002/hyp.3360090305.

Blöschl, G., Sivapalan, M., Wagener, T., Viglione, A., Savenije, H., 2013. Runoff Prediction in Ungauged Basins: Synthesis Across Processes, Places and Scales. Cambridge University Press.

Blume, T., Zehe, E., Bronstert, A., 2007. Rainfall—runoff response, event-based runoff coefficients and hydrograph separation. Hydrological Sciences Journal, 52(5): 843-862. doi: 10.1623/hysj.52.5.843.

Bradley, A.A., Kruger, A., Meselhe, E.A., Muste, M.V.I., 2002. Flow measurement in streams using video imagery. Water Resources Research, 38(12): 1315. doi: 10.1029/2002wr001317.

Brown, V.A., McDonnell, J.J., Burns, D.A., Kendall, C., 1999. The role of event water, a rapid shallow flow component, and catchment size in summer stormflow. Journal of Hydrology, 217(3-4): 171-190. doi: 10.1016/s0022-1694(98)00247-9.

Brutsaert, W., 2008. Long-term groundwater storage trends estimated from streamflow records: Climatic perspective. Water Resources Research, 44(2): W02409. doi: 10.1029/2007wr006518.

Brutsaert, W., Lopez, J.P., 1998. Basin-scale geohydrologic drought flow features of riparian aquifers in the Southern Great Plains. Water Resources Research, 34(2): 233-240. doi: 10.1029/97wr03068.

Brutsaert, W., Nieber, J.L., 1977. Regionalized drought flow hydrographs from a mature glaciated plateau. Water Resources Research, 13(3): 637-643. doi: 10.1029/WR013i003p00637.

Brutsaert, W., Sugita, M., 2008. Is Mongolia's groundwater increasing or decreasing? The case of the Kherlen River basin. Hydrological Sciences Journal, 53(6): 1221-1229. doi: 10.1623/hysj.53.6.1221.

Carroll, R.J., Ruppert, D., Stefanski, L.A., Crainiceanu, C.M., 2010. Measurement error in nonlinear models: a modern perspective. CRC press.

Chapman, T.G., 2003. Modelling stream recession flows. Environmental Modelling & Software, 18(8–9): 683-692. doi: http://dx.doi.org/10.1016/S1364-8152(03)00070-7.

Chapman, T.G., Falkenmark, M., 1989. Comparative hydrology : an ecological approach to land and water resources. United Nations Educational, Scientific and Cultural Organization, Paris.

Ciach, G.J., Krajewski, W.F., 1999. Radar–Rain Gauge Comparisons under Observational Uncertainties. Journal of Applied Meteorology, 38(10): 1519-1525. doi: 10.1175/1520-0450(1999)038<1519:rrgcuo>2.0.co;2.

Clark, M.P. et al., 2009. Consistency between hydrological models and field observations: linking processes at the hillslope scale to hydrological responses at the watershed scale. Hydrological Processes, 23(2): 311-319. doi: 10.1002/hyp.7154.

Council, N.R., 1991. Opportunities in the Hydrologic Sciences. The National Academies Press.

Council, N.R., 2012. Challenges and Opportunities in the Hydrologic Sciences. The National Academies Press.

Dagan, G., Bresler, E., 1983. Unsaturated flow in spatially variable fields: 1. Derivation of models of infiltration and redistribution. Water Resour. Res., 19(2): 413-420. doi: 10.1029/WR019i002p00413.

de Araújo, J.C., González Piedra, J.I., 2009. Comparative hydrology: analysis of a semiarid and a humid tropical watershed. Hydrological Processes, 23(8): 1169-1178. doi: 10.1002/hyp.7232.

Dooge, J.C.I., 1973. Linear theory of hydrologic systems. Tech. Bull. 1468: 327 pp. Agric. Res. Serv., U.S. Dep. of Agric., Washington, D. C.

Dooge, J.C.I., 1986. Looking for hydrologic laws. Water Resources Research, 22(9S): 46S-58S. doi: 10.1029/WR022i09Sp0046S.

Draper, N.R., Smith, H., Pownell, E., 1966. Applied regression analysis, 3. Wiley New York.

Duan, Q., Sorooshian, S., Gupta, V., 1992. Effective and efficient global optimization for conceptual rainfall-runoff models. Water Resources Research, 28(4): 1015-1031. doi: 10.1029/91wr02985.

Dunne, T., Black, R.D., 1970. An Experimental Investigation of Runoff Production in Permeable Soils. Water Resources Research, 6(2): 478-490. doi: 10.1029/WR006i002p00478.

Eagleson, P.S., 1994. The evolution of modern hydrology (from watershed to continent in 30 years). Advances in Water Resources, 17(1–2): 3-18. doi: http://dx.doi.org/10.1016/0309-1708(94)90019-1.

Eckhardt, K., 2005. How to construct recursive digital filters for baseflow separation. Hydrological Processes, 19(2): 507-515. doi: 10.1002/hyp.5675.

Ehret, U., Zehe, E., 2011. Series distance – an intuitive metric to quantify hydrograph similarity in terms of occurrence, amplitude and timing of hydrological events. Hydrol. Earth Syst. Sci., 15(3): 877-896. doi: 10.5194/hess-15-877-2011.

Eng, K., Brutsaert, W., 1999. Generality of drought flow characteristics within the Arkansas River Basin. Journal of Geophysical Research: Atmospheres, 104(D16): 19435-19441. doi: 10.1029/1999JD900087.

Entekhabi, D. et al., 2010. The Soil Moisture Active Passive (SMAP) Mission. Proceedings of the IEEE, 98(5): 704-716. doi: 10.1109/JPROC.2010.2043918.

Fan, Y., Bras, R.L., 1995. On the concept of a representative elementary area in catchment runoff. Hydrological Processes, 9(7): 821-832. doi: 10.1002/hyp.3360090708.

Faurès, J.-M., Goodrich, D.C., Woolhiser, D.A., Sorooshian, S., 1995. Impact of small-scale spatial rainfall variability on runoff modeling. Journal of Hydrology, 173(1–4): 309-326. doi: http://dx.doi.org/10.1016/0022-1694(95)02704-S.

Faures, J.M., Goodrich, D.C., Woolhiser, D.A., Sorooshian, S., 1995. Impact Of Small-Scale Spatial Rainfall Variability On Runoff Modeling. Journal of Hydrology, 173(1-4): 309-326. doi: 10.1016/0022-1694(95)02704-s.

Federer, C.A., 1973. Forest transpiration greatly speeds streamflow recession. Water Resources Research, 9(6): 1599-1604. doi: 10.1029/WR009i006p01599.

Fenicia, F., Savenije, H.H.G., Matgen, P., Pfister, L., 2006. Is the groundwater reservoir linear? Learning from data in hydrological modelling. Hydrol. Earth Syst. Sci., 10(1): 139-150. doi: 10.5194/hess-10-139-2006.

Foglia, L., Hill, M.C., Mehl, S.W., Burlando, P., 2009. Sensitivity analysis, calibration, and testing of a distributed hydrological model using error-based weighting and one objective function. Water Resources Research, 45(6): W06427. doi: 10.1029/2008wr007255.

Foley, J.A. et al., 2005. Global consequences of land use. science, 309(5734): 570-574.

Frisbee, M.D., Phillips, F.M., Campbell, A.R., Liu, F., Sanchez, S.A., 2011. Streamflow generation in a large, alpine watershed in the southern Rocky Mountains of Colorado: Is streamflow generation simply the aggregation of hillslope runoff responses? Water Resources Research, 47(6): W06512. doi: 10.1029/2010wr009391.

Fuller, W.A., 2009. Measurement error models, 305. Wiley. com.

Garbrecht, J., Martz, L., 1994. Grid size dependency of parameters extracted from digital elevation models. Computers & Geosciences, 20(1): 85-87.

Genereux, D., 1998. Quantifying uncertainty in tracer-based hydrograph separations. Water Resources Research, 34(4): 915-919.

Georgakakos, K.P., 1986. A generalized stochastic hydrometeorological model for flood and flash-flood forecasting: 2. Case studies. Water Resources Research, 22(13): 2096-2106. doi: 10.1029/WR022i013p02096.

Gomi, T., Sidle, R.C., Richardson, J.S., 2002. Understanding Processes and Downstream Linkages of Headwater Systems. BioScience, 52(10): 905-916. doi: 10.1641/0006-3568(2002)052[0905:upadlo]2.0.co;2.

Graham, C.B., Woods, R.A., McDonnell, J.J., 2010. Hillslope threshold response to rainfall: (1) A field based forensic approach. Journal of Hydrology, 393(1–2): 65-76. doi: http://dx.doi.org/10.1016/j.jhydrol.2009.12.015.

Grayson, R.B., Western, A.W., 1998. Towards areal estimation of soil water content from point measurements: time and space stability of mean response. Journal of Hydrology, 207(1-2): 68-82. doi: 10.1016/s0022-1694(98)00096-1.

Grayson, R.B., Western, A.W., Chiew, F.H.S., Bloschl, G., 1997. Preferred states in spatial soil moisture patterns: Local and nonlocal controls. Water Resources Research, 33(12): 2897-2908. doi: 10.1029/97wr02174.

Gribovszki, Z., Szilágyi, J., Kalicz, P., 2010. Diurnal fluctuations in shallow groundwater levels and streamflow rates and their interpretation – A review. Journal of Hydrology, 385(1–4): 371-383. doi: http://dx.doi.org/10.1016/j.jhydrol.2010.02.001.

Griffiths, G.A., Clausen, B., 1997. Streamflow recession in basins with multiple water storages. Journal of Hydrology, 190(1–2): 60-74. doi: 10.1016/s0022-1694(96)03060-0.

Gupta, V.K., Dawdy, D.R., 1995. Physical interpretations of regional variations in the scaling exponents of flood quantiles. Hydrological Processes, 9(3-4): 347-361. doi: 10.1002/hyp.3360090309.

Gupta, V.K., Mantilla, R., Troutman, B.M., Dawdy, D., Krajewski, W.F., 2010. Generalizing a nonlinear geophysical flood theory to medium-sized river networks. Geophysical Research Letters, 37(11): n/a-n/a. doi: 10.1029/2009gl041540.

Gupta, V.K., Mesa, O.J., 1988. Runoff generation and hydrologic response via channel network geomorphology — Recent progress and open problems. Journal of Hydrology, 102(1–4): 3-28. doi: http://dx.doi.org/10.1016/0022-1694(88)90089-3.

Gupta, V.K., Waymire, E., Wang, C.T., 1980. A representation of an instantaneous unit hydrograph from geomorphology. Water Resources Research, 16(5): 855-862. doi: 10.1029/WR016i005p00855.

Halford, K.J., Mayer, G.C., 2000. Problems Associated with Estimating Ground Water Discharge and Recharge from Stream-Discharge Records. Ground Water, 38(3): 331-342. doi: 10.1111/j.1745-6584.2000.tb00218.x.

Hall, F.R., 1968. Base-Flow Recessions—A Review. Water Resources Research, 4(5): 973-983. doi: 10.1029/WR004i005p00973.

Hammond, M., Han, D., 2006. Recession curve estimation for storm event separations. Journal of Hydrology, 330(3–4): 573-585. doi: 10.1016/j.jhydrol.2006.04.027.

Harman, C.J., Sivapalan, M., Kumar, P., 2009. Power law catchment-scale recessions arising from heterogeneous linear small-scale dynamics. Water Resources Research, 45(9): W09404. doi: 10.1029/2008wr007392.

Harmel, R.D., Cooper, R.J., Slade, R.M., Haney, R.L., Arnold, J.G., 2006. Cumulative uncertainty in measured streamflow and water quality data for small watersheds. Transactions of the ASABE, 49(3): 689-701.

Harvey, D.W., 1968. Pattern, Process, and the Scale Problem in Geographical Research. Transactions of the Institute of British Geographers(45): 71-78. doi: 10.2307/621393.

Helmers, M.J. et al., 2012. Sediment Removal by Prairie Filter Strips in Row-Cropped Ephemeral Watersheds. J. Environ. Qual., 41(5): 1531-1539. doi: 10.2134/jeq2011.0473.

Hernandez-Santana, V. et al., 2013. Native prairie filter strips reduce runoff from hillslopes under annual row-crop systems in Iowa, USA. Journal of Hydrology, 477(0): 94-103. doi: http://dx.doi.org/10.1016/j.jhydrol.2012.11.013.

Hewlett, J.D., Hibbert, A.R., 1967. Factors affecting the response of small watersheds to precipitation in humid areas. Forest hydrology: 275-290.

Hirsch, R.M., 1979. An evaluation of some record reconstruction techniques. Water Resources Research, 15(6): 1781-1790. doi: 10.1029/WR015i006p01781.

Hooper, R.P., Shoemaker, C.A., 1986. A Comparison of Chemical and Isotopic Hydrograph Separation. Water Resources Research, 22(10): 1444-1454. doi: 10.1029/WR022i010p01444.

Hortness, J.E., 2006. Estimating low-flow frequency statistics for unregulated streams in Idaho. U.S. Geological SurveyScientific Investigations Report 2006-5035. doi:

Horton, R.E., 1933. The role of infiltration in the hydrologic cycle. Transactions, American Geophysical Union, 14: 446-460.

Hubbert, M.K., 1957. Darcy's law and the field equations of the flow of underground fluids. International Association of Scientific Hydrology. Bulletin, 2(1): 23-59. doi: 10.1080/02626665709493062.

Jencso, K.G., McGlynn, B.L., Gooseff, M.N., Bencala, K.E., Wondzell, S.M., 2010. Hillslope hydrologic connectivity controls riparian groundwater turnover: Implications of catchment structure for riparian buffering and stream water sources. Water Resources Research, 46(10): W10524. doi: 10.1029/2009wr008818.

Jencso, K.G. et al., 2009. Hydrologic connectivity between landscapes and streams: Transferring reach- and plot-scale understanding to the catchment scale. Water Resour. Res., 45(4): W04428. doi: 10.1029/2008wr007225.

Jones, J., 2006. Intersite Comparisons of Rainfall-Runoff Processes, Encyclopedia of Hydrological Sciences. John Wiley & Sons, Ltd.

Jones, J.A., Grant, G.E., 1996. Peak Flow Responses to Clear-Cutting and Roads in Small and Large Basins, Western Cascades, Oregon. Water Resour. Res., 32(4): 959-974. doi: 10.1029/95wr03493.

Juston, J.M. et al., 2013. Smiling in the rain: Seven reasons to be positive about uncertainty in hydrological modelling. Hydrological Processes, 27(7): 1117-1122. doi: 10.1002/hyp.9625.

Kienzler, P.M., Naef, F., 2008a. Subsurface storm flow formation at different hillslopes and implications for the 'old water paradox'. Hydrological Processes, 22(1): 104-116. doi: 10.1002/hyp.6687.

Kienzler, P.M., Naef, F., 2008b. Temporal variability of subsurface stormflow formation. Hydrol. Earth Syst. Sci., 12(1): 257-265. doi: 10.5194/hess-12-257-2008.

Kirchner, J.W., 2006. Getting the right answers for the right reasons: Linking measurements, analyses, and models to advance the science of hydrology. Water Resources Research, 42(3). doi: 10.1029/2005wr004362.

Kirchner, J.W., 2009. Catchments as simple dynamical systems: Catchment characterization, rainfall-runoff modeling, and doing hydrology backward. Water Resour. Res., 45(2): W02429. doi: 10.1029/2008wr006912.

Kitanidis, P.K., Bras, R.L., 1980. Real-time forecasting with a conceptual hydrologic model: 2. Applications and results. Water Resources Research, 16(6): 1034-1044. doi: 10.1029/WR016i006p01034.

Klemeš, V., 1983. Conceptualization and scale in hydrology. Journal of Hydrology, 65(1–3): 1-23. doi: http://dx.doi.org/10.1016/0022-1694(83)90208-1.

Krajewski, W.F., Ciach, G.J., Habib, E., 2003. An analysis of small-scale rainfall variability in different climatic regimes. Hydrological Sciences Journal, 48(2): 151-162. doi: 10.1623/hysj.48.2.151.44694.

Kroll, C., Luz, J., Allen, B., Vogel, R., 2004. Developing a Watershed Characteristics Database to Improve Low Streamflow Prediction. Journal of Hydrologic Engineering, 9(2): 116-125. doi: doi:10.1061/(ASCE)1084-0699(2004)9:2(116).

Kuo, W.-L. et al., 1999. Effect of grid size on runoff and soil moisture for a variable-source-area hydrology model. Water Resources Research, 35(11): 3419-3428. doi: 10.1029/1999WR900183.

Liang, X., Lettenmaier, D.P., Wood, E.F., Burges, S.J., 1994. A simple hydrologically based model of land surface water and energy fluxes for general circulation models. J. Geophys. Res., 99(D7): 14415-14428. doi: 10.1029/94jd00483.

Loague, K., Gander, G.A., 1990. R-5 revisited: 1. Spatial variability of infiltration on a small rangeland catchment. Water Resour. Res., 26(5): 957-971. doi: 10.1029/WR026i005p00957.

Loperfido, J.V., Just, C.L., Papanicolaou, A.N., Schnoor, J.L., 2010. In situ sensing to understand diel turbidity cycles, suspended solids, and nutrient transport in Clear Creek, Iowa. Water Resources Research, 46(6): W06525. doi: 10.1029/2009wr008293.

Lyon, S.W. et al., 2012. Specific discharge variability in a boreal landscape. Water Resources Research, 48(8): W08506. doi: 10.1029/2011wr011073.

Mandapaka, P.V., Krajewski, W.F., Mantilla, R., Gupta, V.K., 2009. Dissecting the effect of rainfall variability on the statistical structure of peak flows. Advances in Water Resources, 32(10): 1508-1525. doi: http://dx.doi.org/10.1016/j.advwatres.2009.07.005.

Mantilla, R., 2007. Physical basis of statistical scaling in peak flows and stream flow hydrographs for topologic and spatially embedded random self-similiar channel networks. Ph.D. Thesis, University of Colorado at Boulder, Ann Arbor, 160 pp.

Mantilla, R., Gupta, V.K., 2005. A GIS numerical framework to study the process basis of scaling statistics in river networks. Geoscience and Remote Sensing Letters, IEEE, 2(4): 404-408. doi: 10.1109/LGRS.2005.853571.

Mantoglou, A., Gelhar, L.W., 1987. Stochastic modeling of large-scale transient unsaturated flow systems. Water Resources Research, 23(1): 37-46. doi: 10.1029/WR023i001p00037.

McDonnell, J.J., Bonell, M., Stewart, M.K., Pearce, A.J., 1990. Deuterium variations in storm rainfall: Implications for stream hydrograph separation. Water Resour. Res., 26(3): 455-458. doi: 10.1029/WR026i003p00455.

McDonnell, J.J. et al., 2007. Moving beyond heterogeneity and process complexity: A new vision for watershed hydrology. Water Resour. Res., 43(7): W07301. doi: 10.1029/2006wr005467.

McGlynn, B., McDonnell, J., Stewart, M., Seibert, J., 2003. On the relationships between catchment scale and streamwater mean residence time. Hydrological Processes, 17(1): 175-181. doi: 10.1002/hyp.5085.

McGlynn, B.L., McDonnell, J.J., 2003. Role of discrete landscape units in controlling catchment dissolved organic carbon dynamics. Water Resources Research, 39(4): 1090. doi: 10.1029/2002wr001525.

McGlynn, B.L., McDonnell, J.J., Seibert, J., Kendall, C., 2004. Scale effects on headwater catchment runoff timing, flow sources, and groundwater-streamflow relations. Water Resour. Res., 40(7): W07504. doi: 10.1029/2003wr002494.

McGlynn, B.L., Seibert, J., 2003. Distributed assessment of contributing area and riparian buffering along stream networks. Water Resources Research, 39(4): 1082. doi: 10.1029/2002WR001521.

McGuire, K.J. et al., 2005. The role of topography on catchment-scale water residence time. Water Resources Research, 41(5). doi: 10.1029/2004wr003657.

McMillan, H., Krueger, T., Freer, J., 2012. Benchmarking observational uncertainties for hydrology: rainfall, river discharge and water quality. Hydrological Processes, 26(26): 4078-4111. doi: 10.1002/hyp.9384.

Mendoza, G.F., Steenhuis, T.S., Walter, M.T., Parlange, J.Y., 2003. Estimating basin-wide hydraulic parameters of a semi-arid mountainous watershed by recession-

flow analysis. Journal of Hydrology, 279(1–4): 57-69. doi: http://dx.doi.org/10.1016/S0022-1694(03)00174-4.

Merz, R., Bloeschl, G., Parajka, J., 2006. Spatio-temporal variability of event runoff coefficients. Journal of Hydrology, 331(3-4): 591-604. doi: 10.1016/j.jhydrol.2006.06.008.

Merz, R., Blöschl, G., 2004. Regionalisation of catchment model parameters. Journal of Hydrology, 287(1–4): 95-123. doi: http://dx.doi.org/10.1016/j.jhydrol.2003.09.028.

Milly, P.C.D. et al., 2008. Stationarity Is Dead: Whither Water Management? Science, 319(5863): 573-574. doi: 10.1126/science.1151915.

Minshall, N.E., 1960. Predicting storm runoff on small experimental watersheds.

Moore, I.D., Grayson, R.B., 1991. Terrain-based catchment partitioning and runoff prediction using vector elevation data. Water Resources Research, 27(6): 1177-1191. doi: 10.1029/91WR00090.

Moore, R.J., 1985. The probability-distributed principle and runoff production at point and basin scales. Hydrological Sciences Journal, 30(2): 273-297. doi: 10.1080/02626668509490989.

Mutzner, R. et al., 2013. Geomorphic signatures on Brutsaert base flow recession analysis. Water Resources Research, 49(9): 5462-5472. doi: 10.1002/wrcr.20417.

Nash, J.E., 1957. The form of the instantaneous unit hydrograph. IASH Publ., 45: 114-121.

Nathan, R.J., McMahon, T.A., 1990. Evaluation of automated techniques for base flow and recession analyses. Water Resour. Res., 26(7): 1465-1473. doi: 10.1029/WR026i007p01465.

Neumann, J.v., 1932. Proof of the quasi-ergodic hypothesis. Proceedings of the National Academy of Sciences of the United States of America, 18(1): 70.

Ogden, F., Dawdy, D., 2003. Peak Discharge Scaling in Small Hortonian Watershed. Journal of Hydrologic Engineering, 8(2): 64-73. doi: doi:10.1061/(ASCE)1084-0699(2003)8:2(64).

Ogden, F.L., Julien, P.Y., 1993. Runoff sensitivity to temporal and spatial rainfall variability at runoff plane and small basin scales. Water Resources Research, 29(8): 2589-2597. doi: 10.1029/93WR00924.

Oudin, L., Andréassian, V., Perrin, C., Michel, C., Le Moine, N., 2008. Spatial proximity, physical similarity, regression and ungaged catchments: A comparison of regionalization approaches based on 913 French catchments. Water Resources Research, 44(3): W03413. doi: 10.1029/2007wr006240.

Oudin, L., Kay, A., Andréassian, V., Perrin, C., 2010. Are seemingly physically similar catchments truly hydrologically similar? Water Resour. Res., 46(11): W11558. doi: 10.1029/2009wr008887.

Palmroth, S. et al., 2010. Estimation of long-term basin scale evapotranspiration from streamflow time series. Water Resources Research, 46(10): W10512. doi: 10.1029/2009WR008838.

Pappenberger, F., Beven, K.J., 2006. Ignorance is bliss: Or seven reasons not to use uncertainty analysis. Water Resources Research, 42(5): W05302. doi: 10.1029/2005WR004820.

Pauwels, V.R.N., Verhoest, N.E.C., De Troch, F.P., 2002. A metahillslope model based on an analytical solution to a linearized Boussinesq equation for temporally variable recharge rates. Water Resources Research, 38(12): 1297. doi: 10.1029/2001WR000714.

Pickett, S.A., 1989. Space-for-Time Substitution as an Alternative to Long-Term Studies. In: Likens, G. (Ed.), Long-Term Studies in Ecology. Springer New York, pp. 110-135.

Pilgrim, D.H., Huff, D.D., Steele, T.D., 1979. Use of specific conductance and contact time relations for separating flow components in storm runoff. Water Resour. Res., 15(2): 329-339. doi: 10.1029/WR015i002p00329.

Quinn, P., Beven, K., Chevallier, P., Planchon, O., 1991. The prediction of hillslope flow paths for distributed hydrological modelling using digital terrain models. Hydrological Processes, 5(1): 59-79. doi: 10.1002/hyp.3360050106.

Rayburn, A.P., Schulte, L.A., 2009. Landscape change in an agricultural watershed in the U.S. Midwest. Landscape and Urban Planning, 93(2): 132-141. doi: http://dx.doi.org/10.1016/j.landurbplan.2009.06.014.

Reggiani, P., Hassanizadeh, S.M., Sivapalan, M., Gray, W.G., 1999. A unifying framework for watershed thermodynamics: constitutive relationships. Advances in Water Resources, 23(1): 15-39. doi: http://dx.doi.org/10.1016/S0309-1708(99)00005-6.

Reggiani, P., Rientjes, T.H.M., 2005. Flux parameterization in the representative elementary watershed approach: Application to a natural basin. Water Resources Research, 41(4): W04013. doi: 10.1029/2004wr003693.

Reggiani, P., Sivapalan, M., Hassanizadeh, S.M., 1998. A unifying framework for watershed thermodynamics: balance equations for mass, momentum, energy and entropy, and the second law of thermodynamics. Advances in Water Resources, 22(4): 367-398. doi: http://dx.doi.org/10.1016/S0309-1708(98)00012-8.

Reggiani, P., Sivapalan, M., Hassanizadeh, S.M., 2000. Conservation equations governing hillslope responses: Exploring the physical basis of water balance. Water Resources Research, 36(7): 1845-1863. doi: 10.1029/2000WR900066.

Risley, J., Moradkhani, H., Hay, L., Markstrom, S., 2010. Statistical Comparisons of Watershed-Scale Response to Climate Change in Selected Basins across the United States. Earth Interactions, 15(14): 1-26. doi: 10.1175/2010ei364.1.

Robinson, D. et al., 2008. Soil moisture measurement for ecological and hydrological watershed-scale observatories: A review. Vadose Zone Journal, 7(1): 358-389.

Rodr ́guez-Iturbe, I., Devoto, G., Vald ́s, J.B., 1979. Discharge response analysis and hydrologic similarity: The interrelation between the geomorphologic IUH and the storm characteristics. Water Resources Research, 15(6): 1435-1444. doi: 10.1029/WR015i006p01435.

Rodriguez-Iturbe, I., Rinaldo, A., 1997. Fractal river networks: chance and self-organization. Cambridge University Press, New York.

Rodr ́guez-Iturbe, I., Vald ́s, J., 1979. The geomorphologic structure of hydrologic response. Water Resour. Res., 15(6): 1409-1420. doi: 10.1029/WR015i006p01409.

Rupp, D.E., Owens, J.M., Warren, K.L., Selker, J.S., 2004. Analytical methods for estimating saturated hydraulic conductivity in a tile-drained field. Journal of Hydrology, 289(1–4): 111-127. doi: http://dx.doi.org/10.1016/j.jhydrol.2003.11.004.

Rupp, D.E., Schmidt, J., Woods, R.A., Bidwell, V.J., 2009. Analytical assessment and parameter estimation of a low-dimensional groundwater model. Journal of Hydrology, 377(1–2): 143-154. doi: http://dx.doi.org/10.1016/j.jhydrol.2009.08.018.

Rupp, D.E., Selker, J.S., 2006a. Information, artifacts, and noise in dQ/dt−Q recession analysis. Advances in Water Resources, 29(2): 154-160. doi: 10.1016/j.advwatres.2005.03.019.

Rupp, D.E., Selker, J.S., 2006b. On the use of the Boussinesq equation for interpreting recession hydrographs from sloping aquifers. Water Resources Research, 42(12): W12421. doi: 10.1029/2006wr005080.

Savenije, H.H.G., 2001. Equifinality, a blessing in disguise? Hydrological Processes, 15(14): 2835-2838. doi: 10.1002/hyp.494.

Scherrer, S., Naef, F., Faeh, A.O., Cordery, I., 2007. Formation of runoff at the hillslope scale during intense precipitation. Hydrol. Earth Syst. Sci., 11(2): 907-922. doi: 10.5194/hess-11-907-2007.

Schilling, K.E., 2005. Relation of baseflow to row crop intensity in Iowa. Agriculture, Ecosystems & Environment, 105(1–2): 433-438. doi: http://dx.doi.org/10.1016/j.agee.2004.02.008.

Schilling, K.E., Helmers, M., 2008. Effects of subsurface drainage tiles on streamflow in Iowa agricultural watersheds: Exploratory hydrograph analysis. Hydrological Processes, 22(23): 4497-4506. doi: 10.1002/hyp.7052.

Schilling, K.E., Libra, R.D., 2003. Increased Baseflow In Iowa Over The Second Half Of The 20th Century. JAWRA Journal of the American Water Resources Association, 39(4): 851-860. doi: 10.1111/j.1752-1688.2003.tb04410.x.

Schulz, K., Seppelt, R., Zehe, E., Vogel, H.J., Attinger, S., 2006. Importance of spatial structures in advancing hydrological sciences. Water Resources Research, 42(3): W03S03. doi: 10.1029/2005WR004301.

Seyfried, M.S., Grant, L.E., Du, E., Humes, K., 2005. Dielectric Loss and Calibration of the Hydra Probe Soil Water Sensor. Vadose Zone Journal, 4(4): 1070-1079. doi: 10.2136/vzj2004.0148.

Seyfried, M.S., Grant, L.E., Marks, D., Winstral, A., McNamara, J., 2009. Simulated soil water storage effects on streamflow generation in a mountainous snowmelt environment, Idaho, USA. Hydrological Processes, 23(6): 858-873. doi: 10.1002/hyp.7211.

Seyfried, M.S., Wilcox, B.P., 1995. Scale and the Nature of Spatial Variability: Field Examples Having Implications for Hydrologic Modeling. Water Resour. Res., 31(1): 173-184. doi: 10.1029/94wr02025.

Shaman, J., Stieglitz, M., Burns, D., 2004. Are big basins just the sum of small catchments? Hydrological Processes, 18(16): 3195-3206. doi: 10.1002/hyp.5739.

Shaw, S.B., McHardy, T.M., Riha, S.J., 2013. Evaluating the influence of watershed moisture storage on variations in baseflow recession rates during prolonged rain-free periods in medium-sized catchments in New York and Illinois, USA. Water Resources Research: 1-7. doi: 10.1002/wrcr.20507.

Shaw, S.B., Riha, S.J., 2012. Examining individual recession events instead of a data cloud: Using a modified interpretation of dQ/dt–Q streamflow recession in glaciated watersheds to better inform models of low flow. Journal of Hydrology, 434–435(0): 46-54. doi: http://dx.doi.org/10.1016/j.jhydrol.2012.02.034.

Sivapalan, M., 2003. Process complexity at hillslope scale, process simplicity at the watershed scale: is there a connection? Hydrological Processes, 17(5): 1037-1041. doi: 10.1002/hyp.5109.

Sivapalan, M., 2009. The secret to 'doing better hydrological science': change the question! Hydrological Processes, 23(9): 1391-1396.

Sivapalan, M., Jothityangkoon, C., Menabde, M., 2002. Linearity and nonlinearity of basin response as a function of scale: Discussion of alternative definitions. Water Resources Research, 38(2): 4-1-4-5. doi: 10.1029/2001wr000482.

Sivapalan, M. et al., 2003. IAHS Decade on Predictions in Ungauged Basins (PUB), 2003–2012: Shaping an exciting future for the hydrological sciences. Hydrological Sciences Journal, 48(6): 857-880. doi: 10.1623/hysj.48.6.857.51421.

Smakhtin, V.U., 2001. Low flow hydrology: a review. Journal of Hydrology, 240(3–4): 147-186. doi: 10.1016/s0022-1694(00)00340-1.

Smakhtin, V.Y., Hughes, D.A., Creuse-Naudin, E., 1997. Regionalization of daily flow characteristics in part of the Eastern Cape, South Africa. Hydrological Sciences Journal, 42(6): 919-936. doi: 10.1080/02626669709492088.

Small, S.J. et al., 2013. An asynchronous solver for systems of ODEs linked by a directed tree structure. Advances in Water Resources, 53(0): 23-32. doi: http://dx.doi.org/10.1016/j.advwatres.2012.10.011.

Sorooshian, S., Dracup, J.A., 1980. Stochastic parameter estimation procedures for hydrologie rainfall-runoff models: Correlated and heteroscedastic error cases. Water Resources Research, 16(2): 430-442. doi: 10.1029/WR016i002p00430.

Spence, C., 2007. On the relation between dynamic storage and runoff: A discussion on thresholds, efficiency, and function. Water Resour. Res., 43(12): W12416. doi: 10.1029/2006wr005645.

Spence, C., 2010. A Paradigm Shift in Hydrology: Storage Thresholds Across Scales Influence Catchment Runoff Generation. Geography Compass, 4(7): 819-833. doi: 10.1111/j.1749-8198.2010.00341.x.

Ssegane, H., Amatya, D.M., Tollner, E.W., Dai, Z., Nettles, J.E., 2013. Estimation of Daily Streamflow of Southeastern Coastal Plain Watersheds by Combining Estimated Magnitude and Sequence. JAWRA Journal of the American Water Resources Association: n/a-n/a. doi: 10.1111/jawr.12077.

Stoelzle, M., Stahl, K., Weiler, M., 2012. Are streamflow recession characteristics really characteristic? Hydrol. Earth Syst. Sci. Discuss., 9(9): 10563-10593. doi: 10.5194/hessd-9-10563-2012.

Sujono, J., Shikasho, S., Hiramatsu, K., 2004. A comparison of techniques for hydrograph recession analysis. Hydrological Processes, 18(3): 403-413. doi: 10.1002/hyp.1247.

Szilagyi, J., Parlange, M.B., 1998. Baseflow separation based on analytical solutions of the Boussinesq equation. Journal of Hydrology, 204(1–4): 251-260. doi: 10.1016/s0022-1694(97)00132-7.

Szilagyi, J., Parlange, M.B., Albertson, J.D., 1998. Recession flow analysis for aquifer parameter determination. Water Resources Research, 34(7): 1851-1857. doi: 10.1029/98wr01009.

Tallaksen, L.M., 1995. A review of baseflow recession analysis. Journal of Hydrology, 165(1–4): 349-370. doi: http://dx.doi.org/10.1016/0022-1694(94)02540-R.

Troch, P.A. et al., 2013. The importance of hydraulic groundwater theory in catchment hydrology: The legacy of Wilfried Brutsaert and Jean-Yves Parlange. Water Resources Research: 5099-5116. doi: 10.1002/wrcr.20407.

Troch, P.A. et al., 2009. Dealing with Landscape Heterogeneity in Watershed Hydrology: A Review of Recent Progress toward New Hydrological Theory. Geography Compass, 3(1): 375-392. doi: 10.1111/j.1749-8198.2008.00186.x.

Troch, P.A., De Troch, F.P., Brutsaert, W., 1993. Effective water table depth to describe initial conditions prior to storm rainfall in humid regions. Water Resour. Res., 29(2): 427-434. doi: 10.1029/92wr02087.

Tromp-van Meerveld, H.J., McDonnell, J.J., 2006a. On the interrelations between topography, soil depth, soil moisture, transpiration rates and species distribution at the hillslope scale. Advances in Water Resources, 29(2): 293-310. doi: http://dx.doi.org/10.1016/j.advwatres.2005.02.016.

Tromp-van Meerveld, H.J., McDonnell, J.J., 2006b. Threshold relations in subsurface stormflow: 1. A 147-storm analysis of the Panola hillslope. Water Resources Research, 42(2). doi: 10.1029/2004wr003778.

Ts'o, D., Gilbert, C., Wiesel, T., 1986. Relationships between horizontal interactions and functional architecture in cat striate cortex as revealed by cross-correlation analysis. The Journal of Neuroscience, 6(4): 1160-1170.

Uchida, T., Asano, Y., Onda, Y., Miyata, S., 2005a. Are headwaters just the sum of hillslopes? Hydrological Processes, 19(16): 3251-3261. doi: 10.1002/hyp.6004.

Uchida, T., Tromp-van Meerveld, I., McDonnell, J.J., 2005b. The role of lateral pipe flow in hillslope runoff response: an intercomparison of non-linear hillslope response. Journal of Hydrology, 311(1–4): 117-133. doi: http://dx.doi.org/10.1016/j.jhydrol.2005.01.012.

Uhlenbrook, S., Hoeg, S., 2003. Quantifying uncertainties in tracer-based hydrograph separations: a case study for two-, three-and five-component hydrograph separations in a mountainous catchment. Hydrological Processes, 17(2): 431-453.

van de Giesen, N., Steenhuis, T.S., Parlange, J.Y., 2005. Short- and long-time behavior of aquifer drainage after slow and sudden recharge according to the linearized Laplace equation. Advances in Water Resources, 28(10): 1122-1132. doi: http://dx.doi.org/10.1016/j.advwatres.2004.12.002.

Van Heel, M., 1987. Similarity measures between images. Ultramicroscopy, 21(1): 95-100. doi: http://dx.doi.org/10.1016/0304-3991(87)90010-6.

Van Nieuwenhuyse, B.H.J., Antoine, M., Wyseure, G., Govers, G., 2011. Pattern-process relationships in surface hydrology: hydrological connectivity expressed in landscape metrics. Hydrological Processes, 25(24): 3760-3773. doi: 10.1002/hyp.8101.

Vannote, R.L., Minshall, G.W., Cummins, K.W., Sedell, J.R., Cushing, C.E., 1980. The River Continuum Concept. Canadian Journal of Fisheries and Aquatic Sciences, 37(1): 130-137. doi: 10.1139/f80-017.

Villarini, G. et al., 2011. On the frequency of heavy rainfall for the Midwest of the United States. Journal of Hydrology, 400(1–2): 103-120. doi: http://dx.doi.org/10.1016/j.jhydrol.2011.01.027.

Vogel, R.M., Kroll, C.N., 1992. Regional geohydrologic-geomorphic relationships for the estimation of low-flow statistics. Water Resour. Res., 28(9): 2451-2458. doi: 10.1029/92wr01007.

Vogel, R.M., Kroll, C.N., 1996. Estimation of baseflow recession constants. Water Resour Manage, 10(4): 303-320. doi: 10.1007/bf00508898.

Wagener, T., Sivapalan, M., Troch, P., Woods, R., 2007. Catchment Classification and Hydrologic Similarity. Geography Compass, 1(4): 901-931. doi: 10.1111/j.1749-8198.2007.00039.x.

Wagener, T. et al., 2010. The future of hydrology: An evolving science for a changing world. Water Resources Research, 46. doi: 10.1029/2009wr008906.

Wang, C.T., Gupta, V.K., Waymire, E., 1981. A geomorphologic synthesis of nonlinearity in surface runoff. Water Resources Research, 17(3): 545-554. doi: 10.1029/WR017i003p00545.

Weerts, A.H., El Serafy, G.Y.H., 2006. Particle filtering and ensemble Kalman filtering for state updating with hydrological conceptual rainfall-runoff models. Water Resources Research, 42(9): W09403. doi: 10.1029/2005wr004093.

Weiler, M., McDonnell, J., 2004. Virtual experiments: a new approach for improving process conceptualization in hillslope hydrology. Journal of Hydrology, 285(1–4): 3-18. doi: http://dx.doi.org/10.1016/S0022-1694(03)00271-3.

Weiler, M., McDonnell, J.J., 2006. Testing nutrient flushing hypotheses at the hillslope scale: A virtual experiment approach. Journal of Hydrology, 319(1–4): 339-356. doi: http://dx.doi.org/10.1016/j.jhydrol.2005.06.040.

Weisman, R.N., 1977. The Effect of Evapotranspiration on Streamflow Recession. Hydrological Sciences Bulletin, 22(3): 371-377. doi: 10.1080/02626667709491731.

Western, A.W., Grayson, R.B., Bloschl, G., Willgoose, G.R., McMahon, T.A., 1999. Observed spatial organization of soil moisture and its relation to terrain indices. Water Resources Research, 35(3): 797-810. doi: 10.1029/1998wr900065.

Western, A.W. et al., 2004. Spatial correlation of soil moisture in small catchments and its relationship to dominant spatial hydrological processes. Journal of Hydrology, 286(1-4): 113-134. doi: 10.1016/j.jhydrol.2003.09.014.

Weyman, D.R., 1970. THROUGHFLOW ON HILLSLOPES AND ITS RELATION TO THE STREAM HYDROGRAPH. International Association of Scientific Hydrology. Bulletin, 15(3): 25-33. doi: 10.1080/02626667009493969.

Whitehead, P.G., Robinson, M., 1993. Experimental basin studies—an international and historical perspective of forest impacts. Journal of Hydrology, 145(3–4): 217-230. doi: http://dx.doi.org/10.1016/0022-1694(93)90055-E.

Wittenberg, H., 1994. Nonlinear analysis of flow recession curves. IAHS Publications-Series of Proceedings and Reports-Intern Assoc Hydrological Sciences, 221: 61-68.

Wittenberg, H., 1999. Baseflow recession and recharge as nonlinear storage processes. Hydrological Processes, 13(5): 715-726. doi: 10.1002/(sici)1099-1085(19990415)13:5<715::aid-hyp775>3.0.co;2-n.

Wittenberg, H., Sivapalan, M., 1999. Watershed groundwater balance estimation using streamflow recession analysis and baseflow separation. Journal of Hydrology, 219(1–2): 20-33. doi: 10.1016/s0022-1694(99)00040-2.

Wolock, D.M., Fan, J., Lawrence, G.B., 1997. Effects of basin size on low-flow stream chemistry and subsurface contact time in the Neversink River watershed, New York. Hydrological Processes, 11(9): 1273-1286. doi: 10.1002/(sici)1099-1085(199707)11:9<1273::aid-hyp557>3.0.co;2-s.

Wolock, D.M., Price, C.V., 1994. Effects of digital elevation model map scale and data resolution on a topography-based watershed model. Water Resources Research, 30(11): 3041-3052. doi: 10.1029/94WR01971.

Wood, E.F., Sivapalan, M., Beven, K., 1990. Similarity and scale in catchment storm response. Reviews of Geophysics, 28(1): 1-18. doi: 10.1029/RG028i001p00001.

Wood, E.F., Sivapalan, M., Beven, K., Band, L., 1988. Effects of spatial variability and scale with implications to hydrologic modeling. Journal of Hydrology, 102(1–4): 29-47. doi: 10.1016/0022-1694(88)90090-x.

Woods, R., 2006. Hydrologic concepts of variability and scale. Encyclopedia of hydrological sciences.

Woods, R., Sivapalan, M., Duncan, M., 1995. Investigating the representative elementary area concept: An approach based on field data. Hydrological Processes, 9(3-4): 291-312. doi: 10.1002/hyp.3360090306.

Yang, D., Herath, S., Musiake, K., 2002. A hillslope-based hydrological model using catchment area and width functions. Hydrological Sciences Journal, 47(1): 49-65. doi: 10.1080/02626660209492907.

Zecharias, Y.B., Brutsaert, W., 1988. Recession characteristics of groundwater outflow and base flow from mountainous watersheds. Water Resour. Res., 24(10): 1651-1658. doi: 10.1029/WR024i010p01651.

Zehe, E., Becker, R., Bárdossy, A., Plate, E., 2005. Uncertainty of simulated catchment runoff response in the presence of threshold processes: Role of initial soil moisture and precipitation. Journal of hydrology, 315(1): 183-202.

Zehe, E., Bloschl, G., 2004. Predictability of hydrologic response at the plot and catchment scales: Role of initial conditions. Water Resources Research, 40(10). doi: 10.1029/2003wr002869.

Zehe, E., Blöschl, G., 2004. Predictability of hydrologic response at the plot and catchment scales: Role of initial conditions. Water Resour. Res., 40(10): W10202. doi: 10.1029/2003wr002869.

Zehe, E., Sivapalan, M., 2009. Threshold behaviour in hydrological systems as (human) geo-ecosystems: manifestations, controls, implications. Hydrology and Earth System Sciences, 13(7): 1273-1297.

Zhang, W., Montgomery, D.R., 1994. Digital elevation model grid size, landscape representation, and hydrologic simulations. Water Resour. Res., 30(4): 1019-1028. doi: 10.1029/93wr03553.

Zhang, Y.K., Schilling, K.E., 2006. Increasing streamflow and baseflow in Mississippi River since the 1940s: Effect of land use change. Journal of Hydrology, 324(1–4): 412-422. doi: http://dx.doi.org/10.1016/j.jhydrol.2005.09.033.

Zhang, Z., Kroll, C., 2007. The baseflow correlation method with multiple gauged sites. Journal of Hydrology, 347(3–4): 371-380. doi: http://dx.doi.org/10.1016/j.jhydrol.2007.09.025.